UCL Université catholique de Louvain

École polytechnique de Louvain (EPL)

epl

3D interconnected nanowires networks on silicon substrate for energy storage applications

Dissertation presented by
Valentin MATTON

for obtaining the Master's degree in
Physical engineering

Supervisors
Piraux LUC, Vlad ALEXANDRU

Readers
van Velthem PASCAL, Gohy JEAN-FRANÇOIS

Academic year 2016-2017

Master thesis realised at the Institute of Condensed Matter and Nanosciences in the Université Catholique de Louvain in Louvain-La-Neuve under the supervision of professors Luc Piraux and Alexandru Vlad

Acknowledgement

By this, I would like to thank the persons who helped me in the achievement of my master's thesis.

First, I would like to thank my two supervisors Luc Piraux and Alexandru Vlad for the oversight of my work and the guidance they provided me during this whole year. This master thesis was a real pleasure to do, and I thank them for choosing me to do it.

My sincere thanks to Pascal Van Velthem who helped me a lot in the beginning to make my first electrodepositions. He helped me when it did not work and spent time with me discovering which problem it was one at the time. He also makes SEM session with me as well as the cathodic sputtering on Si/SiO_2 substrates and was always there when I had questions and was very helpful.

I would like to express my gratitude to Xuelian Liu who helped me a lot during the entire year. She helped me to do my first batteries and supercapacitors. She explained to me the working of the glovebox, the drying oven, the cyclic voltammetry, the battery tester, the hydraulic crimper, the making of the slurry for the supercapacitors, the ball mill and was also very available to all my questions and answered them very enthusiastically.

Thanks a lot to Vivien Van Kerckhoven who was of vital importance for the use of the Picosecond laser in Winfab. Indeed, every time I needed to use this laser, Vivien was always available to do it. He also helped me when I had problems during the electrodeposition.

I highly benefited from the advises given by Laura Höltschi. She spent time to answer questions I had about batteries and the comfort she brought me when I was in doubt.

I also thank Pedro Miguel Pereira de Sá who also helped me for my first electrodeposition and explained to me the working of the tubular furnace as well as the AGM. He has been very helpful all along the year when I had questions.

I would also like to thank Tristan da Câmara Santa Clara Gomes who also helped me for the AGM measurements and was also always available when I had questions.

I will also mention Delphine Magnin that did a SEM session with me at the beginning of the year.

Discussions with Bruno Ernould and Louis Sieuw have been insightful.

Special thanks to Olivier Alves for his help and its unwavering motivation he gave me during this year.

I thank Shanshan for her help to understand the working of the cyclic voltammetry.

Abstract

This master thesis has the aim of finding out the feasibility of 3D interconnected nanowires networks on silicon substrate for energy storage applications without damaging the silicon. The studied network is made of nickel-nickel oxide core-shell nanowires grown by polymer template-assisted followed by thermal annealing. Research have been conducted in batteries, supercapacitors and interdigit electrodes using this 3D nanostructure.

Electrodes have been successfully produced, as well as functional batteries having this electrode as a cathode. These batteries show no degradation of the silicon substrate, and an enhanced cycle performance compared batteries based on bulk transition metal compounds.

The morphology of the 3D nanowires nanostructure has been observed by scanning electron microscopy, and the chemical composition of the interdigit electrode with energy dispersive X-ray spectroscopy. Magnetic moment measurements have been conducted with an alternating gradient magnetometer to observe the influence of the thermal annealing. The batteries have then been tested with the galvanostatic charge and discharge method as well as electrochemical impedance spectroscopy. The made supercapacitors have been supplementary analysed with cyclic voltammetry.

Abbreviations

During this thesis, several abbreviations have been used to reduce the complexity and shorten the text.

- **230 nm batteries**: Batteries with an electrode with made of nanowires of 230nm in diameter before annealing.
- **40 nm batteries**: Batteries with an electrode with made of nanowires of 40 nm in diameter before annealing.
- **SEM** : Scanning electron microscope
- **EIS** : Electrochemical impedance spectroscopy
- **AGM** : Alternating gradient magnetometer
- **EDX** : Energy-dispersive X-ray spectroscopy
- **SEI** : Solid electrolyte interface
- **xC** : Charge-discharge current of a cell.
- **VS** : Versus
- **EDLC** : Electrical double-layer capacitor
- **ESR** : Equivalent series resistance
- **PVDF** : Polyvinylidene fluoride
- **PC** : Polycarbonate
- **Sccm** : Standard Cubic Centimeters per Minute
- **DC** : Direct current
- **AC** : Alternating current
- **EC** : Ethylene carbonate
- **DEC** : Diethyl carbonate
- **CV** : Cyclic voltammetry
- **1D** : One dimension
- **2D** : Two dimensions
- **3D** : Three dimensions
- **bef** : Before
- **aft** : After

Symbols

- **E**$^{\circ}$: Standard electromotive force in volts
- **R**: The gas constant in $\frac{kgm^2}{s^2mol}$
- **n** : Number of exchanged electrons
- **T** : Temperature in Kelvin or degree Celcius
- **F** : Faraday's constant in $\frac{Coulombs}{mol}$
- **Q** : The charge in Coulomb
- **m** : The mass in g
- M_w : The molar mass in g/mol
- **i** : Current in ampere
- ϕ : Cathodic efficiency in %
- γ : Magnetic moment in emu

Contents

1 Introduction **1**

2 Batteries **3**
2.1 Definition . . . 3
2.2 General Characteristics . . . 3
2.2.1 Voltage of a Cell . . . 3
2.2.2 Specific Capacity . . . 4
2.2.3 The Specific Energy . . . 5
2.2.4 The Specific Power . . . 5
2.2.5 Depth of Discharge . . . 5
2.2.6 Cycle Life . . . 5
2.2.7 Memory Effect . . . 5
2.2.8 Self-Discharge . . . 5
2.2.9 Solid-Electrolyte Interphase . . . 5
2.2.10 HOMO-LUMO Levels . . . 6
2.3 Type of Batteries . . . 6
2.3.1 Primary Batteries . . . 7
2.3.1.1 Voltaic Pile . . . 7
2.3.1.2 Daniell Cell . . . 7
2.3.2 Secondary Batteries . . . 7
2.3.2.1 Lead-Acid Batteries . . . 7
2.3.2.2 Nickel Cadmium Batteries . . . 8
2.3.2.3 Nickel-Metal Hybrid . . . 8
2.4 Lithium Batteries . . . 9
2.4.1 Lithium Metal . . . 9
2.4.2 Lithium-ion Batteries . . . 10
2.4.2.1 Electrodes . . . 11
2.4.2.2 Nanostructured Electrode . . . 13
2.4.2.3 Electrolyte . . . 13
2.4.3 Lithiation of Silicon . . . 14

3 Supercapacitor **17**
3.1 Electrical Double-Layer Capacitors . . . 17
3.2 Pseudocapacitors . . . 18
3.3 Hybrid Capacitors . . . 18
3.4 Comparison Batteries VS Supercapacitors . . . 19
3.5 Interdigit Electrodes . . . 20

I Experimental part **22**

4 Sample preparation **23**
4.1 Electrode with Nanowires on Silicon Substrate . . . 23
4.1.1 Track-Etched PC Membranes . . . 23
4.1.2 Substrate . . . 24
4.1.3 Potentiostatic Electrochemical Deposition . . . 25
4.1.3.1 Device . . . 25
4.1.3.2 Charge, Current and Mass relation . . . 26
4.1.4 PC Dissolution . . . 27
4.1.5 Thermal Annealing . . . 27
4.1.6 Drying . . . 27
4.2 Substrate with Nickel Oxide Film . . . 28
4.2.1 Slurry Preparation . . . 28
4.2.2 Ball Mill . . . 28
4.2.3 Coating of the Slurry . . . 28
4.2.4 Drying . . . 28
4.2.5 Electrode's Fabrication . . . 28
4.3 Batteries Assembly . . . 29
4.3.1 Without Nanowires . . . 29
4.3.2 With Nanowires . . . 29
4.4 Supercapacitor Assembly . . . 30
4.4.1 Without Nanowires . . . 30
4.4.2 With Nanowires . . . 30
4.5 Interdigit Electrodes . . . 30
4.5.1 Picosecond Laser . . . 32
4.5.2 Other Etching Structures . . . 33

5 Characterisation Techniques **34**
5.1 Structural Analysis . . . 34
5.1.1 Scanning Electron Microscopy . . . 34
5.2 Chemical Analysis . . . 35
5.2.1 Energy Dispersive X-ray Spectroscopy . . . 35
5.3 Magnetic Characterisation . . . 36
5.3.1 Alternating Gradient Magnetometer . . . 36
5.4 Electrochemical Characterisation . . . 37
5.4.1 Electrochemical Impedance Spectroscopy . . . 37
5.4.2 Galvanostatic Charge and Discharge Cycles . . . 38
5.4.3 Cyclic Voltammetry . . . 39

II Results and discussion **41**

6 Electrode characterisation **42**
6.1 SEM . . . 42
6.1.1 Before Annealing . . . 42
6.1.2 After Annealing . . . 43
6.2 AGM . . . 44
6.2.1 230 nm Nanowires . . . 44
6.2.2 40 nm Nanowires . . . 44

7 Batteries Performance Testing **46**
7.1 Electrochemical Characterisation . . . 46
7.1.1 Galvanostatic Charge and Discharge . . . 46
7.1.1.1 Specific Capacity VS Cycles . . . 46
7.1.1.1.a Batteries Without Nanowires . . . 46
7.1.1.1.b Batteries With Nanowires . . . 47
7.1.1.1.c Comparison . . . 49
7.1.1.2 Charge-Discharge Voltage profiles . . . 50
7.1.1.2.a 230 nm Batteries . . . 50
7.1.1.2.b 40 nm Batteries . . . 53
7.1.1.2.c 230 nm Battery Cycled Between 0.01 V and 3 V . . . 55
7.1.2 Electrochemical Impedance Spectroscopy . . . 57
7.1.2.1 Batteries Without Nanowires . . . 57
7.1.2.2 Batteries With Nanowires . . . 58

8 Supercapacitor Performance Testing **60**
8.1 Electrochemical Characterisation . . . 60
8.1.1 Without Nanowires . . . 60
8.1.1.1 EIS . . . 60
8.1.1.2 Galvanostatic Charge and Discharge Test . . . 61
8.1.1.2.a Na_2SO_4 Supercapacitors . . . 62
8.1.1.2.b H_2SO_4 Supercapacitors . . . 64
8.1.1.2.c KOH Supercapacitor . . . 65
8.1.1.3 Cyclic Voltammetry . . . 67
8.1.2 With Nanowires: . . . 68
8.1.2.1 EIS . . . 68
8.1.2.2 Galvanostatic Charge and Discharge . . . 69
8.1.2.3 Cyclic Voltammetry . . . 69

9 Interdigit Electrode **71**
9.1 Morphological Characterisation . . . 71
9.1.1 Optical Microscopy . . . 71
9.1.2 SEM . . . 72
9.2 Chemical Characterisation . . . 75
9.2.1 EDX . . . 75
9.3 Electrical Measurement . . . 76
9.4 Other Etching Structures . . . 76

10 Conclusion **78**

Bibliography **80**

11 Appendix **87**
11.1 Calculation of Nickel Oxide Mass . . . 87
11.1.1 Faraday's Law . . . 87
11.2 Experimental Issues . . . 88
11.2.1 Electrodes Problems . . . 88
11.2.1.1 Break of the Substrate . . . 88
11.2.1.2 Detachments of Nanowires . . . 88
11.2.2 Broken Machines . . . 88
11.2.2.1 Electrodeposition Set-up . . . 88
11.2.2.2 The Tubular Oven . . . 88

11.2.2.3 Malfunction of the Drying Oven 88
11.2.2.4 Malfunction of the Glovebox 89
11.2.2.5 Picolaser Failure 89
11.3 Unusable Results 90
11.3.1 Electrodeposition 90
11.3.2 Galvanostatic Charge and Discharge 90
11.3.3 AGM 90

Chapter 1

Introduction

Lithium batteries are nowadays very popular in cell phones and other little demanding power devices. These will certainly become increasingly important as the storage of energy at big scale will become essential. Indeed, we are now facing the lack of clean energy production, but moreover, of ways to store it. Batteries seem to have many advantages that could give a boost to the renewable energy market and therefore, to the clean energy transition. This transition is done by moving from a centralised energy distribution, with big power plants using fossil fuels, to a multitude of smaller energy production units like wind turbines, solar panels, hydroelectric power or geothermal energy. These energies are becoming increasingly popular and cheaper. Between 2009 and 2014, the price dropped by about 75% and 33% respectively for solar PV panels and wind turbines [1]. These renewable energies suffer however from a major drawback: Their intermittence. Indeed, renewable energies are mostly nonconstant, and an overproduction coupled with more storage is needed to create a 100% renewable energy grid[2].

Secondary batteries are a good option to explore for such energy storage. Some prototypes are already working like in Japan[3] to store the overproduction of solar energy. Batteries will also probably be the future of zero emission cars, that become increasingly attractive especially since the Tesla 3 has been announced. The reason is its relatively low cost, good performances, and an increased autonomy. The low cost comes from an annual price drop of 14% of the fabrication costs of batteries for the industry between 2007 and 2014[4]. The decrease will continue, helped by the construction of the Tesla's Gigafactory, which will reduce the price even more, by doing economy of scale incorporating all steps of the battery production in one place. It will be fully operating in 2018 and will produce as much lithium-ions battery in one year as the entire world in 2013[5].

The most promising type of batteries are the lithium-ion batteries because of their higher power and energy density. These are also lighter and more compact [6] than other technologies. These do not suffer from memory effect like nickel-cadmium batteries do [7], and do not suffer from dendrites formation like lithium metal batteries do [Chapter 34 of [8]]. These can work at a higher potential because lithium has the lowest reduction potential of -3.04V. Also, lithium has one of the smallest radius of one single charged ion, which facilitates its diffusion inside the electrolyte and, therefore, the battery performance [9].
Some problems hinder the performances of batteries like the decomposition of the electrolyte above 4.2V versus Li/Li^+, which limit the working voltage of the cathode[10]. Also, the commonly used electrodes in lithium-ions batteries have a relatively low specific capacity. LiC_6 has 372 mAh/g and 320 mAh/g theoretically and experimentally respectively, and $LiCoO_2$ has 274 mAh/g and 140 mAh/g respectively[11].

Nanostructured electrodes are therefore of great interest to increase the specific capacity, the cycle life, and the specific power [10]. One of this nanostructure is the nanowires, which has been

made during this project.

Our first objective was to experiment if it is possible to have a mechanically stable 3D interconnected nanowire structure, on a substrate of silicon-silicon oxide, coated with titanium and platinium. 3D structures tend to be more stable than vertical nonconnected nanowires, but the adhesion of them with a substrate needs to be investigated. The structure is made of nickel-nickel oxide nanowires (See figure 1.1) which have been grown using cathodic electrodeposition method, followed by thermal annealing to make the shell. Nickel has been chosen because it is low cost, abundant[12] and it is a transition metal that offers a high theoretical specific capacity of 717 mAh/g thanks to a conversion mechanism with lithium [13]. This core-shell has the advantage of having its metallic core that offers a great electrical collector, and a higher surface area per unit of volume than 2D electrodes, which enhance the reactivity of the electrode with the electrolyte[12].

The second objective was to characterise the morphology of the nanowires by scanning electron microscopy, as well as the proportion of annealed metal during the annealing process using an alternating gradient magnetometer.

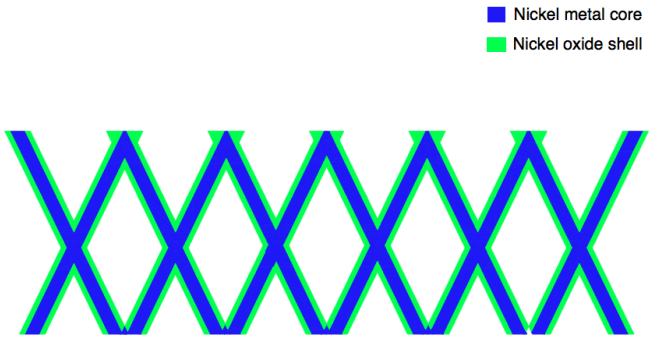

Figure 1.1: 3D interconnected Ni-NiO core-shell nanowires

The third objective was to experiment the possibility to make batteries out of electrodes containing silicon without reacting with it, leading the path to integrated storage energy directly on silicon-based chips[14]. Indeed, despite the fact that this material has an astonish specific capacity of 4200 mAh/g[15], it has the disadvantage of swelling up to 400% in volume during lithiation [16], leading to the rapid destruction of the electrode. The lithiation of silicon must, therefore, be avoided. To prevent that, the galvanostatic cycles of the batteries have been done between 0.3V and 3V, which is a potential window higher than the potential of lithiation of silicon[17].

The fourth objective was to build supercapacitors, made with the same electrodes used in the batteries, and to compare the results with an already existing research about transition metal oxides in supercapacitors[18][19].

Our final objective was to build interdigit electrodes, by etching parts of the initial electrode, using a picosecond laser, to create two electrically insulated electrodes on the same substrate. This configuration has the advantage of reducing the diffusion length path of ions between the adjacent electrodes, and hence, increasing the performance.

Chapter 2

Batteries

2.1 Definition

A battery is an electrochemical energy storage system. It's composed of several parts [20][Chapter 1 of [8]]:

- The anode which is the electrode where the oxidation takes place and where electrons are released into an external circuit during the discharge of the battery.
- The cathode that is the other electrode where the reduction reaction takes place and is the one that receives electrons from an external circuit when discharged.
- The electrolyte in a battery is a fluid, a gel or a solid which facilitates the passage of the ions from one electrode to the other during the charge and discharge but must not be electronically conductive[21]. It must also be non-reactive with the materials composing the battery.
- The separator that separates the anode electrically from the cathode. It is insulating at the passage of electrons but not to the electrolyte and therefore the ions. It permits thus to the electrons to pass through an external circuit leading to the conversion of chemical energy into electrical energy.

During this work, all the mention about anodes and cathodes will be made considering that the battery is in discharge mode. Indeed, for rechargeable batteries, anodes and cathodes are inverted between charge and discharge, but here the anode refers to the same electrode during discharge and charge process.

2.2 General Characteristics

A battery is characterised by several parameters that all have their importance in function of the type of battery an application needs[22] :

2.2.1 Voltage of a Cell

Let's take two half-cell reactions as followed which are respectively the reduction and the oxidation with their standard electromotive force[Chapter 2 of [8]] :

$$aA + ne^- \rightleftarrows cC \qquad \mathrm{E}^\circ_{\mathrm{Red}} \tag{2.1}$$

$$bB \rightleftarrows dD + ne^- \qquad \mathrm{E}^\circ_{\mathrm{Oxy}} \tag{2.2}$$

This leads to a complete cell reaction:

$$aA + bB \rightleftarrows cC + dD \qquad \mathrm{E}^\circ = \mathrm{E}^\circ_{\mathrm{Oxy}} + \mathrm{E}^\circ_{\mathrm{Red}} \tag{2.3}$$

The standard electromotive force E° of the cell is calculated by summing the oxidation potential occurring at the anode and the reduction potential occurring at the cathode.

$$E^\circ_{Red} + E^\circ_{Oxy} = E^\circ \tag{2.4}$$

The best standard electromotive force for a battery cell is therefore obtain using two redox couple which have the largest difference of standard electromotive force.

Then, using the Nernst equation, the temperature, concentration of materials and other sources of variation factors are taken into account and give the real potential of the cell at a certain condition.
The cell-potential will be described as follow :

$$E = E^\circ - \left(\frac{RT}{nF}\right) ln \left(\frac{a_C^c a_D^d}{a_A^a a_B^b}\right) \tag{2.5}$$

$$with \begin{cases} E & \text{The real potential of the cell} \\ E^\circ & \text{The standard electromotive force of the cell} \\ \mathrm{R} & \text{The gas constant} \\ \mathrm{T} & \text{The temperature in [K]} \\ \mathrm{n} & \text{Number of moles of exchanged electrons} \\ \mathrm{F} & \text{The Faraday's constant (96485 } [\frac{Coulombs}{mol}]) \\ a_X^x & \text{The activity of the specie X present in x number of moles} \end{cases}$$

2.2.2 Specific Capacity

The specific capacity of a cell depends on the materials composing its electrodes. First of all, one can calculate the theoretical specific capacity of each electrode. This is done using the Faraday's law that states[23] :

$$m = \frac{QM_w}{nF} \tag{2.6}$$

where we rearranged the terms into :

$$\frac{Q}{m} = \frac{nF}{M_w} \tag{2.7}$$

$$C^{elec}_{theo} = \frac{nF}{3.6M_w} \tag{2.8}$$

In order to obtain the specific capacity of the cell, one has to do the following operation[Chapter 1 of [8]] :

$$C_{cell} = \frac{C^{anode}_{theo} \times C^{cathode}_{theo}}{C^{anode}_{theo} + C^{cathode}_{theo}} \tag{2.9}$$

$$where \begin{cases} m & \text{Mass of active material} \\ C^{elec}_{theo} & \text{Theoretical specific capacity of an electrode } [\frac{mAh}{g}] \\ C_{cell} & \text{Theoretical specific capacity of the cell } [\frac{mAh}{g}] \\ C^{anode}_{theo} & \text{Theoretical specific capacity of the anode } [\frac{mAh}{g}] \\ C^{catohde}_{theo} & \text{Theoretical specific capacity of the catohde } [\frac{mAh}{g}] \\ n & \text{The number of exchange electrons per ion} \\ F & \text{The Faraday constant (96485 } [\frac{Coulombs}{mol}]) \\ M_w & \text{The molar mass of the active material } [\frac{g}{mol}] \end{cases}$$

2.2.3 The Specific Energy

The specific energy of a cell is the product of the theoretical potential of the cell times its theoretical specific capacity. It is expressed in Wh/g. This value will never be achieved in real life since the potential of a cell decreased in function of the state of charge since the concentration of the species will change and, as seen in the Nernst equation (2.5), this changes the potential of the cell. The potential will also never be decreased to zero since a minimum potential is needed for the devices it supplies. Also, the specific capacity of a cell is never achieved either since the entire material of the battery is never available to react because a part of it is electrically disconnected or is lost in the formation of the SEI[24]. Also, other materials like the current collectors or the separator do not take part in the reactions. These add mass and volume in the cell and reduce the specific energy.[Chapter 1 of [8]]

2.2.4 The Specific Power

The specific power is the amount of power per unit of mass a battery can deliver. It is expressed in W/kg. [Preface of [8]].

2.2.5 Depth of Discharge

The depth of discharge indicates the percentage or the amount of capacity which has been used from the cell. For example, for a 2000 [mAh] battery, if 1500 [mAh] has been used, the depth of discharge is 75% or 1500 [mAh][25].

2.2.6 Cycle Life

The cycle life is the number of times a battery can be totally discharged and charged before losing some capacity and only be able to deliver 80% of the first capacity[26]. The cycle life is optimum at a certain temperature and decreased when deviating from it. Also, partial discharges and charges can enhance the life cycle of a battery. A low current delivery from the battery also helps to extend the cycle life[27].

2.2.7 Memory Effect

The memory effect is the trend of a battery to remember how it was used in previous cycles and to adapt its electrical properties to these cycles. For example, when trying to increase the depth of charge of such a battery, it appears impossible to recover the total specific capacity[Chapter 26 of [8]].

2.2.8 Self-Discharge

Recoverable loss of capacity of a cell over time. It is expressed in % of the rated capacity per month and is strongly influenced by the temperature and the used technology[28].

2.2.9 Solid-Electrolyte Interphase

Solid-electrolyte interphase or SEI is an important phenomenon to explore since it is responsible for many characteristics of a battery like the cyclability, the rate capability, the battery performance, the irreversible charge loss,..[29]. The formation of a SEI occurs principally during the first cycle. It is a consequence of the irreversible reduction of the electrolyte because of their instability at the negative anode's potential during charging[24]. Therefore, the products deposits on the negative anode of Li-ion batteries forming a passive layer composed of organic and inorganic electrolyte decomposition products as well as lithium which is consumed. This layer will then protect further degradation of the electrolyte by blocking the electron transport from the electrolyte to the anode

while letting the ions pass (See Figure 2.1). After that, the cycles are done reversibly. Without this behavior, the SEI would thicken at every cycle, and the battery performance would drop very rapidly. The average thickness of a SEI can vary between few Å to a hundred of Å.[Chapter 34 of [8]][29]

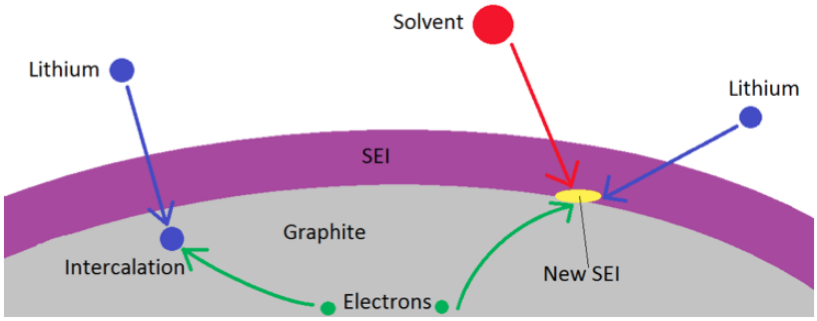

Figure 2.1: SEI formation and lithium ion conduction path through it for lithium ion batteries.[24]

2.2.10 HOMO-LUMO Levels

For the cell to be stable, the electrochemical potential of the anode, μ_a must be lower in energy than the LUMO[1] level of the electrolyte to prevent this last to be reduced. Conversely, the electrochemical potential of the cathode, μ_b, must be higher than that of the HOMO[2] level of the electrolyte to prevent this last to be oxidised (See Figure 2.2). The HOMO-LUMO levels of the electrolytes represent its gap.[6]

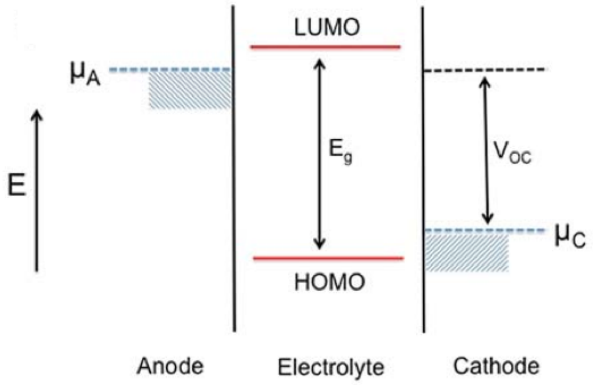

Figure 2.2: Relative energy diagram for lithium-ions anode and cathode potential and electrolyte energy gap.[6]

2.3 Type of Batteries

Hereafter are the mention of the two first primary batteries that are the base of what is now known on the subject. Afterward, a presentation of several major secondary batteries will be done to finish with the major battery of interest which is the lithium-ion battery. All the direct chemical reactions presented during this section are discharged reactions and are reversible. The opposite reactions are therefore the reactions occurring during the charging process.

[1]LUMO stands for lowest unoccupied molecular orbital
[2]HOMO stands for highest occupied molecular orbital

2.3.1 Primary Batteries

Primary batteries are also called non-rechargeable batteries. When these batteries are being discharged, the chemical energy stored inside is irreversibly converted into electrical energy. Their specific energy capacity is higher that of secondary batteries but only at low current and intermittent load[30]. Indeed, when these are used under a discharged rate of 1C as commonly for secondary batteries, their specific capacity drop dramatically[31].

2.3.1.1 Voltaic Pile

The first battery ever made was the voltaic pile invented by an Italian physicist Alessandro Volta in 1799 and was composed of the stacking of copper and zinc disk separated by a brine-soaked paper as an electrolyte.

2.3.1.2 Daniell Cell

In 1836, John Frederick Daniell created a new cell that resolved the problem of hydrogen production from the voltaic cell. It was composed of two contained separated by a porous membrane. The first container containing a zinc electrode immersed in zinc sulfate which acted as the anode and the second container contained a copper electrode immersed in copper(2)sulphate which served as the cathode[32].

2.3.2 Secondary Batteries

Secondary batteries, also called rechargeable batteries, make the use of "two electrochemically reversible cathodic and anodic reactions in one electrolyte"[33]. These have a lower specific capacity than primary batteries but are more efficient at a higher load than these lasts. These also have a flatter discharge potential curve and higher performance at low temperature. [Chapter 1 of [8]]

2.3.2.1 Lead-Acid Batteries

Twenty-three years later in 1859, the first rechargeable or secondary battery was created by the French physicist Gaston Planté. It is the lead-acid battery that is composed of lead dioxide for the cathode, metallic lead for the anode and sulphuric acid diluted in water for the electrolyte[Chapter 23 of [8]]. Some impurities are nowadays added to improve electrical properties. An example is antimony that enhances the deep cycling but increases the water consumption, because of the production of hydrogen and oxygen. Therefore, it increases the need to do a regular overcharge called an equalising which consist of raising the potential of the battery to 2.5 [V/cell] to remove sulfate crystals that appear with time on the electrodes[34]. Another example is calcium which has the effect of reducing the self-discharge but leads to the growth of the lead-calcium electrode due to the oxidation occurring during an overcharge. Other elements like selenium, cadmium or Arsenic can also be added. The following equation describes the chemical reaction taking place in a lead battery acid during discharge. During charge, the equation are inverted:
At the anode:

$$Pb \rightleftarrows Pb^{2+} + 2e^- \tag{2.10}$$

$$Pb^{2+} + SO_4^{2-} \rightleftarrows PbSO_4 \tag{2.11}$$

At the cathode:

$$PbO_2 + 4H^+ + 2e^- \rightleftarrows Pb^{2+} + 2H_2O \tag{2.12}$$

$$Pb^{2+} + SO_4^{2-} \rightleftarrows PbSO_4 \tag{2.13}$$

The overall reaction is, therefore:

$$Pb + PbO_2 + 2H_2SO_4 \rightleftarrows 2PbSO_4 + 2H_20 \tag{2.14}$$

Such batteries do not support deep cycles well because of the strain, which will reduce the capacity at each cycle. Also, when stored, these batteries must be fully charged to prevent the sulfation which reduces the capacity. The typical life span of lead-acid batteries is about 250 cycles. This kind of battery is still used today because of its low cost, and it is capable of delivering high current making it a particularly interesting choice for car starters for example. Also, it does not present memory effects, and their charge retention is by the best among rechargeable batteries[35].

2.3.2.2 Nickel Cadmium Batteries

Nickel Cadmium batteries are alkaline secondary batteries and were discovered in 1899 by the Swedish engineer Waldemar Jungner.
The positive electrode is composed of nickel oxyhydroxide, the negative electrode of cadmium and the electrolyte is alkaline. The first batteries were vented cells consisting of pocket-plate. The pocket plate type cells were very rugged. After a while, these pocket plates were changed by sintered-plates enhancing the energy density, the performance at high discharge rate and the performance at low temperature[Chapter 27 of [8]]. The real industrial application of sealed cells began in 1947 when a problem concerning generated gases during charge has been fixed by using an oxygen recombination feature[36][Chapter 27 of [8]]. Nickel-cadmium batteries have the advantages of having a long life cycle, a relatively stable potential of 1.2 [V/cell] throughout the whole discharge cycle and the capability of being charged very fast and delivers high current because of their low internal resistance[37]. The disadvantages are its high self-discharge rate, its relatively low capacity in comparison with other technologies or the memory effect that can, however, be reduced by doing periodic full discharges. The memory effect happens because of the formation of crystals on the electrodes. Another disadvantage is the fact that cadmium is toxic and this leads to the interdiction of them for most applications. It also needs a lot of maintenance[7]. The half-cell chemical equations characterising the discharge of a nickel-cadmium are the following:
The first describe the oxidation occurring at the anode converting cadmium to cadmium hydroxide and two electrons

$$Cd + 2OH^- \rightleftarrows Cd(OH)_2 + 2e^- \tag{2.15}$$

The second equation describes the reduction of nickel oxyhydroxide of the cathode into nickel hydroxide and the acceptance of an electron

$$2NiO_2H + 2H_2O + e^- \rightleftarrows 2OH^- + 2Ni(OH)_2 \tag{2.16}$$

The overall reaction is, therefore:

$$2NiO_2H + Cd + 2H_20 \rightleftarrows Cd(OH)_2 + 2Ni(OH)_2 \tag{2.17}$$

2.3.2.3 Nickel-Metal Hybrid

The beginning of the research for such cells started in 1967 but was rapidly slowed by the instabilities linked to the metal-hybrids. It is only in the year 1980s, after the discovery made in hybrid alloys, that the NiMH battery became a major player in the battery market[36]. It has the advantages that it does not contain any trace of cadmium and in thus consider as more environmentally friendly. It possesses a metal alloy as the anode that can desorb and adsorb hydrogen during discharge and charge, and a nickel oxyhydroxide cathode like the nickel-cadmium battery. The electrolyte is composed of an aqueous solution of potassium hydroxide. It possesses

a higher specific capacity and a longer service life but a lower specific power and a higher price. During the discharge, the nickel oxyhydroxide is reduced to nickel hydroxide, and the metal hybrid MH is oxidised to the metal alloy M. These two reactions can be respectively written as follows:

$$NiO_2H + H_2O + e^- \rightleftarrows Ni(OH)_2 + OH^- \tag{2.18}$$

$$MH + OH^- \rightleftarrows H_20 + e^- \tag{2.19}$$

The overall discharge reaction can, therefore, be written as:

$$MH + NiO_2H^- \rightleftarrows Ni(OH)_2 + M \tag{2.20}$$

Attention has to be paid during the charging process. Indeed, the hydroxide ion is converted into water and oxygen. To avoid a pressure building, the anode is designed to have a higher specific capacity than the cathode leading to the migration of the oxygen through the separator when the cathode is fully charged. There, the oxygen will oxidise the anode and produce water and pure metal[Chapter 29 of [8]].

2.4 Lithium Batteries

2.4.1 Lithium Metal

Lithium metal batteries are based on the use of a lithium metal anode. It is a quiet logical choice since lithium is the material with one of the highest specific capacity, 3860 mAh/g, that exists[10]. With its 0.59 g/cm^3, it is also light, and it possesses one of the lowest electrochemical potentials of -3.04 V compared to the standard hydrogen electrode[38] leading it to be one of the strongest metal reducing agent[39]. By coupling it with low standard reduction potential species or, in other words, to a material having a high electrochemical potential, a high cell potential cell can be obtained, leading to a higher energy density.

Several security problems have however prevented rechargeable lithium metal batteries to be successfully commercialised and lead to the change of orientation of the research toward lithium-ions batteries. These problems come from the high reactivity of lithium with the electrolyte. Indeed, during the charge, the lithium is not equally electrodeposited on the anode. Therefore, a mossy deposition occurs and the formation of sharp lithium peaks called dendrites can happen. These dendrites are a real problem because these can create a short circuit by perforating the separator and have a bigger surface area than the plane lithium of the anode at the origin. Therefore, the reactivity of the lithium is enhanced, and a runaway of the processes can lead to too much thermal energy production and hence the destruction of the cell.
Another point is that lithium is not thermodynamically stable in the electrolyte. That means that there will be the creation of a passivation film or SEI at the surface of the anode. This film is composed of lithium that reacted with the electrolyte. The problem is not the creation of the SEI, but it is the continuous renewal of it. Indeed, during each cycle, the lithium will go from the anode to the cathode and back to the anode. During this cycle, new lithium metal that did not participate in the previous reaction is exposed to the electrolyte, and a new SEI is formed. The lithium is thus consumed at each cycle. To improve the cycle life of such batteries, the amount of lithium is more than three to five times higher than it should be[Chapter 34 of [8]].

This kind of batteries are the batteries made during this thesis. The purpose of choosing lithium metal instead of lithium-ion is to test the electrodes VS the lithium metal anode which has a way bigger specific capacity than the theoretical specific capacity of the made cathode. Therefore, the limiting factor of the battery is the cathode made of core-shell nickel-nickel oxide

nanowires and measurements can be done only on this cathode when measure are made on the cell. These are also called half-cell.

Breakthrough
An MIT spinout called SolidEnergy recently made a lithium metal battery that can be made with already existing battery equipment of lithium ions factories. This new battery is claimed to be safer than conventional lithium batteries and contains twice as much capacity. It has been done by "coating the lithium metal foil with a thin solid electrolyte that doesn't need to be heated to function"[40] not like the previous used solid polymers. Another electrolyte is also employed in the cell. It is a quasi-ionic liquid electrolyte that is not flammable. The separator received some chemical modifications and the cell designed has also been modified to stop the liquid electrolyte to react with the lithium metal negatively[40].

2.4.2 Lithium-ion Batteries

The use of carbon for the anode, of commercially used lithium-ion batteries, is the big difference between lithium metal and lithium-ion cells. Indeed, in the second case, there is no more lithium metal since the lithium atoms are always incorporated into another material composing the anode or into the structure of the cathode material. The change permits to obtain a more secure cell without changing a lot the potential of the anode compared to the cathode. Indeed, it has been measured that the potential of carbon-lithium versus lithium is nearly zero and leads therefore to nearly the same open circuit cell potential. In the beginning, several carbon compounds have been used like coke offering a specific capacity of 180 mAh/g which are stable in the presence of propylene carbonate based electrolytes. Carbon based anodes materials use the intercalation principle to store lithium. This ability to store lithium is highly dependent on their morphology and structure. Graphite is largely used nowadays because of its even higher specific capacity of 372 mAh/g for the LiC_6 and its flatter voltage discharge curve than coke.
The first lithium-ion battery cathode was made of $LiCo0_2$ which is a cubic packed array of oxide ions with Co (III) and lithium ions occupying octahedral voids in alternate sheets. It has a specific capacity of 140 mAh/g and a potential of 3.9 V against lithium. Other compounds are nowaydays used like $LiCo_{1-x}Ni_xO_2$, with x included between 0.1 and 0.3 which has a lower price than $LiCoO_2$ and higher structural stability or $LiNi_{1/3}Mn_{1/3}Co_{1/3}O_2$ which has a higher specific capacity of 200 mAh/g.
In such cells, the lithium ions shuttle back and forth between the electrodes during the discharge-charge cycle (See Figure2.3)
The anode, cathode and overall reactions for typical lithium ion batteries during discharge can be written respectively as follows:

$$Li_xC \rightleftarrows C + xLi^+ + xe^- \tag{2.21}$$

$$Li_{1-x}CoO_2 + xLi^+ + xe^- \rightleftarrows LiCoO_2 \tag{2.22}$$

$$Li_{1-x}CoO_2 + Li_xC \rightleftarrows LiCoO_2 + C \tag{2.23}$$

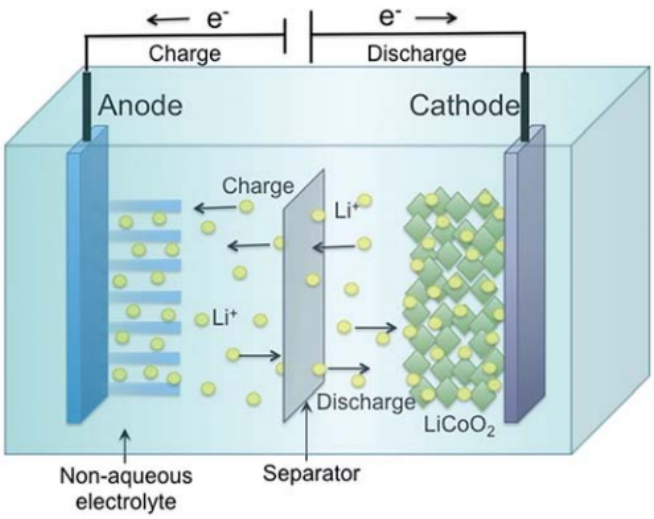

Figure 2.3: Charge-discharge scheme of a lithium-ion battery[6]

2.4.2.1 Electrodes

Three major kind of electrodes exists (See figure 2.4), the intercalation the alloying and the conversion electrodes for lithium batteries[41].

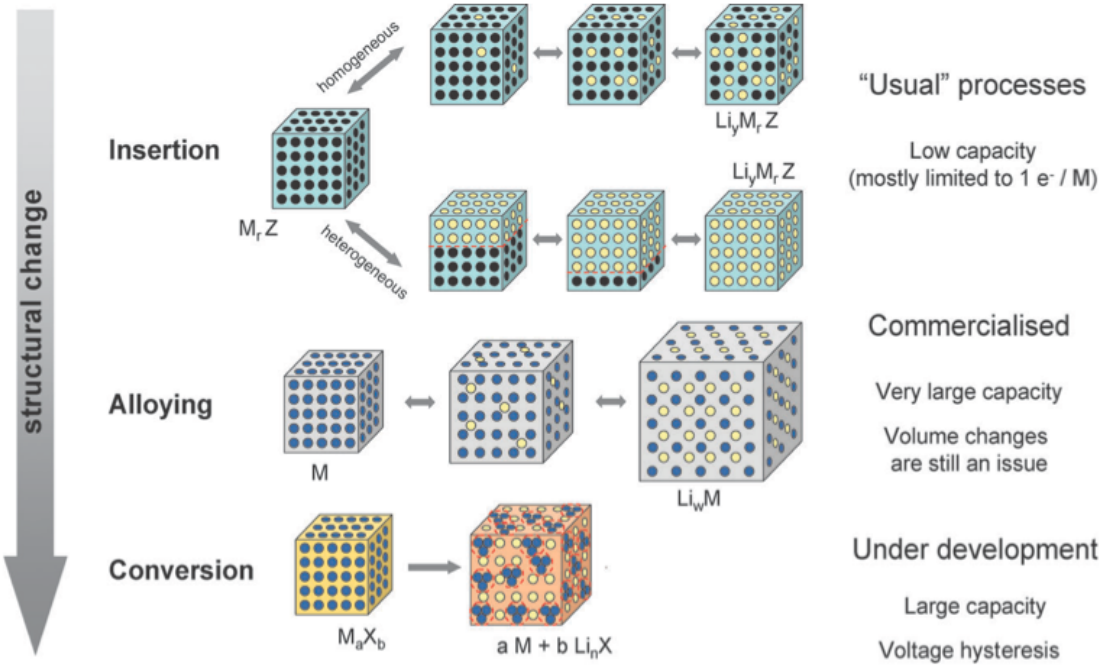

Figure 2.4: Different kind of reaction mechanisms in lithium electrode materials. Black circle: voids; Blue circles: metal; Yellow circles: lithium.[41]

1) Insertion or intercalation

In these materials, the redox process that occurs involves a topotactic[3] reversible intercalation of the lithium ions in low-energy interstitial sites in the structure of the electrode's material[42]. The ability to store lithium inside the material depend on its diffusivity inside it. This diffusivity depends on nature and the form of the host material. The main examples of intercalation compound are LiC_6 as an anode and $LiCoO_2$ as a cathode[6].

2) Alloying

Alloying processes are based on the creation of an alloy of lithium with the compound composing the electrode. These have the big advantage to possess very high specific capacity as high as 4200 mAh/g for silicon forming $Li_{22}Si_5$ [10], but the significant disadvantage is that the compound undergoes a very large volume expansion during lithiation. This volume expansion leads to accelerated degradation of the performance of the electrode. More detailed information about alloying mechanism are covered in section 2.4.3 that threat about the issue of silicon and the different solution based on nanotechnologies to get over them.

3) Conversion:

Conversion reactions are the last that have been discovered among the three mentioned reactions. It has only been confirmed in 2000 by Poizot et al. that reversible conversion reactions are possible at ambient temperature. Conversion reactions are often based on the use of binary transition metal compounds M_aX_b (M: the transition metal, X compounds like O, P, S, N, F,..). During the conversion reaction, there is a full reduction of a transition metal to its metal state by transferring more than two electrons. This is because of their variable valence states that facilitates more electron-storing sites[43], enabling very high specific capacity between 650 mAh/g and 1500 mAh/g. The discharge reaction can be written as follows[16]:

$$MX_a + bLi^+ + be^- \rightleftarrows M + bLiX_{b/a} \tag{2.24}$$

$$with \quad \begin{cases} \text{a=b} & \text{X=F} \\ \text{a=b/2} & \text{X=O} \\ \text{a=b/3} & \text{X=N, P} \end{cases}$$

As seen on figure 2.5, the first discharge or lithiation process leads to the formation of a composite of metal nanoparticles (1-5 nm) included in a Li_2O matrix[44].
During the first charge or delithiation process, the metal nanoparticles are oxidised by electron transfer through the LiO_2 matrix, which can be kinetically limited by the solid-solid reaction between the metal nanoparticles and the LiO_2. This is the cause of the large hysteresis in voltage plateau[4]. Finally, the formed products are nanoparticles of metal oxide that do not have the same crystalline structure as the initial one. This can be referred as an electrochemical pulverization process[13]. These electrodes present a high specific capacity but present a relatively large expansion during lithiation even if it is smaller than for alloying electrodes[10]

[3]Structural change to a crystalline solid with the final and original lattices related to each other by one or more crystallographic equivalent

[4]difference between the voltage for the same state of charge during lithiation and delithiation

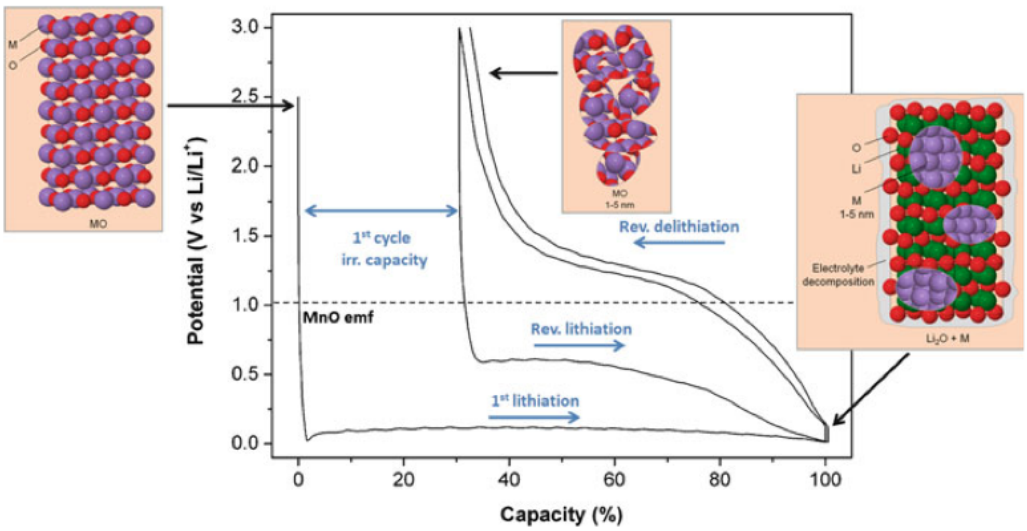

Figure 2.5: Typical voltage profile of a lithium metal battery with metal oxide as cathode for the two first cycles[16]

2.4.2.2 Nanostructured Electrode

Nanostructured materials are a promising way of improving electrodes materials in general. The use of nanoparticles improve the ability to store lithium but at the cost of life cycle because of large volume expansion leading to cracks. Also, the grain boundaries and voids decrease the battery performance. Also, the miniaturisation leads to a higher surface to volume ratio leading to more reactivity and therefore to more side reactions involving the formation of the SEI. The electrical and lithium transport is also weakened by the random path the structure offers for their movement.
One dimension nanostructures like nanotubes or nanowires are therefore promising due to their directional electronic and ionic transport permitting a high electron collection efficiency. The mechanical structure is also more stable as this will be seen during this thesis.
Other structure like core-shell nanostructure, like the one made during this master thesis or heterogeneous nanostructures like MnO nanoflakes grown on nickel foam, are interesting because of their high specific capacity of about 700 mAh/g.

Different materials like carbon-based materials, metal oxide, silicon, metal alloys and many others look very promising for the future of batteries.

2.4.2.3 Electrolyte

A good electrolyte for lithium ion batteries need to fill several characteristics[Chapter 34 of [8]]:

- It must have a good ionic conductivity, typically higher than 10^{-3} S/cm, at a temperature of -40°C to 90°C to obtain a battery with a minimal internal resistance
- A transference number of lithium ion closed to one. The transference number describes the ability of the electrolyte to permits the diffusion of ions inside it. A close to one number describes a medium where no or little ion concentration gradient. Indeed, at high rates, such gradient can cause the failure of the battery[45].
- A wide electrochemical voltage windows, typically between 0 and 5 V. The electrochemical window is the range of potential between which the compound is neither oxidised neither reduced and thus inert[46].

- An excellent thermal stability to be used in different conditions
- Compatibility with the other materials employed in the cell

Here are shown the most common electrolytes used in the lithium-ion industry as well as new kind of electrolytes that could enhance batteries performance:

- **Aprotic organic electrolyte**: These are the most commonly used electrolyte in conventional lithium-ion batteries. Such electrolytes possess a high ionic conductivity greater than 10^{-3} S/cm[41]. These are composed of a solution of lithium salt, typically $LiPF_6$ and are always mixed with two to four aprotic organic carbonate solvents which possess a high dielectric content enables them to dissolve much lithium. Some examples of used solvents are dioxolane, propylene carbonate, ethylene carbonate or EC, diethyl carbonate or DEC and ethyl methyl carbonate which are the most common among them. EC is always present since it is essential for the reversibility of the chemical reaction at the anode because it decomposes to form a SEI at 0.8V preventing other solvents molecules to co-intercalating with lithium in the graphite anode.
- **Polymer electrolyte**: These exist in two different forms[Chapter 34 of [8]]:
  - **A solid polymer electrolyte** where lithium salts are included in matrices of polymers and then cast in thin films. These electrolytes can also be used as separators between the cathode and the anode. Advantages of such electrolytes are the elimination of the dendrites problem, enhanced safety because of the absence of organic electrolytes, a good processability and good flexibility [41]. A disadvantage of such polymers is their low ionic conductivity of about 10^{-8} S/cm for polyethylene oxide and lithium salts like $LiClO_4$ and $LiN(CF_3SO_2)_2$. The value of ionic conductivity of about 10^{-5} S/cm has then been achieved using comb-shaped polyethylene oxide with lithium salts[Chapter 34 of [8]]. These solid polymers must be heated to work properly[40].
  - **A gel polymer electrolyte** is composed of the same polymer matrix, but the difference is that liquid electrolyte is injected in that matrix followed by an immobilisation procedure like crosslinking or casting. Such electrolyte has as advantages a higher ionic conductivity of 10^{-3} S/cm, the ability to take any wanted form, faster charging/discharging rates and a higher power density.[47]
- Other electrolytes such as **solid-state electrolytes** such as lithium phosphorus oxynitride or **inorganic electrolyte** like SO_2-based $LiAlCl_4$.

2.4.3 Lithiation of Silicon

For this thesis, all the tested electrodes were composed of a silicon substrate. It will be seen later that the potentials used during the galvanostatic charge and discharge prevent the silicon to react with lithium. However, it is interesting to discover how this material is performing when it is lithiated by conversion because silicon presents the highest theoretical specific capacity: 4200 mAh/g. This element is the second most abundant on earth and has a working potential of 0.5 V against lithium. Thus, it has a great potential as anode material. This incredible high specific capacity is more than ten times the value discussed for the LiC_6 of 372 mAh/g. Taking all these advantages into account, it is not surprising that many research are carried out on silicon[48].

However, a major drawback hinders silicon batteries on the market: The expansion during lithiation. This expansion is of about 300-400% for Li_xSi, with x between 3.5 to 4.2[16], in comparison to about 12% for LiC_6[49]. This huge expansion leads to three consequences[50] presented in Figure 2.6:

1. The pulverisation of a part of the silicon leading to losses in electrical contacts between the electrolyte, the current collector and the active material leading to a rapid fade in capacity.

2. High compressive stress inside the active material slows down further lithiation. In severe cases, the lithiation can be stopped, and the core of the active material becomes inaccessible to the electrolyte and reduce the specific capacity.

3. The SEI breaks during every delithiation leading to the exposure of new silicon to the electrolyte that will react with the electrolyte resulting in the formation of a new SEI. Therefore, the growth of the SEI is unstable and continue at each cycle, consuming lithium and reducing the ionic conductivity between the electrolyte and the silicon.

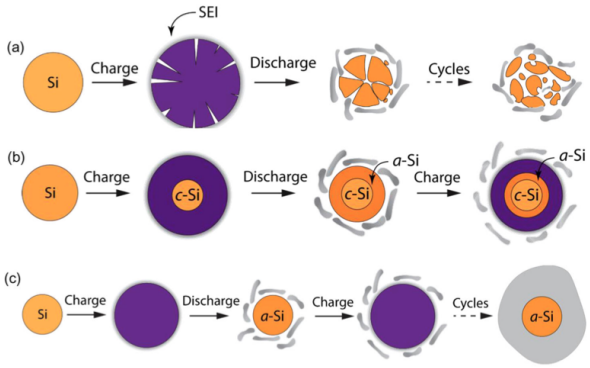

Figure 2.6: Degradation mechanisms of silicon during lithiation-delithiation cycles[51]

One of the solutions to improve mechanical stability and therefore the life cycle of a silicon anode is to reduce the size of the active particles. It has been shown that at the micrometer scale, even if there is a little improvement in performance, there is still a fast fading of the capacity and short cycle life due to the pulverisation of silicon[17]. It has been shown that thinner silicon film, 1 μm and 250 nm, show a capacity close to the theoretical one, but still show a fast degradation of the capacity after about 15 and 30 cycles respectively.
Therefore, other configurations have been tried. One of them is the coating of the silicon on a nickel substrate. Before the coating, the nickel exhibits a passivating layer of nickel oxide that creates strong bonds with silicon after the coating because of the strong affinity of silicon for oxygen. This configuration showed a good specific capacity of 1700-2200 mAh/g after 750 cycles at 2C. Other ways to improve the performances are the inclusion of Si micro/nanoscale nanopowder into an active/inactive matrix or binding silicon with binders[48]. There is also the use of silicon thin films composed of nanocrystalline particles of 12 nm in diameter, or thin films of continuous amorphous silicon, of 100 nm. These provide a specific capacity of 1100 mAh/g and 3500 mAh/g respectively at the first cycle and 550 mAh/g and 2000 mAh/g at the 50th cycle[52].

Two other solutions are based on the use of nanowires.
The first is the use of silicon nanowires directly grown on a metallic substrate, which acts as a current collector (See Figure 2.7). This configuration permits to the silicon nanowires to not fractured themselves because of the easy strain relaxing in the nanowires. All nanowires participate to the capacity, since every nanowire is electrically connected to the substrate, and the charge transport to the substrate is a 1D electronic pathway leading it to be efficient.

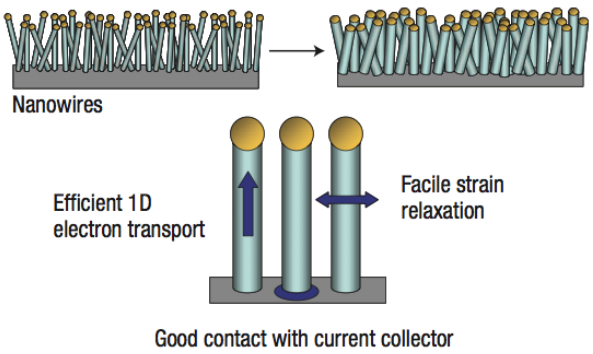

Figure 2.7: Schematic of the aspect of the nanowires during electrochemical cycling.

The second, which correspond the most to the nickel-nickel oxide core-shell nanowires done is this thesis is the use of silicon core-shell nanowires. The core is composed of a crystalline silicon core acting as a mechanical support and an electrical conductor, and the shell consists of amorphous silicon and is the electrochemically active material. This choice has been motivated since it has been discovered that amorphous silicon better resists to the pulverisation occurring during cycling[48].

Chapter 3

Supercapacitor

Supercapacitors are, like batteries, energy storage systems. These are electrochemical capacitors based on the use of an electrolyte instead of a dielectric and possess a very high capacitance. Other characteristics are a very long lifetime up to 10^5 cycles[53], a lower energy capacity than batteries but a higher specific density that can reach 10 kW/kg. These are thus very suitable for high power applications like hybrid electrical vehicles, power back-up in portable electronics or load-levelling. The energy density (E) of supercapacitors depends on the voltage (V) and the capacitance (C) of the electrode and can be written as:

$$E = \frac{CV^2}{2} \tag{3.1}$$

These are formed of two electrodes, an electrolyte, and a separator to disconnect the two electrodes electrically. Three different kinds of supercapacitors can be distinguished in function of the material and the energy storage method[54]: The electrical double-layer capacitor, the pseudocapacitor, and the hybrid capacitor.

3.1 Electrical Double-Layer Capacitors

The electrical double-layer capacitors or EDLC store energy electrostatically or in a non-faradaic way[1]. This non-faradaic mechanism permits to this type of supercapacitor to have a high power density, to be very stable and to have a long cycle life. Therefore, materials with large surface area are used as activated carbon, which is the most used material in ELDC because of its very high surface area and its low cost, carbon nanofibers, mesoporous carbon, carbon nanotubes, graphene, and carbide-derived carbon[56]. The advantages of carbon-based materials are their lower price, better-established fabrication techniques and generally a larger surface area than conducting polymer or metal oxides.
During the charge, a voltage is applied, and the negative ions diffuse to the positive electrode and the positive ions diffuse to the negative electrode. When the ions arrive at the electrodes, these formed an electrical double layer at the interface between the electrode and the electrolyte because the electrodes have been made to avoid recombination of the ions with the electrode[57]. During the discharge, the ions go back to the electrolyte, and the electrical double layer decomposes (See Figure 3.1). In these capacitors, at most the surface area of the electrodes is high, at most the capacitance of the supercapacitor will be because the energy stored depend on the amount of possible ion adsorption. Also, a decrease in the distance between the electrode will increase the capacity.

The electrolyte is also critical to improving the efficiency of such capacitors. In the case of electrical double-layer capacitors, aqueous electrolytes, like H_2SO_4 or KOH, or organic

[1] A non-faradaic mechanism accumulates the charge electrostatically with the positive and negative charge on each electrode respectively and with no transfer of charge between the electrolyte and the electrode[55][53].

electrolytes, like acetonitrile are used. The aqueous electrolyte has a low viscosity and has, therefore, a high mobility and can, therefore, work with low pore size electrodes. It is however not able to operate at a voltage greater than that of the electrolysis of water at a potential of -1.23 V compared to the standard hydrogen electrode[58]. The organic electrolyte permit to reach a potential of about 2.5 V, at the cost of a lower specific power due to their higher viscosity and electrical conductivity, but have a higher specific capacity due to the square dependence on the potential.[53].

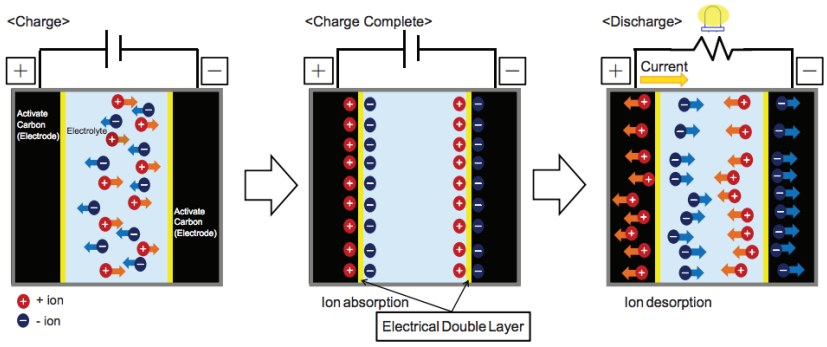

Figure 3.1: Typical three-step process during the use of an EDLC supercapacitor.

3.2 Pseudocapacitors

Pseudocapacitors store energy faradaically[2] thanks to "fast and reversible redox reactions between the electrolyte and electro-active species on the electrode surface"[59]. This storage can be done by adsorption of the ions from the electrolyte, reduction-oxidation reactions that involve ions from the electrolyte, and intercalation processes by doping or undoping conductive polymers which are less dependent on the surface but are based on micropores where ions can go into[53]. It permits to this kind of supercapacitors to achieve higher capacitance than EDLC[57] but still lower than batteries. However, their specific power and cycle life are lower than ELDC[53]. Two kinds of electrodes materials can be used:

- **Conductive Polymers**: Conductive polymers like polyaniline, polypyrrole, and poly[3,4-ethylenedioxythiophene][54] have a relatively high capacitance, conductivity, and a low equivalent series resistance or ESR compared to the carbon-based materials used in EDLC. However, it has been discovered that mechanical stress occurring during the reduction-oxidation process limit the stability and make them not suitable for long cycle life.
- **Metal Oxides**: Metal oxide like manganese oxide, nickel oxide, vanadium oxide, titanium oxide TiO2 and mostly ruthenium oxide[54] have been widely used for pseudocapacitors because of their high conductivity.

3.3 Hybrid Capacitors

Hybrid supercapacitors use the principle of both faradaic and non-faradaic mechanism to store charges. This lead to supercapacitors having a cycle life close to that of EDLC and specific capacity close to that of pseudocapacitors. To make such capacitors, three different electrodes configurations have been investigated: The composite, the asymmetric and the battery-type.

[2]In faradaic process, the charge storage is done by transferring electrons across the double layer leading to a change in the oxidation or chemical state of the electrode surface[55]

- **The Composite**: In this configuration, each electrode contains both two different materials. One that will store charges by faradaic mechanism and the other that will do it without the faradaic mechanism. These are composed of carbon-based materials with conducting polymer or metal oxide materials. The first has a high surface area and provide a good capacitive double layer. It also provides a structure having a good surface area for the second material that will do the Faradaic mechanism. Good results have been obtained using electrodes composed of carbon nanotubes and polypyrrole[57].

- **The Asymmetric**: Such capacitors use an EDLC anode and a pseudocapacitor cathode. An example that has been well studied is the couple activated carbon for the anode and conducting polymer for the cathode. These types of supercapacitors have higher specific energy and power than comparable EDLCs and higher cycling cyclability than comparable pseudocapacitors[57].

- **The Battery-Type**: This configuration combines the higher specific capacity from a battery electrode for the anode and the higher specific power of a supercapacitor electrode for the cathode the whole immersed in an organic electrolyte containing lithium salts[60]. Some researches have been conducted and lead to the use of a $LiNi_{0.5}Mn_{1.5}O_4$ cathode with an active carbon anode using a 1.0 M $LiPF_6$ ethylene carbonate/dimethyl carbonate (1:2 in volume solution) electrolyte. These battery-type supercapacitors showed an 80% capacity retention after 1000 cycles[61].

3.4 Comparison Batteries VS Supercapacitors

As seen in the two previous sections concerning batteries and supercapacitors, there are two different kinds of energy storage systems. In this small section, a comparison is made to highlight the difference and the similitudes between the two. The figure 3.2 shows the range of specific energy and specific power achievable with the different devices.

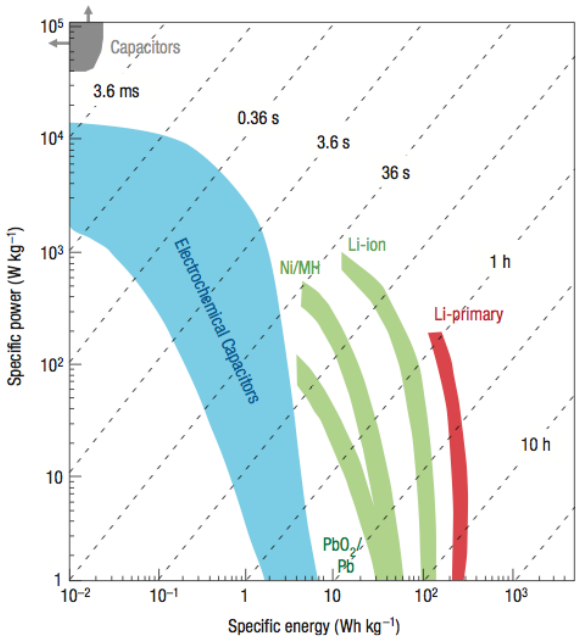

Figure 3.2: Specific power against specific energy or Ragone plot for batteries, supercapacitors, and capacitors. The time constant represents the total discharge duration at maximum power density.[62]

Both batteries and pseudocapacitors are based on faradaic processes. However, in the case to the pseudocapacitors, the reactions only take place on the surface of the active material leading them to be faster. Therefore, there is no limitation due to diffusion of species resulting in a more rapid reaction but also to a lower capacity.

3.5 Interdigit Electrodes

This kind of electrodes has begun to be studied in the early 1970s. These can be used for many applications going from optical and surface acoustic wave devices to thin-film acoustic-electronic transducers and tunable devices, humidity and chemical sensors[63] or even on-chip energy storage integrated thin-film amorphous silicon solar cells[14]. Most of them are made of an inert substrate on which two electrodes are deposited. The pattern can also be done by cutting the surface with a conventional DVD laser[64], CO_2 laser[65], printing the pattern with aerosols jet printing or by using lift-off techniques[66].

The performances of an interdigit electrode highly depend on its structure. The most simple structure is the linear one. There are also more sophisticated structures like fractals[65] which is a mathematical object having an invariant structure by the change of scale. All these structures have a different surface to volume ratio (SA:V) and a different ionic path as shown on figures 3.3 and 3.4. One can observe that large differences are present between several fractals structure and, that these last have an SA:V far greater than the traditional simplest planar structure. The decrease of the total ionic path is crucial because it means that the distance for the ion to travel from the electrolyte to the electrode is shorter, meaning that the ions will arrive faster on the electrode-electrolyte interface, and therefore increase the performances[65].

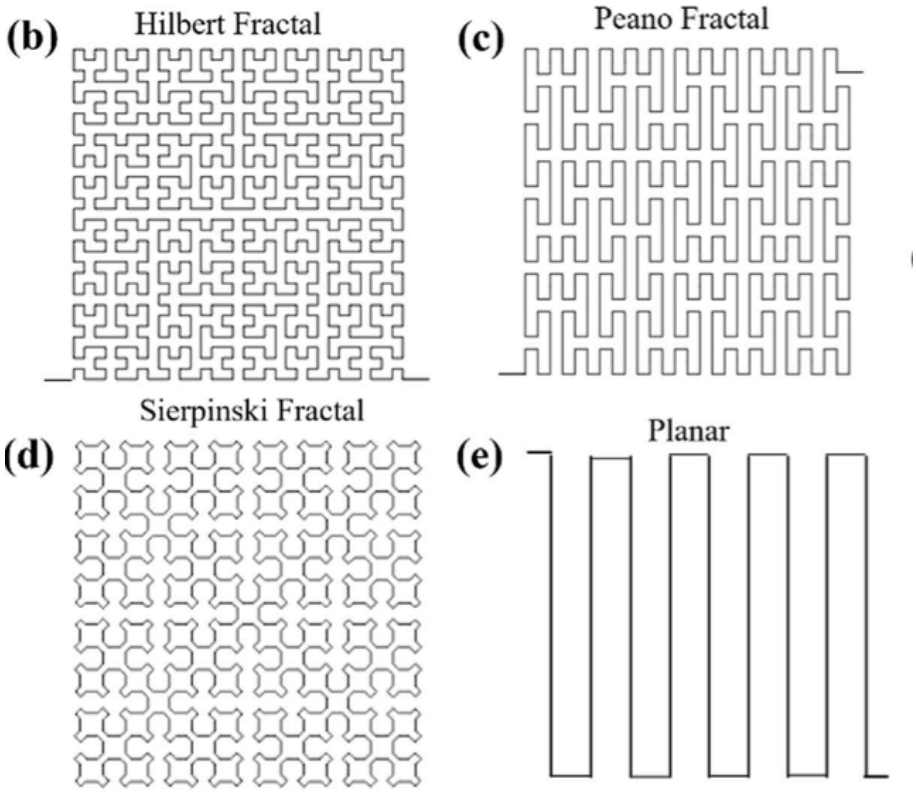

Figure 3.3: Representation of three fractals structure for electrodes pattern[65]

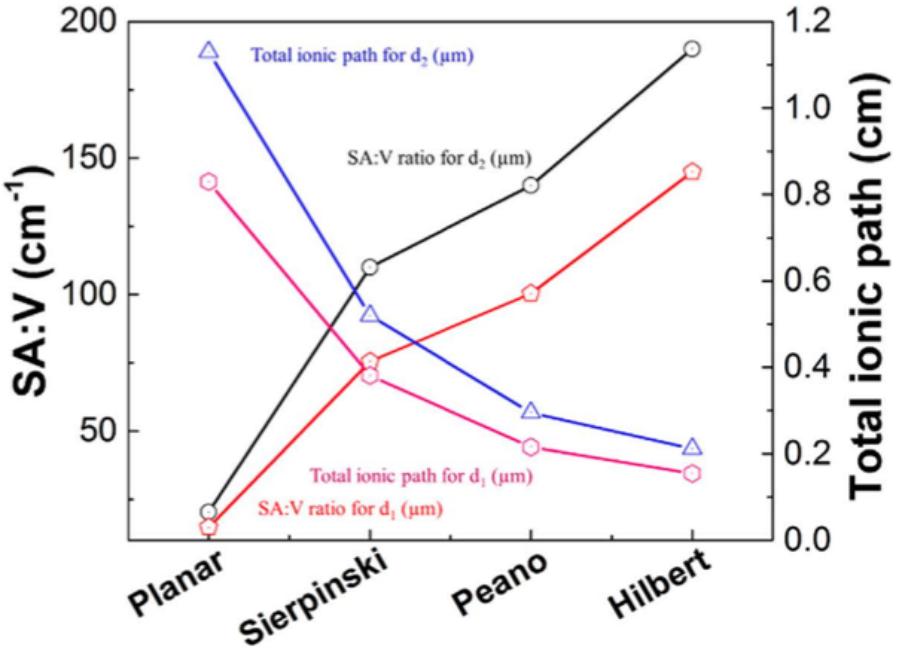

Figure 3.4: Variation of the surface area to volume ratio (SA:V) and the total ionic path in function of the structure.[65]

Part I

Experimental part

Chapter 4

Sample preparation

In this section, all the steps used to assemble the batteries, supercapacitors and interdigit electrodes will be developed.

4.1 Electrode with Nanowires on Silicon Substrate

The first thing that needed to be done is the fabrication of the electrodes. The different steps concerning their fabrication and parameters used to make them will now be discussed.

4.1.1 Track-Etched PC Membranes

The membranes used for the deposition come from the company it4ip. These originate from the $ipPore^{TM}$ *Track Etched Membrane* series, are made of Hydrophilic polycarbonate (PC) and have a volumetric porosity of about 20%. The pores in the membranes were made using the nuclear track-etched technology where a representation of the different steps is shown on Figure 4.1. This technology uses energetic heavy ions, Ar^{9+} at 5.5 [Mev/amu], under a vacuum of 10^{-2} [mbar] to bombard a polymer film (1)→(2). This bombardment destroys chemical bonds and formed damaged tracks. The pores are then formed by principally etching these broken chemical bonds with an aqueous solution of 0.5 [M] of NaOH at 70 °C [67] (3)→(4). In fact, the NaOH will etch the entire PC membrane, but it will etch the damaged track faster than the intact PC.

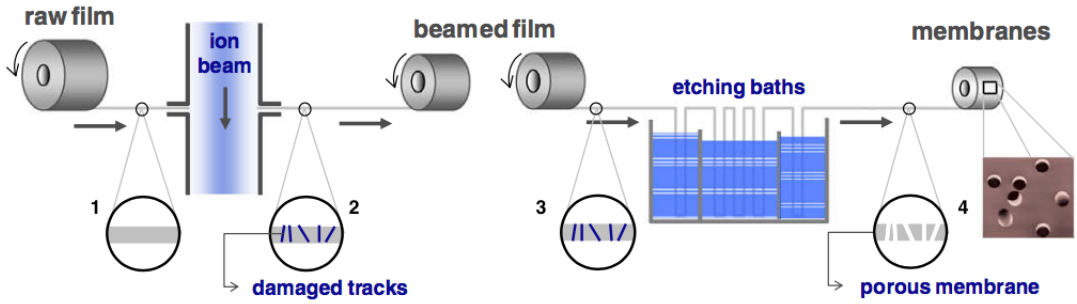

Figure 4.1: Representation of the different steps of fabrication of a track-etched membrane[68]

During this master thesis, two kinds of membranes were used:

- The first was a polycarbonate membrane with pores of 230 nm in diameter inclined with an angle of about 25° and about -25° with the vertical. The pores are all in the same plane meaning these are interconnected along one plane and not along others. The pore density is 5×10^8 $pores/cm^2$.

- The second was a polycarbonate membrane with pores of 40 nm in diameter inclined with angles between +25° and 25° with a porosity of 20% and with the same pore density of 5×10^8 $pores/cm^2$.

To use the membrane as an electrode, these were cut in samples of 6 mm in diameter thanks to a punch.

4.1.2 Substrate

The substrate used to make the electrode is made of the stacking of several layers: silicon (Si), silicon oxide ($SiO2$), titanium (Ti), platinium (Pt) with a disk of copper (Cu) for some samples. All the fabrication steps will be now explained and are represented on Figure 4.2.
The first layer is made of silicon with the crystallographic direction (100) and bought at *Siegert wafers*(1). This layer has been cleaned using H_2SO_4 and H_20 for 10 min then 30 s with an aqueous solution of 2% of HF. A humid thermal oxidation at 1000° C is then done to obtain a 300 nm thick SiO_2 layer(2).

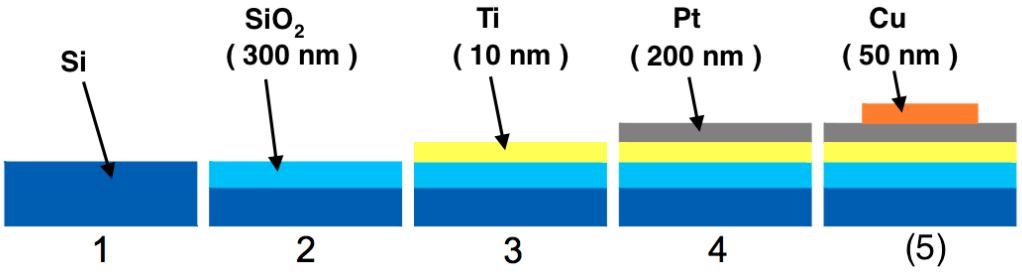

Figure 4.2: Representation of all fabrication steps to obtain the final substrate used during the electrodeposition of the nickel nanowires.

Cathodic sputtering
The second part of the fabrication of the substrates was the cathodic sputtering which is a deposition technique allowing to deposit thin films of materials onto a substrate. This method is based on the creation of a plasma between two electrodes inside a chamber under medium vacuum filled with an inert gas such as argon. The charged ion particles forming the plasma are then accelerated onto the negative electrode (cathode) where the source material is disposed, e.g., copper or platinium, which leads to the erosion of this last with the emission of neutral particles of the source material. These particles deposit on the positive electrode (cathode) where the substrate is present forming a thin layer[69]. The speed of the deposition depends on the applied current used to form the plasma. When this current is higher, there is more erosion of the source material and therefore more deposition on the substrate.

In this case, Ti, Pt and, only for the electrodes used for the supercapacitors, the Cu layers were deposited. The Ti layer has the purpose to be an adhesive layer between the Pt and the silicon oxide since it is known that Pt has a low adhesion to silicon and silicon oxide[70]. The conditions used were a temperature of 15 °C, a DC and 50 sccm of Argon.
The three targets have first be cleaned to remove the native oxide on the surface using high currents:

- Ti : 1 min at 0.5 A (3)
- Pt : 1 min at 2.5 A (4)

- Cu : 1 min at 2.5 A (5)

After that, the sputtering has been realised under the following conditions:

- Ti deposited for 3 min 53 s with a 0.1 A current to form a 10 nm layer.
- Pt deposited for 17 min 52 s with a 0.1 A current to form a 200 nm layer.
- Cu deposited for 8 s with a 2 A current through a Ni mask to form a 50 nm thick disk.

Mask creation for Cu deposition
To deposit the Cu in a disk shape, a mask of Ni has been cut with the Picosecond laser from Oxford Lasers J-Series located in Winfab in Louvain-La-Neuve. The parameters were a power of about 3.85 W, a frequency of 200 kHz and a wavelength of 355 nm for the laser beam. The working of such a laser is explained in section 4.5.1 The laser cut disks of 6 mm in diameter spaced between them by 15 mm. Another mask with disks of 7 mm in diameter was done to make easier to center the 6 mm disk cut in the membrane on the 7 mm Cu disks during the electrodeposition which will now be explained.

4.1.3 Potentiostatic Electrochemical Deposition

4.1.3.1 Device

Every electrodeposition has been done using the Potentiostat/Galvanostat Model 263A from Princeton Applied Research controlled by the Pulsed Chrono-Amperometry program. The system used to make the electrodeposition is made of several parts.

- A double junction Ag/AgCl reference electrode saturated with KCl 3M
- An aluminium sheet with the sample electrically connected to it
- The platinum counter electrode
- An aqueous electrolyte

The purpose of the reference electrode is to set a reference to the voltage to control the voltage applied during the deposition. Indeed, the potential of this electrode is always equal to E=-0.197 V compared to standard hydrogen electrode. The aluminium sheet is placed under the silicon substrate and is bend to make an electrical contact between the platinium on the silicon substrate and the anode. The platinium counter electrode is the anode in this configuration, is inert and serves to close the electrical circuit. The aqueous electrolyte was a mix of $NiSO_4.6H_20$ 0.5M and H_3BO_3 0.3M in the very beginning but has been changed into $NiSO_4.6H_20$ 1M and H_3BO_3 0.3M for the rest of the master thesis. This change has been done since it appears that the electrodeposition was faster with the second one and that no change in structural integrity and adhesion was found. H_3B0_3 is a buffer solution preventing the pH of the electrolyte to change too much while a strong acid or base is added to it[71]. Indeed, during the electrodeposition, some reactions occurs whose main are presented.
First, the reduction of the nickel ions into nickel metal at the cathode forming the nanowires (Eq 4.1) and secondly, the production of oxygen at the anode (Eq 4.2)

$$Ni^{2+} + 2e^- \rightarrow Ni \tag{4.1}$$

$$H_2O \rightarrow 2H^+ + \frac{1}{2}O_2 + 2e^- \tag{4.2}$$

Therefore, the electrolyte should become more acid during the deposition if the boric acid was not there to acts as a buffer.

- The first step was a short pulse step. In this stage, the applied voltage was alternated between -1.05 V for 40 ns and -0.70 V for ten ns for a total time of 1000s. This stage has found to be useful in the lab of Luc Piraux to permit to the nickel to well stick to the last layer of the substrate (Pt or Cu) and so having a stronger adhesion of the 3D nanowire structure on the substrate. During both substeps, the deposition continues but the deposition at -0.7V is much slower permitting to avoid the formation of a depletion region at the interface between the electrolyte and the surface of the sample. The used short pulse is thus not a real short pulse, but a two stages deposition.
- The second step is a continuous one. At this moment, the applied voltage was continued at -1.05 V until a certain amount of specific charge was deposited.

These tensions were chosen in order discovery to only deposit the nickel without having too much side reactions like the electrolysis of water. The total deposited charge permits us to calculate the mass of deposited material.

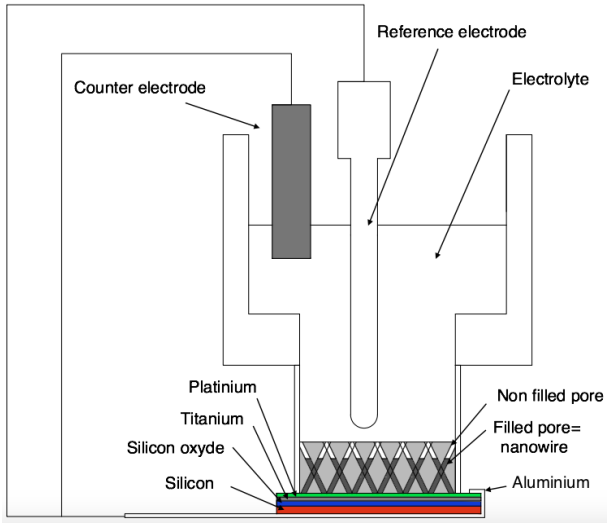

Figure 4.3: Autocad representation of the electrodeposition device

Figure 4.4: Real picture of the electrodeposition device

4.1.3.2 Charge, Current and Mass relation

The charge deposited during the electrodeposition enables us to calculate the mass of material that has been deposited. This can be done using the Faraday's law shown in equation (2.6):

$$m = \frac{QM_w}{nF} \tag{4.3}$$

with the charge Q, the molar mass M_w, the number of exchanged electrons n and the Faraday's constant F.
The deposited charge related to the deposition current by:

$$Q = \int_0^T idt \tag{4.4}$$

with i the deposition current and T the total deposition time.

The reality is a little more complex since the total current does not serve to deposit the desired compound. Indeed, some parasite reactions, such as partial reduction of the metal ion or the reduction of the metal oxide present on the surface of the substrate can occur. The following side reactions can also occur:

$$H^+ + e^- \rightarrow \frac{1}{2}H_2 \tag{4.5}$$

$$2H^+ + \frac{1}{2}0_2 + 2e^- \rightarrow H2O \tag{4.6}$$

It has thus been calculated that the cathodic efficiency for the deposition of nickel is 96%[72]. It means that 96% of the current has been effectively used to deposit the nickel from the solution. This values may change in function of the deposition current. At the extreme, if the deposition current is higher than the limiting current, described by the charge transfer of the ion, the side reactions become the most important reactions[73].

4.1.4 PC Dissolution

The dissolution of the polycarbonate has been done by plunging the sample into dichloromethane for 10 min and agitated it from time to time to ensure that the solvent dissolved all the polycarbonate and to ensure that mechanical stability of the nanowires on the substrate in strong enough before going to the next steps. After this, the samples were plunged into distilled water to clean them then let to dry in air at ambient temperature.

4.1.5 Thermal Annealing

The thermal annealing step was then done to create a shell of nickel oxide around the nanowires. This led to the formation of core-shell nickel-nickel oxide nanowires.

The thermal annealing has been done using the Eurothem 2416CG, 2416P8 oven from the company Carbolite. The oven was preheated to the desired temperature then the sample was put inside for a certain amount of time depending on the desired conditions. Several annealing conditions were used:

- Nanowires of 230 nm: 1 h at 450°C
- Nanowires of 40 nm: 15 min at 350°C
- Nanowires of 40 nm: 45 min at 350°C

4.1.6 Drying

Batteries need to be made in a glovebox were neither H_2O nor O_2 are allowed. To remove the water from the sample, these were placed in a Vacutherm vacuum heating and drying oven from Heraeus Instruments (See Figure 4.5) at 70 °C at a low pressure of about 50 mbar for minimum 24 h. The combination of hot temperature and low pressure permits speeding up the evaporation of the adsorbed water on the sample.
It has to be mentioned that a sheet of Cu has been placed under the substrate of Si and bent to touch the Pt surface. This has been done to permit electrical contact between the Ni nanowires and the electrode of the cell via the electrical conduction of platinium.

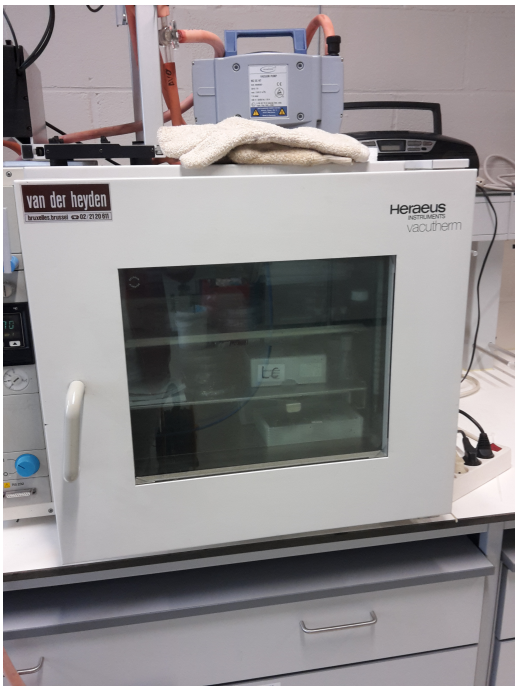

Figure 4.5: Picture of the Vacutherm vacuum heating and drying oven from Heraeus Instruments

4.2 Substrate with Nickel Oxide Film

4.2.1 Slurry Preparation

The slurry contains 80% NiO (the active material), 10% carbon black which plays the role of conductive additive and 10% Polyvinylidene fluoride (PVDF) which acts as a binder. The PVDF was diluted at 3% in mass in a solution of N-Methyl-2-pyrrolidone (NMP).

4.2.2 Ball Mill

The ball mill used is a grinder composed of a steel container where steel balls and the slurry are put inside. By spinning, the balls will grind and blend the slurry's components.

4.2.3 Coating of the Slurry

The slurry has been coated on a Cu or Al foil using a film coating machine with a dryer from the TOB company. The thickness of the coating has been fixed to 200 μm. In the case of the batteries, only Cu has been used.

4.2.4 Drying

The slurry has been dried for 30 min at 70°C to form a film. Then, the desorbed water was removed using the same oven for the same time as the silicon-based electrodes mentioned in section 4.1.6.

4.2.5 Electrode's Fabrication

The coated copper or aluminium sheet is punched in disc shape of 0.5 inches $\approx$ 1.27 cm in diameter. A paper sheet has been placed under the Cu/Al sheet to minimise its deformation

during the punching. The disks were then weighted with a balance to take the ones that had the more similar mass to make symmetrical supercapacitors.

4.3 Batteries Assembly

4.3.1 Without Nanowires

The electrode made of 2D nickel oxide film coated on copper were moved from the drying oven to the glovebox to minimise any contamination of adsorbed water from the atmosphere.
First, the electrode is placed on the positive side of the battery with the copper substrate in contact with the positive side. Then, two drops of electrolyte are put on the NiO film. The electrolyte used in these batteries was 1M LiPF6 ethylene carbonate/diethyl carbonate (EC/DEC) with a volume ratio of 1:1 from salvionic. Afterward, a Whatmann 1823-150 Glass Microfiber Binder Free Filter cellgard separator sheet of 13 mm in diameter is placed on the sample, and two other drops of the same electrolyte were put on the separator. A lithium tablet is then placed on the separator. A stainless steel disk which acts as the current collector is placed on the lithium tablet and a stainless steel spring is finally placed on top of this stack to compress the pieces when the battery is closed with the negative part of the cell and ensure that all the pieces stay immobile in the battery. This is done by compressing the whole battery under a hydraulic crimper.

4.3.2 With Nanowires

The battery assembly also occurred inside the glovebox. The electrodes made of nickel-nickel oxide nanowires on the silicon substrate were also moved rapidly from the drying oven to the oven. First, the sample is placed on the positive side of the battery with its Si side covered by the Cu sheet in contact with the positive side. Two drops of the same electrolyte as in section 4.3.1 are put on the nanowires. Then, the same separator as in the previous section is placed on the electrode. The rest of the assembly is the same as previously explained in section 4.3.1. The complete AutoCAD representation of an assembled battery is shown on figure 4.6.

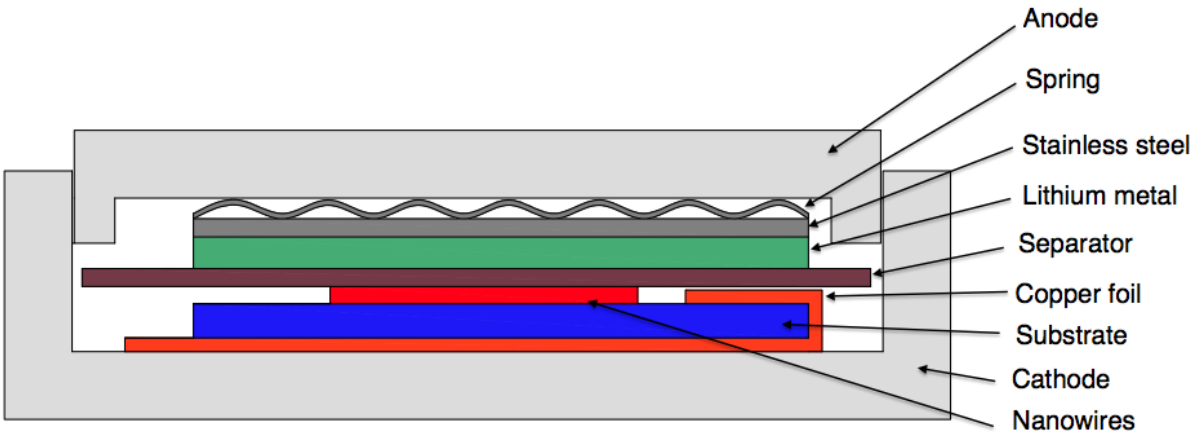

Figure 4.6: Autocad design of an assembled battery

4.4 Supercapacitor Assembly

4.4.1 Without Nanowires

A first disk was placed with the Cu/Al side in contact with the negative part of a CR2032 cell. In fact here, one cannot speak of positive or negative electrode since it is a symmetric supercapacitor and therefore each side can be positive or negative in function of the potential applied to the terminals of the cell.After that, two drops of electrolyte have then been deposited on the side of the disk with the film. Three electrolytes have been tested : Na_2SO_4 1M, H_2SO_4 1M and KOH 6M. A 130520 type celgard separator was then placed on the substrate before putting two more drops of the same electrolyte on the separator. Another disk of similar active material mass was then placed in the opposite orientation compared to the first one. A steel current collector having a disk shape was then put on it followed by a spring to keep everything compact in the cell. The positive side of the cell was then placed on the top of this stack, and finally, the cell was sealed using a hydraulic crimper like the one used for batteries.
No supercapacitors have been made with the Al substrate and KOH electrolyte since the KOH would react with Al producing potassium ions and aluminium hydroxide.

4.4.2 With Nanowires

The mounting process of such supercapacitors is quite similar as the mounting of the batteries with nanowires electrodes of section 4.3.2. However, four major differences can be mentioned.

1. The mounting is done in air.
2. The electrolytes which have been used are Na_2SO_4 or KOH.
3. The separator was the same than the one used for the supercapacitors without nanowires.
4. There is no lithium tablet. Instead, a second electrode is placed in the opposite orientation than the first one, like in section 4.4.1, to make symmetrical supercapacitors.

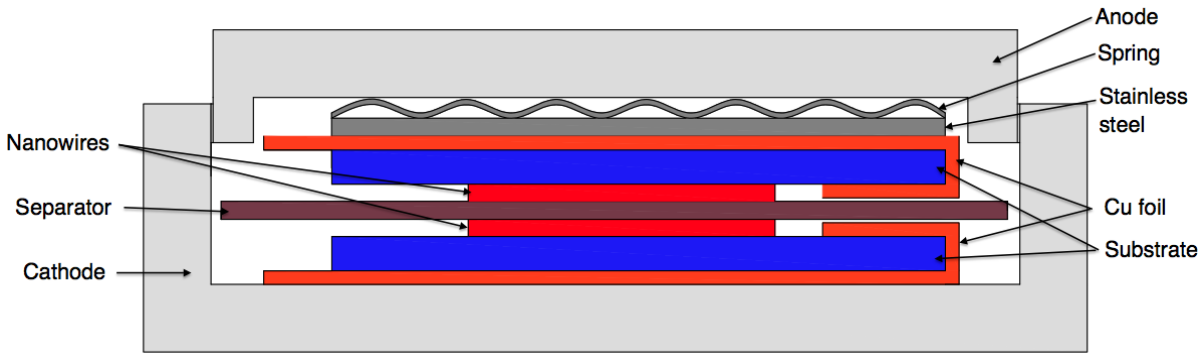

Figure 4.7: Autocad design of an assembled supercapacitor

4.5 Interdigit Electrodes

To make interdigit electrodes, the previous fabrication steps until the end of section 4.1.6 were done.

After that, the sample has been taken to the same laser like the one used to cut the mask for the Cu deposition of subsection 4.1.2. The general pattern, created with the AutoCAD

software, is represented in figure 4.8. On this figure, one can see different colors and zones. The blue color represents the platinium from the substrate which is left intact, the blue zones with the numbers one and two represent the two electrodes where the electrical contacts with measurement devices are done. The red and yellow colors represent the nanowires that are left intact and are all about 200 μm wide. The red ones are electrically connected to the electrode 2 and the yellow ones to the electrode 1. The pink color represents the zone where nanowires are present on the sample. This pink disk has a purpose of calibration for the positioning of the sample under the laser.

To ensure electrical insulation between the first and second electrode, the laser etches the material of the surface to dig until reaching the Si layer. This digging is represented by the dark areas present on the left and right sides of electrodes one and two (1 mm wide) and between the nanowires (about 100 μm wide). A more precise view of the pattern of the nanowires is shown on figure 4.9 and permits to better see the dark areas in the zones where nanowires are present. This round design has been invented to optimise the use of the available material which has the form of a disk.

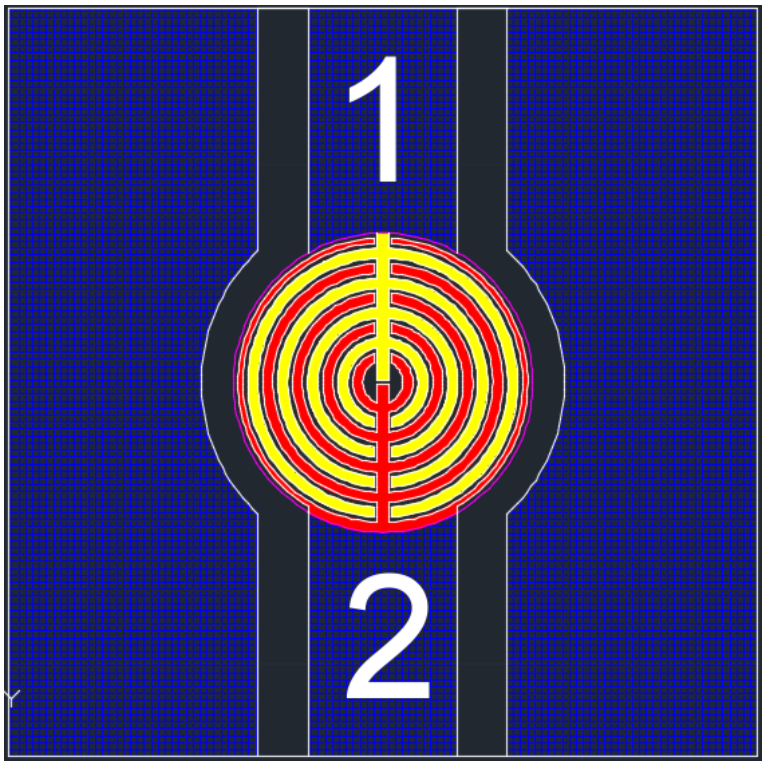

Figure 4.8: Entire Autocad design of the interdigit electrode

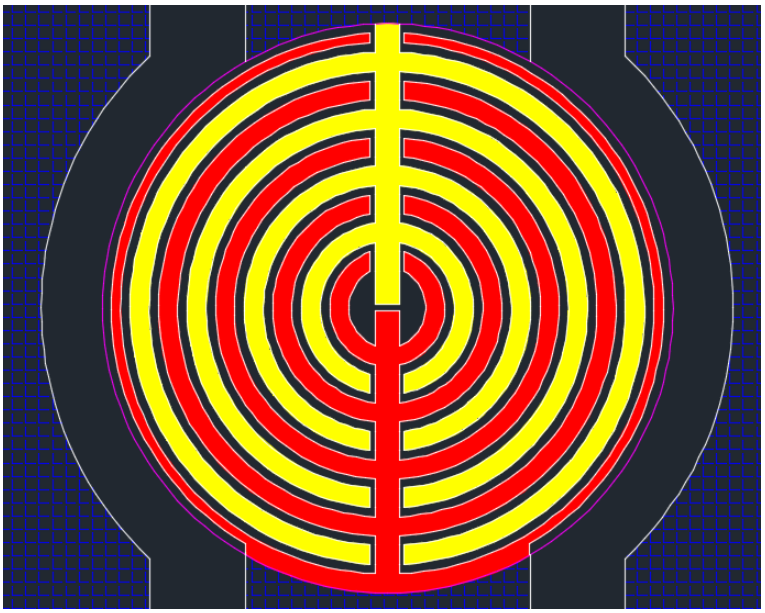

Figure 4.9: Closer view of the Autocad design of the interdigit electrode

4.5.1 Picosecond Laser

To make such complicated structure, a precise cutting technique must be used. The picosecond laser, used in micromachining to drill, cut or scribe a very precise zone of a sample, fulfill the requirement. The working of this laser is based on the emission of very brief light pulses whose orientation is controlled by piezoelectric actuators. On figure 4.10, a comparison of a nanosecond and picolaser is shown. On the first one, the pulse is longer and thermally affects the close vicinity of the impact point. Therefore, the material in this zone heats up, can crack, melt or break into pieces. These pieces can deposit on the surface's material in a small area around the impact point. All these points lead to an imprecise cut of the surface and a contamination of this last.

On the contrary, the pulses of the picosecond laser are shorter and last about ten ps. This leads to the sublimation of the surface with the absence or low heat dispersion and therefore no degradation of the material in the vicinity of the impact zone. Indeed, the hot material is directly ejected from the surface, and the heat does not have time to diffuse in the rest of the material reducing thermal damage[74].

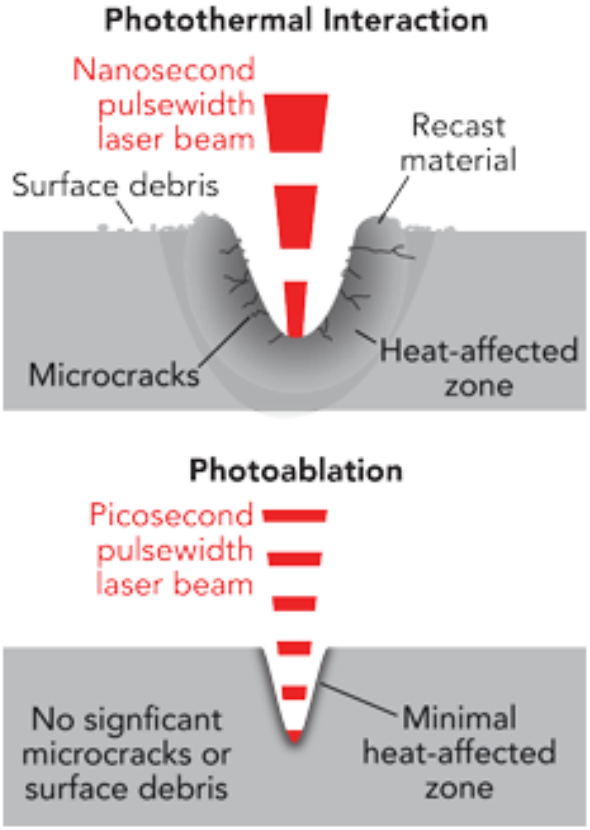

Figure 4.10: Representation of the difference of effects between a nanosecond and a picosecond laser[74]

4.5.2 Other Etching Structures

As it will be discussed in section 9.3, a good electrical insulation between the two electrodes from the interdigit design has not been achieved. Therefore, more simple structures have been tested on the same substrate with different parameters like:

- The power of the laser beam
- The number of passages on each place
- The distance between each line on which the laser pass to make the complete design. A lower distance between the lines means a more precise discretisation of the etched area.
- The overlap which defines the superposition of the different round zones where the laser hits. Indeed, the laser emits pulses that formed a disk shape on the target. A higher overlap indicates a closer distance between the disk and a higher overlap of their surface.
- The width of the etched zone

Chapter 5

Characterisation Techniques

5.1 Structural Analysis

5.1.1 Scanning Electron Microscopy

The scanning electron microscopy is based on an electron microscope or SEM (See figure 5.1). It scans the sample by bombarding it with a focused beam of high-energy electrons. These electrons come from thermionic heating of a tungsten filament, tungsten thin tip for field emission gun or $CeB6$ or $LaB6$ crystals [75] which is accelerated of about 15 keV in a low-pressure environment. These electrons will interact with atoms composing the sample and create several signals [76]. The different types of signal are:

- The secondary electrons that are produced from atoms close to the surface. These are used to show the morphology of the topography of samples.
- Backscattered electrons are electrons from the primary beam that undergo an elastic scattering after a collision with atoms from the sample. These are used to highlight the contrast between different phases composition in multiphase samples because the production of backscattered electrons depends on the atomic number of the material composing the phase. [77]
- X-rays that are produced by inelastic scattering of electrons with electrons of the atoms in the sample. The excited electrons from the material's atom then reduced its energy by changing of orbital. This change in energy orbital induces an emission of X-ray of a fixed wavelength which depends on the orbital change and of the nature of the atom.
- Visible light produced by cathodoluminescence which is a phenomenon in which an electron of the conduction band recombines with a hole of the valence band with the emission of light.

For the electrons to travel the space between the source and the sample and between the sample and the detector, their mean free path must be of the order of magnitude of the distance between these elements. At atmospheric pressure, the primary beam would only travel for about 100 mm in air meaning that the less energetic electrons composing the signal coming from the sample would travel even less far since their energy is lower than the energy of the electrons from the beam. This is why a SEM is operating at low pressure, typically about 10^{-6} mbar [78].

The samples were attached to a holder using a double face carbon tape to avoid the sample from falling in the SEM. Since the sample is made of a 3D metal matrix of core-shell nanowires which are conducting, the electrons will not build up on the surface and not deviate the incident beam of electrons and therefore not degraded the SEM image[77]. Therefore, no particular

attention has been taken to avoid the accumulation of charge.

To obtain a good SEM image quality, the focus and the astigmatism[1] need to be adjusted. The SEM that has been used for the measurements was a JEOL 7600F Schottky Field Emission Scanning Electron Microscope from the UCL.

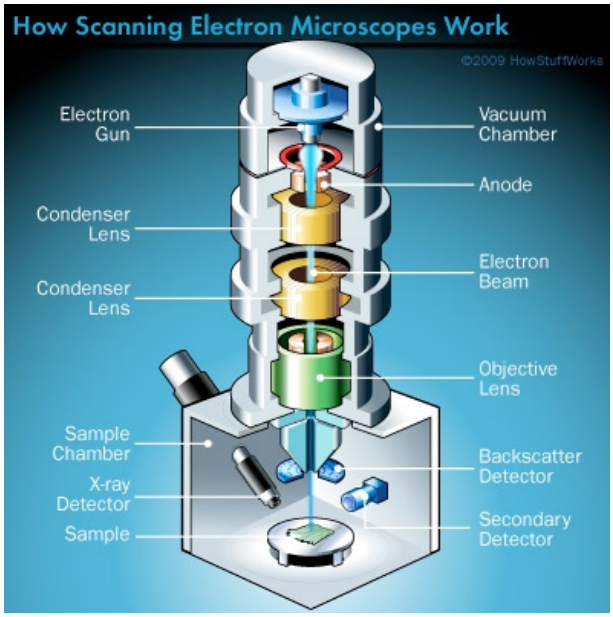

Figure 5.1: Key component of a SEM[80]

5.2 Chemical Analysis

5.2.1 Energy Dispersive X-ray Spectroscopy

The energy dispersive X-ray spectroscopy, EDX or EDS is a chemical microanalysis technique which is often used in combination with a scanning electron microscope. The electrons emitted from the electron gun from the SEM hit the material and can eject core electrons from the material's atoms. The atoms are thus in an unstable energy equilibrium with a hole in their low energy level. Because of this, an electron from a higher energy level rapidly fills the lower energy level that lost an electron. To do that, the electron emits energy in the form of an electromagnetic wave. The energy corresponding to this wave varies in function of the level the electron comes from and the energy level it falls into and is characteristic of the nature of the atom. Generally, the electromagnetic wave is an X-ray. These X-rays can then be detected by a solid-state detector typically composed of lithium-drifted silicon which will create a charge pulse proportional to the X-ray's energy every time an X-ray strikes it. This charge pulse comes from the emission of electrons from the semiconductor composing the detector. Each ejected electron consumes 3.8 eV of energy from the X-ray that hit the semiconductor's atom[81]. The charge's pulse is then converted into a voltage, while maintaining the proportionality to the X-ray energy, by a charge-sensitive preamplifier. A multi-channel analyser receives then the voltage and sorts it by amplitude. To each amplitude of the voltage is associated an X-ray energy itself associated with one particular transition. The data can then be used to know which material is present in the sample. The number of voltage counts of each amplitude permits to know the relative abundance of each material. When there are more counts, it means that more particles of the same nature

[1]Astigmatism is an optical aberration occurring when two orthogonal axes of light are focused at two foci[79]

emitted the same X-ray meaning the material is composed of more of this compound[82].

The acquisition of the X-ray spectrum has been made with a JEOL 7600F Schottky Field Emission Scanning Electron Microscope that contains the option to make EDX analysis. It has been done for 100 s on each place with a 15 keV applied potential.

5.3 Magnetic Characterisation

5.3.1 Alternating Gradient Magnetometer

The alternating gradient magnetometer (AGM) or alternating gradient force magnetometer (AGFM) is a technique in which the magnetic moment of a sample can be measured in function of the applied magnetic field. The sample is fixed on a sample holder using a diamagnetic silicon grease. This sample holder is fixed on the bottom of a piezoelectric element which is itself rigidly fixed via the top. The sample is positioned in the middle of two electromagnetic poles that produces a uniform DC field. The DC field will magnetise the sample. The magnetised sample can then interact with the alternating excitation field produced by the gradients coils. This interaction causes the sample to displace alternatively in the direction of the axis of the gradient causing a deformation of the piezoelectric element[83][84]. Using the piezoelectric effect, the mechanical deformation of a piezoelectric element will create a voltage that will depend on the deformation[85]. The AC field gradient will improve the signal-to-noise discrimination by tuning the frequency of the field gradient to the mechanical resonance frequency of both the probe and the sample. This frequency is generally in the order of 100 to 1000 Hz[86].

The system used in the framework of this master thesis was the PMC MicroMag 2900 Series AGM from LakeShore Cryotechnics. This system has an extremely high sensitivity of 10 nemu rms and a speed of measurement of 10 ms/point. The maximum size of the sample is 5 $\times$ 5 $\times$ 2 mm[84] which is far greater than the samples that were 2 mm in diameter and 20 μm thick.

Figure 5.2: PMC MicroMag 2900 Series AGM[84]

In the case of this measurement, the used sample is a bit different from the samples used to make the electrode. Indeed, no silicon substrate has been used since it would be too thick to be measured. Another type of polycarbonate membrane coated with chromium, which acts as an adhesive layer, and gold, which act as a conductive layer, has been used. This membrane does not have holes at the bottom but has the same density of pores and the same orientation of these last.
The applied magnetic field varied from -14 kOe to 14 kOe at ambient temperature. The measurements were made by saturating the sample at 14 kOe then get back to 0 kOe before making the scan from 0 to 14 then -14 then back to 0 kOe. This has been done to obtain a more symmetric hysteresis loop. This measure of the magnetic moment at saturation has been made before and after annealing of the sample. By comparing the two values of magnetic moment at saturation, it is possible to calculate the proportion of nickel and nickel oxide in the nanowires because nickel is ferromagnetic but not nickel oxide neither gold, polycarbonate or chromium. This is calculated in section 11.1.

5.4 Electrochemical Characterisation

5.4.1 Electrochemical Impedance Spectroscopy

This electrochemical measurement method is also called AC impedance spectroscopy[87]. It is a complete testing method which can characterise the electrodes process dynamics, the ion diffusion inside the cell, the electrode surface phenomenon, the impedance of the cell and several other characteristics. The device used to make the tests were a VersaStat3 and a Parstat 3000 from Princeton Applied Research.

During an electrochemical impedance spectroscopy or EIS test, an alternating voltage is applied to the terminals of the cell and the current which flows through the cell is measured. At each measurement, the excitation signal is of about 1 mV to 10 mV leading to a pseudo-linear response from the cell even if the voltage-current relation of a battery or a supercapacitor is not linear. This permits to use more simple models because linear systems are more easy to describe than non-linear ones. The pseudo-linear behavior can be verified by checking the absence of harmonic of the excitation frequency in the current. Knowing the applied voltage in the response current, it is possible to calculate the impedance of the cell and to plot it in a Nyquist plot which represents the real part of the impedance on the X-axis and the imaginary part on the Y-axis. Each point of a Nyquist plot represents the impedance at one particular frequency. The norm of the vector connecting the origin to a point of the graph represent the impedance, and the angle made by the vector with the X-axis represent the phase shift. Unfortunately, it is not possible to know at which frequency each point has been measured by looking at the plot.
An example of a typical Nyquist plot is shown on figure 5.3. The plot is divided into three zones[88]:

1. High frequencies called the migration zone which provides the resistive characteristics
2. Medium frequencies called charge transfer which represents everything which is linked to the kinetics
3. Low frequencies which represent everything linked to the diffusion of species inside the cell.

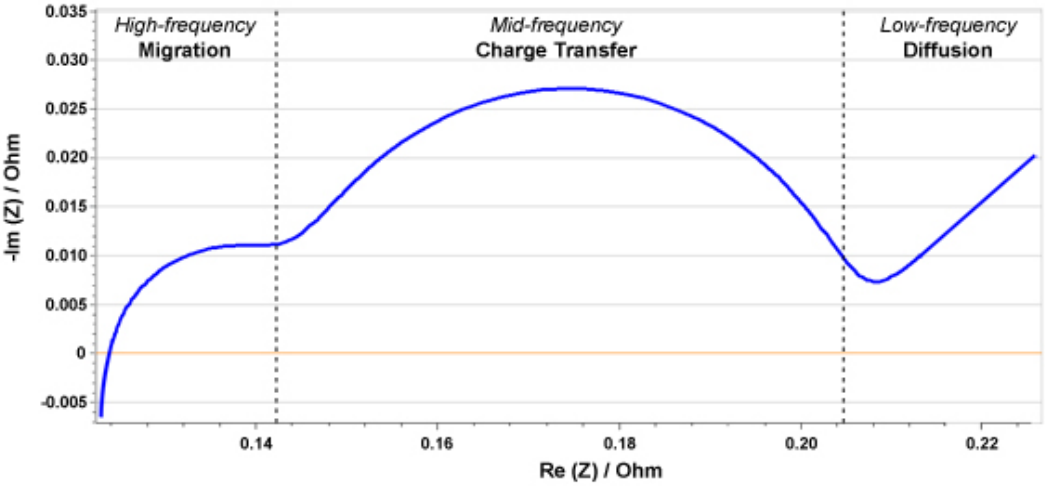

Figure 5.3: Nyquist diagram obtained during a typical EIS test[88]

5.4.2 Galvanostatic Charge and Discharge Cycles

The galvanostatic charge and discharge cycles of batteries and supercapacitors permit to look at the voltage-current behavior of them with respect to time. In the galvanostatic mode, the charge and discharge current is constant during the whole discharge and charge steps[89]. This constant current is often referred as C-rate. This is calculated from the capacity of the batteries and is used to calculate more easily the time needed for a battery to be completely charged or discharged under a certain current[90]. For example, a battery having a specific capacity 1500 mAh will be completely charged, starting from the complete discharge state, in an hour under a current of 1500 mA which is equal to 1 C. The charge and discharge steps are carried out in a voltage range to avoid damaging the electrolyte or the electrodes.

The instrument used to perform the test was a BTS4000 shown on figure 5.4.
The applied voltage range was 0.3 V to 3 V. One can wonder why the voltage was not dropped to 0 V. This has been chosen because of the lithiation of silicon which occurs at 0.33V[17]. This phenomenon has to be avoided since silicon is rapidly destroyed during lithiation/delithiation process due to significant volume changes [91]. Concerning the used current, several have been used such as C/7, C/2, C, 2C and 4C for batteries and 0.1 mA/cm^2 for supercapacitors

Figure 5.4: Picture of the BTS4000 galvanostatic battery testor

5.4.3 Cyclic Voltammetry

The purpose of cyclic voltammetry or CV is to sweep the voltage linearly with time across cells from a lower to a higher and then again to a lower potential called switching potentials. A pair of sweeps in the opposite direction represents a cycle. A typical graph showing the potential in function of time can be seen on figure 5.5. The speed at which the test occurs is called the scan rate and is expressed in mV/s. The result of such a test is called a voltammogram (See figure 5.6) and shows the variation of current in function of the potential. Oxidation and reduction reactions induced by anodic and cathodic current respectively can, therefore, be seen as a sharp increase of decrease of the current. Cyclic voltammetry can provide information about the potential, the energy, the reversibility and continuity of a redox reaction occurring in the voltage range of the test[92]. To make the measurement, the reference electrode, an electrode with a fixed electrochemical potential, and a counter electrode, an inert electrode used to complete the circuit, are connected to one side of the cell. The working electrode load, which is the electrode being tested, is connected on the other side[93].

The device used to make the tests was a BTS 2000 from Arbin Instruments. The used switching potentials and scan rates during the tests depended on the electrolyte contained inside the supercapacitors. The parameters relative to these are shown in Table 5.1 :

Electrolyte	Switching potentials V	Scan rate [mV/s]
Na_2SO_4 [18]	-0.2 to 1.2	5, 25, 50, 100, 200, 300, 400, 500
KOH [19]	-0.1 to 0.2	2, 5, 10, 25, 50, 100, 200, 500

Table 5.1: Parameters used for cycling voltammetry

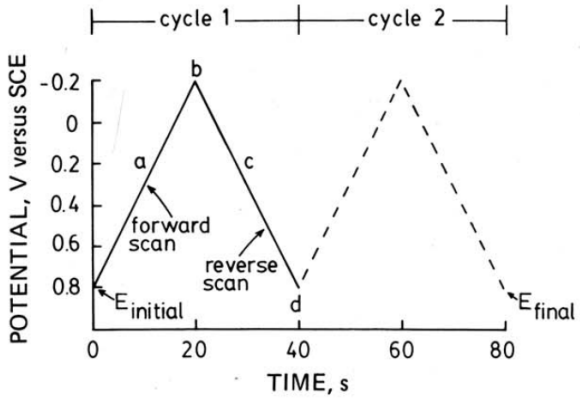

Figure 5.5: Representation of the triangular potential CV scan[94]

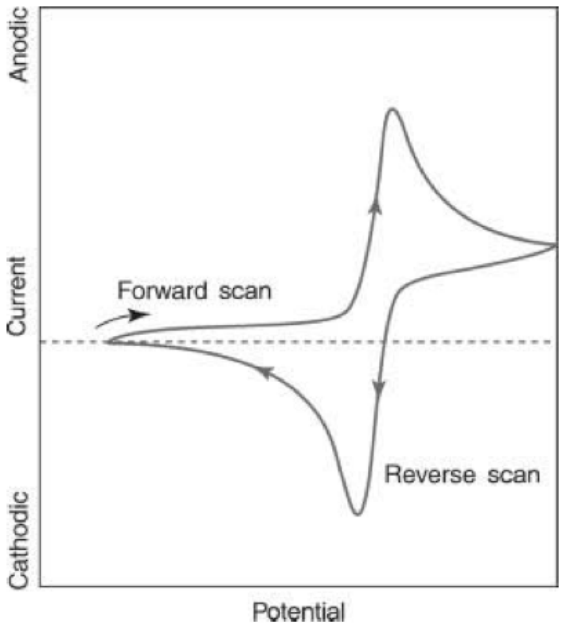

Figure 5.6: Typical voltammogram during a CV test [92]

Part II

Results and discussion

Chapter 6

Electrode characterisation

6.1 SEM

The nanowires 3D network has been observed in SEM before and after annealing to observe the shape modification of the nanowires.

6.1.1 Before Annealing

On figure 6.1, one can see that the 230 nm nanowires remained straight and had an ordered structure. On figure 6.2, one can see that for the 40 nm nanowires, the structure seems to be more chaotic. This view has been done by tilting the sample and by doing a scratch on the sample which is visible on the bottom of the image. There, no nanowires are present. This scratch enables us to see a cross-section of the 3D nanowire structure.

Figures 6.3 and 6.4 show a closer view of the 230 nm and 40 nm nanowires respectively. For the 230 nm, one can see that the surface of the nanowires is very smooth and that the nanowires are straight. On the other hand, it appears that the 40 nm nanowires have bent under their weight because of the high ratio between their length and diameter. Also, there are more or less densely packed in certain zones. A less densely packed zone is visible in the middle of figure 6.4 and is a little darker than the rest of the image.

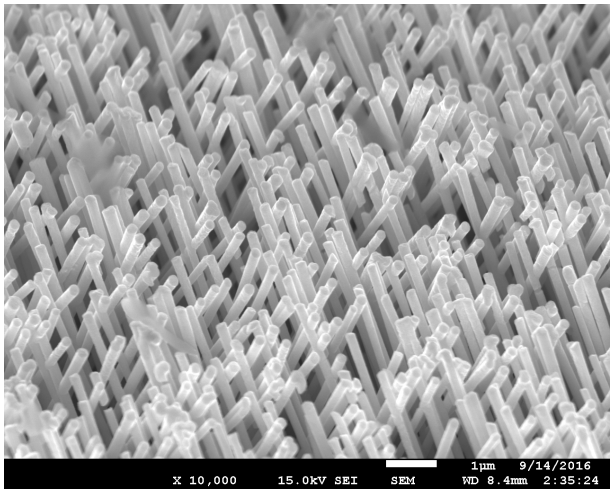

Figure 6.1: SEM view of the 230 nm nanowire network before annealing

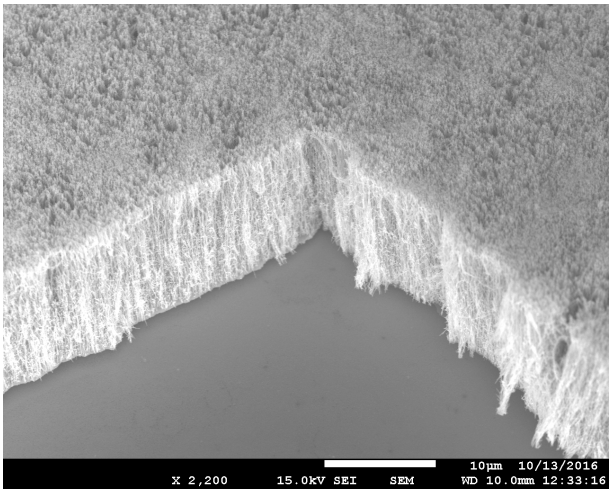

Figure 6.2: SEM view of the 40 nm nanowire network before annealing

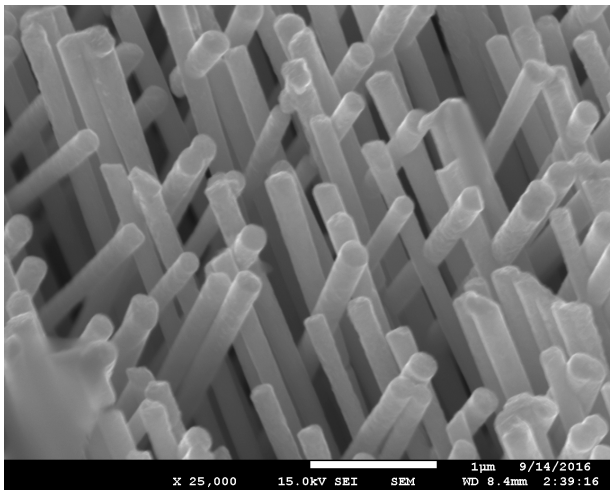

Figure 6.3: Closer SEM view of the 230 nm nanowire network before annealing

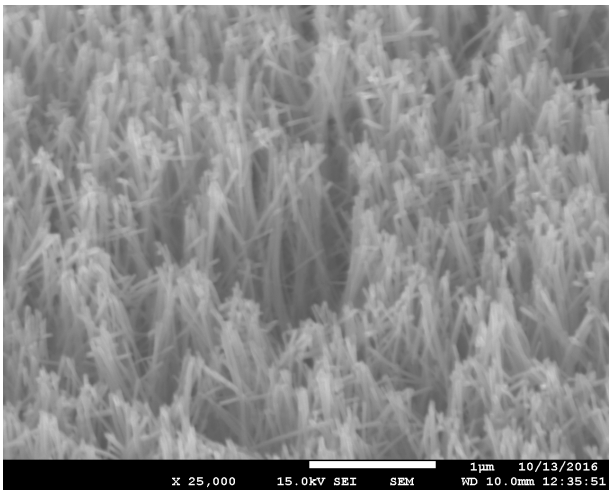

Figure 6.4: Closer SEM view of the 40 nm nanowire network before annealing

6.1.2 After Annealing

The annealing drastically changed the shape of the 230 nm nanowires. As one can see on figure 6.5, the surface of these nanowires became rough. This roughness is the result of the formation of nickel oxide on the surface of the nanowires to form a shell. It can be said with a high probability that the formed oxide is NiO and not Ni_2O_3 for both the thin and large nanowires since another study only discover the formation of NiO at $300°C$ and $500°C$[95].
On the other hand, the 40 nm nanowires do not show a variation of the morphology. This can be attributed to the annealing conditions of these nanowires that produced less NiO.

Because of the lower density of nickel oxide in comparison with nickel, 8.9 g/cm^3[96], and 6.67 g/cm^3[97] respectively, the diameter of the large nanowires expand to a mean diameter of 305 nm showing the oxidation of a part of the nickel composing the nanowires into nickel oxide. The 40 nm nanowires expanded to a diameter of about 42 nm. This value is not very precise since, as can be seen on figure 6.6, the image is not precise.

The composition of the nanowires before and after the annealing are shown in Table 6.3. The calculation done to obtain these proportions are discussed in 11.1.

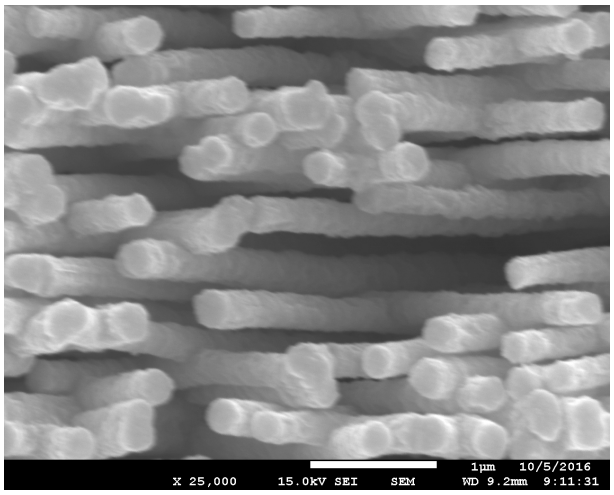

Figure 6.5: SEM view of the 230 nm nanowire network after annealing

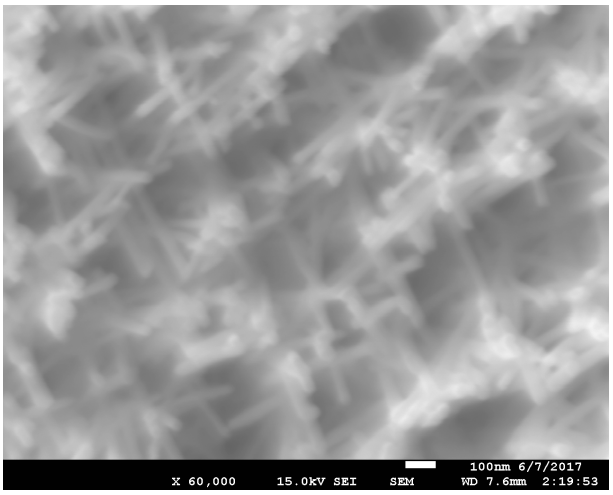

Figure 6.6: SEM view of the 40 nm nanowire network after annealing

6.2 AGM

Each sample of 6 mm in diameter has been cut in three small subsamples of 2 mm in diameter because the AGM measurement needs smaller samples. Therefore, the multiplication of the measurements on several subsamples from a same sample permits to obtain more data and therefore have a better accuracy on the magnetic moment. The ratio of the magnetic moment after annealing by the magnetic moment before annealing permits to obtain the proportion of nickel still present in the nickel metal core. Using the molar mass of nickel and nickel oxide, 58.69 g/mol and 74.69 g/mol respectively, it's possible to obtain the mass proportion of the two compounds.

6.2.1 230 nm Nanowires

For this sample, the measurements on the three subsamples that were cut from this one has been done in an orientation parallel and perpendicular to the plane before annealing. The orientation of the nanowires is not really parallel neither perpendicular because of the angle these exhibit with the substrate. The substrate being attached to the sample holder which is parallel or perpendicular to the applied magnetic field, its impossible to measure a parallel or perpendicular nanowires orientation with this device. Moreover, these two orientations are not compulsory since the goal of this measurement is to obtain the magnetic moment at saturation and not the hysteresis curve which, for its part, is modified by the relative orientation of the nanowires with applied magnetic field. The results are shown in Table 6.1. It can be seen that the magnetic moment at saturation for both orientation is nearly the same within experimental errors confirming that the magnetic moment at saturation is the same for any orientation. By making the ratio between the value of magnetic moment after and before annealing, one obtain 52.44% for the 230 nm nanowires meaning that 52.44% of the nickel mass is present in the nickel core of the nanowires. This percentage is equal to 83.05 % for the 40 nm nanowires. This means that less NiO has been formed corroborating the lower volume expansion of these nanowires.

	Before annealing		After annealing
Sample	Magnetic moment in parallel orientation [memu]	Magnetic moment in perpendicular orientation [memu]	Magnetic moment [memu]
1	3.968958	3.969065	1.776756
2	3.825949	3.972368	2.312992
3	3.933822	3.819251	2.069735
Mean	3.909576	3.920228	2.053161
Final mean	3.914902		2.053161

Table 6.1: Measured magnetic moment at saturation

6.2.2 40 nm Nanowires

The AGM measurements on the 40 nm nanowires electrode has only been done with the substrate in the direction parallel compared to the applied magnetic field. The obtained values of the magnetic moment before and after annealing shown in Table 6.2 permit to calculate that 83.05% of the nickel is still present in the nickel metal core. The higher result is consitent with the lower annealing temperature and shorter annealing time used during the annealing of the 40 nm nanowires. The mass proportions are

	Before annealing	After annealing
Sample	Magnetic moment in parallel orientation [memu]	Magnetic moment [memu]
1	3.607323	2.978378
2	3.329621	2.782730
Mean	3.468472	2.880554

Table 6.2: Measured magnetic moment at saturation

Taking all these informations into account, it is possible to summarise the diffrent information into Table 6.3.

Diameter before annealing nm	Diameter after annealing nm	nickel metal mass proportion %
230	305	52.44
40	42	83.05

Table 6.3: Composition of nanowires before and after annealing

Chapter 7

Batteries Performance Testing

7.1 Electrochemical Characterisation

7.1.1 Galvanostatic Charge and Discharge

7.1.1.1 Specific Capacity VS Cycles

Several kinds of batteries have been tested. There are the batteries made of 230 nm nanowires electrodes, 40 nm nanowires electrodes and the ones with NiO film. The latest has been done to compare the cycle life as well as the specific capacity of NiO when incorporated in a film or nanowires.
All the tests have been done between 0.3V and 3V to avoid any lithiation of silicon starting at potentials less than about 0.33 V[17]. A test has been done between 0.01 V and 3 V to have a look at the lithiation process on a battery with 230 nm nanowires electrode. 0.01 V has been chosen instead of 0 V because the tester did not allow the chose 0 V. Several rates have been chosen: C/7, C/2, C, 2C, and 4C. The mass of the NiO present on the 230 nm and 40 nm nanowires electrodes is about 0.358 mg and about 0.076 mg respectively (See section 11.1).
The discharge and charge currents are thus 0.0358 mA, 0.1283 mA, 0.2567 mA, 0.5134 mA and 1.027 mA respectively for the 230 nm nanowires batteries.
For the 40 nm, the currents are 0.0076 mA, 0.0272 mA, 0.0545 mA, 0.1090 mA and 0.2180 mA respectively.

7.1.1.1.a Batteries Without Nanowires

On figure 7.1, the variation of the specific capacity in function of the cycle number can be observed. The red curve corresponds to a sample containing less active material on the cathode (1.96 mg) than the other (3.576 mg). Both cells were cycled at C/7.

A big decrease can be seen in the first cycle for both batteries, corresponding to the irreversible reactions like the formation of the SEI. From the second cycle, the decrease is more smooth but still quite important. This large decrease can be explained by the progressive pulverisation of the NiO. During every cycle, some parts of it dislocate from the cathode and reduce therefore the specific capacity. This rapid decrease of the specific capacity is consistent with the literature [12]. It can be seen than the electrode containing less active mass has a higher specific capacity than the other all along the test. This can be explained by the higher proportion of active mass that participates in the conversion reaction due to the 2D structure of the film. Indeed, for the heavier cathode, more NiO is hidden from the electrolyte because the thickness of the film is higher and therefore less active mass in comparison with the total active mass can react. The two samples lose rapidly more than 90 % of their specific capacity after only 60 cycles: 40 mAh/g for the lightest and 25 mAh/g for the heavier in comparison with 1058 mAh/g and 1052 mAh/g respectively at the first cycle.

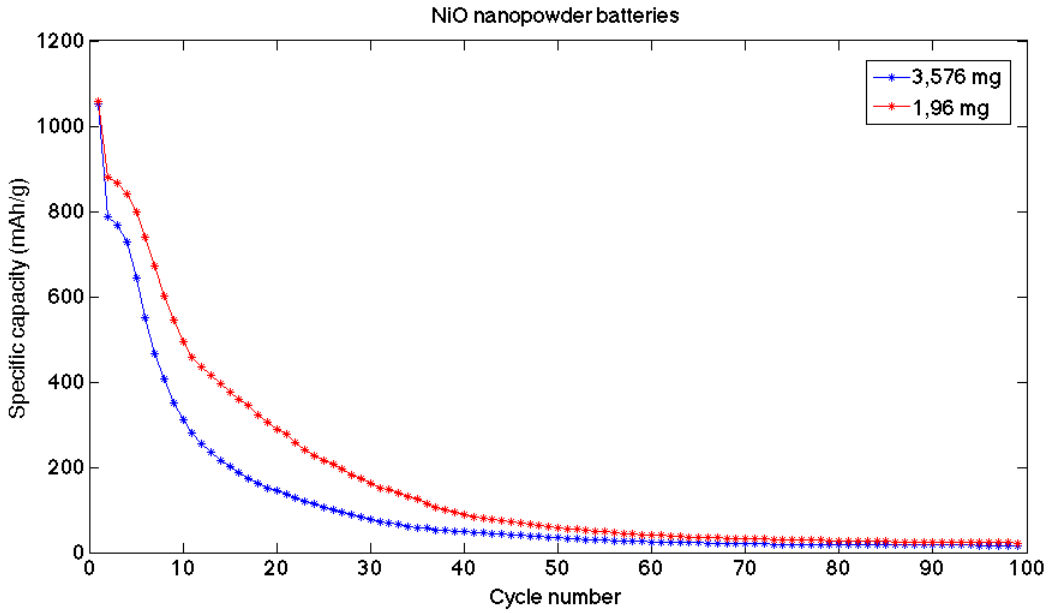

Figure 7.1: Galvanostatic charge-discharge cycles of NiO nanopowder batteries

7.1.1.1.b Batteries With Nanowires

Concerning the electrodes that have been made of 230 nm and 40 nm nanowires (See figures 7.2 and 7.3), five same batteries were tested for each at different speed rate: C/7, C/2, C, 2C, and 4C. All the test do not contain the same amount of cycles because of time issues.

The first thing which can be seen for the 230 nm batteries is that the specific capacity of the batteries is dependent on the rate of charge-discharge. This can be well seen on figure 7.2 where the specific capacity decrease with increasing charge-discharge speed. For the 40 nm batteries (figure 7.3), this relation is not respected. Indeed, the tests at a rate capability of 2C and 4C give the higher specific capacity among all the 40 nm batteries from the hundredth cycle. The battery tested at a C-rate of 2C is even the best from the fiftieth cycle until the end of this test. These unexpected results could be explained by a difference in mass between the samples even if the deposit mass should be the same. There is maybe less active material losses because the nanowires structure was more stable than the other. Indeed, nearly all 3D structure were already a bit damaged with cracks or showed slight separation between the network and the substrate. Another explanation could be an enhanced electronic conductivity of the core which is closer to the NiO-electrolyte interface improving the electrochemical reaction inside the batteries. However, this hypothesis suffers from the drawback that all 40 nm batteries are not all superior in term of performance than their counterpart 230 nm battery.

Secondly, for the test at C/7, C/2, and C for the 230 nm, one can see a small increase of the specific capacity from the second cycle until about the 25th cycle.

Thirdly, for both 230 nm and 40 nm batteries, on the blue curves corresponding to the C/7 rate, one can see a significant perturbation in the data where the specific capacity suddenly drops to about 150 mAh/g for the 230 nm and 350 for the 40 nm batteries. After that, the specific capacity recovers to nearly its previous value. This strange behaviour is the consequence of a power shortage that occurred during the test. This had no consequences on the 230 nm battery but had consequences on the 40 nm battery. In the first case, the slope of the curve seems to be the same before and after the shortage. However, the slope for the second case is higher leading to

faster greater loss of specific capacity after the shortage. A similar but less marked phenomenon is visible at the 250th cycle of the green curve (C-rate) of the 230 nm nanowires battery. This is because the first cycle test on this battery has been planned for 250 cycles initially. After seeing that the results were good, another 250 cycles have been done. The phenomenon is probably due to the self-discharge of the battery between the end of the first and the beginning of the second test cycles.

Another unpredicted behaviour is the increase of the specific capacity of the 230 nm battery tested at C, almost continuously from the cycle 300 to 500. A similar phenomenon occurs on the 40 nm battery also at a C-rate of C for more than 200 cycles. This behaviour could be explained by the change in temperature of the room. Indeed, this test was started at the end of winter and took more than 40 days. Therefore, the higher temperature experienced during spring can be responsible for this because the capacity is enhanced with the temperature as long as the temperature is not too high in which case increased chemical activity could lead to higher self-discharged and other side reactions[92]. The effect is caused by enhanced electrochemical reduction-oxidation at the electrodes. Also, the diffusivity of lithium ions in the electrolyte increases with temperature[98].

The 230 nm battery tester à C/7 suddenly stopped working after a bit more than 150 cycles. This problem might be caused by the emergence of dendrites that have perforated the separator and therefore created a short circuit. Another reason could be a mechanical failure due to the detachment of the 3D nanowire network from the substrate. Indeed, it is reasonable to think that, if the structure of this particular battery was weaker than normal, the repetitive lithiation and delithiation process could have damaged the structure to the point of failure.

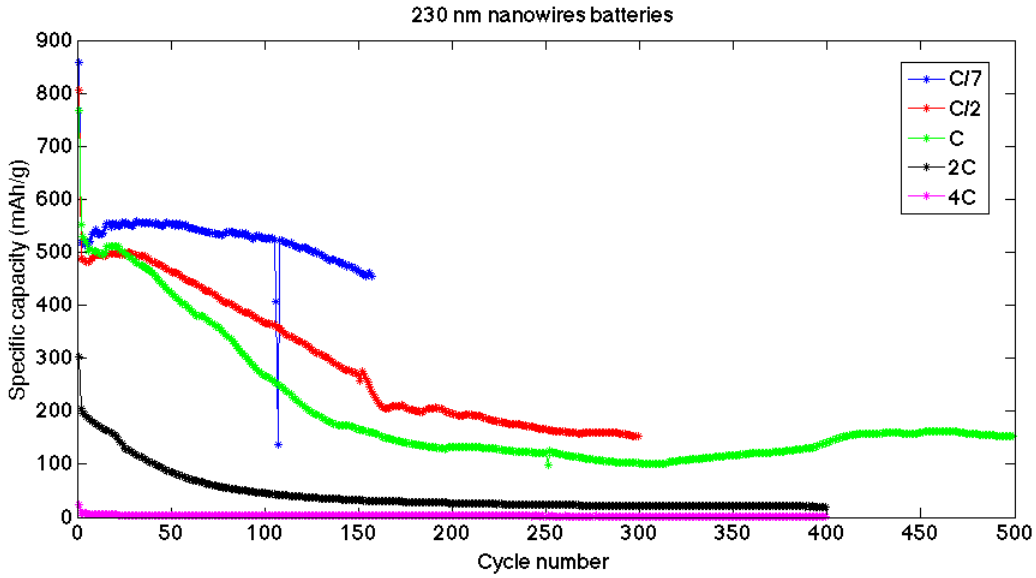

Figure 7.2: Galvanostatic charge-discharge cycles of 230nm nanowires batteries

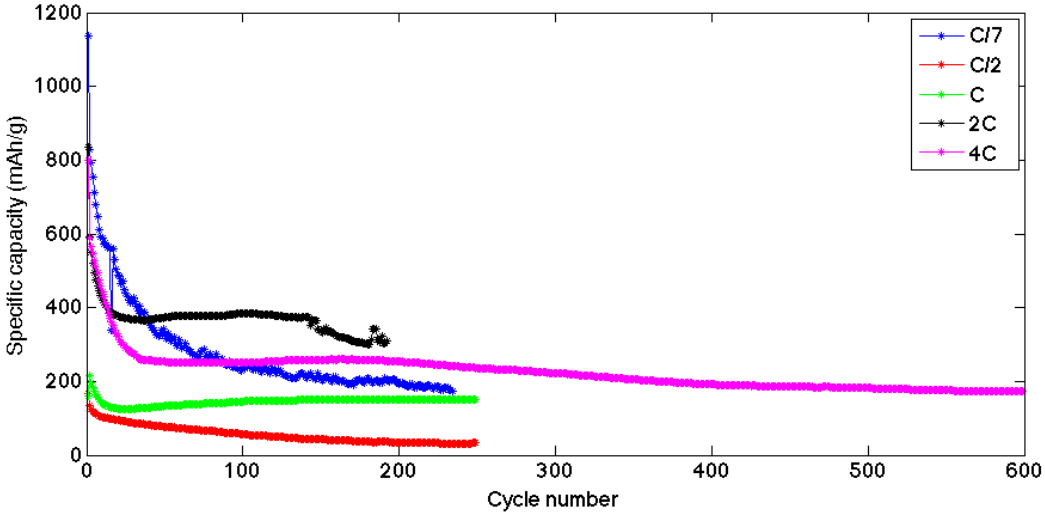

Figure 7.3: Galvanostatic charge-discharge cycles of 40nm nanowires batteries

7.1.1.1.c Comparison

In general, one can see that 230 nm batteries performed better at the beginning of the test cycles for approximately the first 100 cycles. However, these lose their capacity more rapidly leading the 40 nm nanowires batteries to be better when the number of cycles is higher than about 100 cycles. The electrochemical stability of the 40 nm batteries is greater than for the 230 nm batteries because these lose less capacity with time.

To better see the differences, all the previous type of electrode have been compared and are depicted on figures 7.4 and 7.5. All the curves correspond to a C-rate of C/7. The most significant result is the lower electrochemical stability of the electrode without nanowires compared with the electrodes with nanowires. The lower electrochemical stability of the NiO film can be attributed to an unstable formation of SEI and higher pulverisation of the active material.
Also, the specific capacities are very different. The 230 nm batteries seem to possess the higher specific capacity per mass followed by the 40 nm batteries and finally the NiO film which is consistent with the literature [12]. This proves that the active material is better used for the redox reactions and that there is less deterioration of it in the 3D structure.

The graph corresponding to the specific capacity per unit of surface shows that the NiO film, 2D structure, has the highest value until the 35th cycle. This is surprising, but this can be explained by the fact that there is way more active material in the NiO film than in the nanowires. The same explication can be used to explained why the 230 nm nanowires batteries have a higher specific capacity per unit surface than 40 nm nanowires batteries.

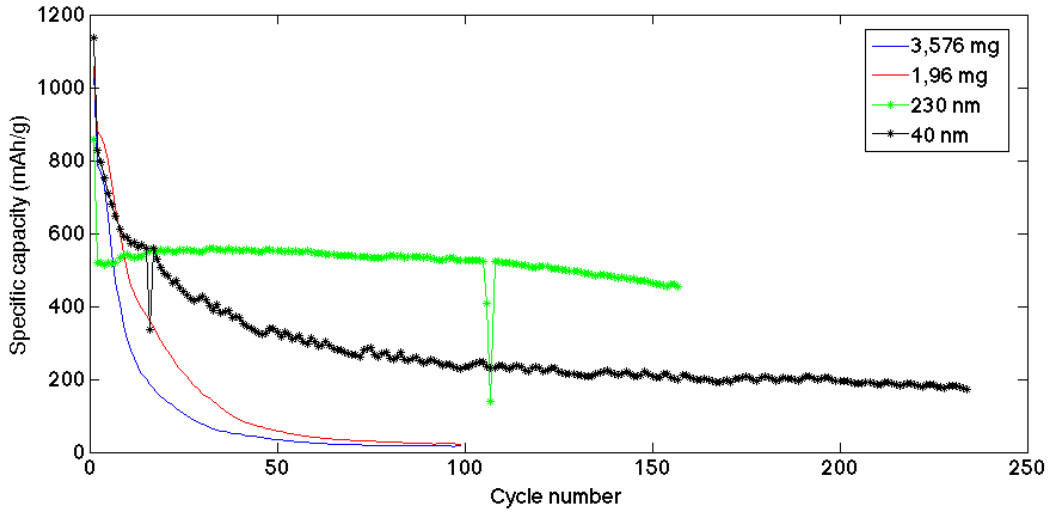

Figure 7.4: Comparison of the specific capacity per unit of mass between the NiO film, the 40 nm and 230 nm batteries

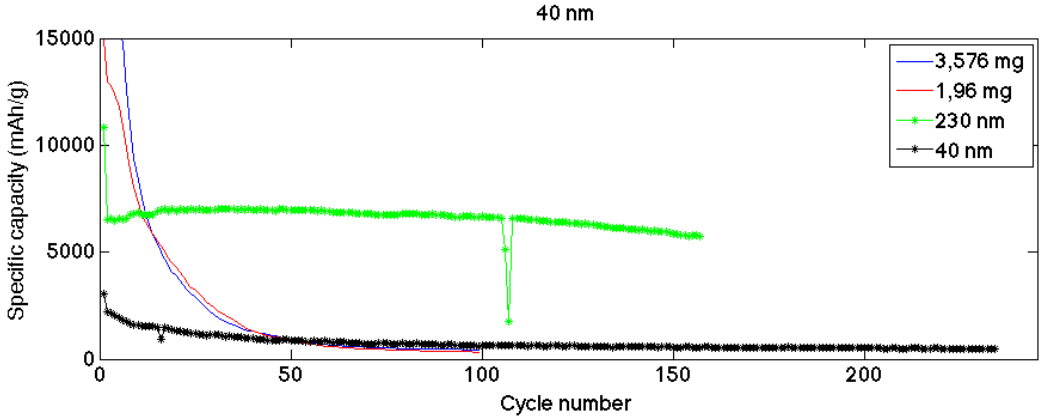

Figure 7.5: Comparison of the specific capacity per unit surface between the NiO film, the 40 nm and 230 nm batteries

7.1.1.2 Charge-Discharge Voltage profiles

A close analysis of the charge-discharge voltage profile of some batteries permits to highlight different behaviour and gives additional informations in addition to the specific capacity VS cycles graphs.

7.1.1.2.a 230 nm Batteries

During the first discharge, a small plateau slope is situated between 1.10 V and 1.25 V (See figure 7.7 and 7.8) and match the potential of lithiation of NiO found in literature [16]. This plateau is however not present in the first test at C/7 (See figure 7.6) for un unknown reason. The second plateau is situated between 0.6 V and 0.7 V (See figure 7.7 to 7.8) in function of the C-rate. This plateau is lower in potential when the C-rate increases due to kinetics effect that reduce the ability of the lithium to access the NiO[99][13]. This result is closer to the behaviour observed for submicrometer particles than nanoparticles of NiO. At the end of the first discharge curve, the profile goes down rapidly. This could be explained by the SEI layers on the electrode

surface[13].
An unexpected slope that begins at 1.5 V occurs on the tested conducted at 2C for the 230 nm batteries. It is believed that the slope is due to kinetics effects.

During the first charge, a plateau slope at about 2.1V is present which potential and slope increase with the number of cycles and with the C-rate. The position of this slope has been found to correspond to the delithiation of sub-microsized particles of NiO[13].

During the fifth discharge, the broad plateau at 0.7 V from the first discharge is shifted towards higher potential values of about 1.4 V and is smaller. This large change in potential suggests that the first cycle was governed by irreversible process linked to the formation of the SEI[16] or/and to the structure change of the nickel oxide from crystalline to an amorphous structure as explained in section 2.4.2.1.

During the fifth charge cycle, the delithiation curve is slightly shifted towards higher potentials but without major variations.

During the 50th charge, a second plateau slope seems to appear at 1.5 V, and the plateau of delithiation of NiO becomes a slope.

It has to be noted that nearly none of the previously mentioned plateaus and plateau slopes do appear in the last, which has been test conducted at 2C. Also, a long slope is present in all discharge cycles. This is probably due to the very high testing speed that limits the reaction kinetically inside the battery.

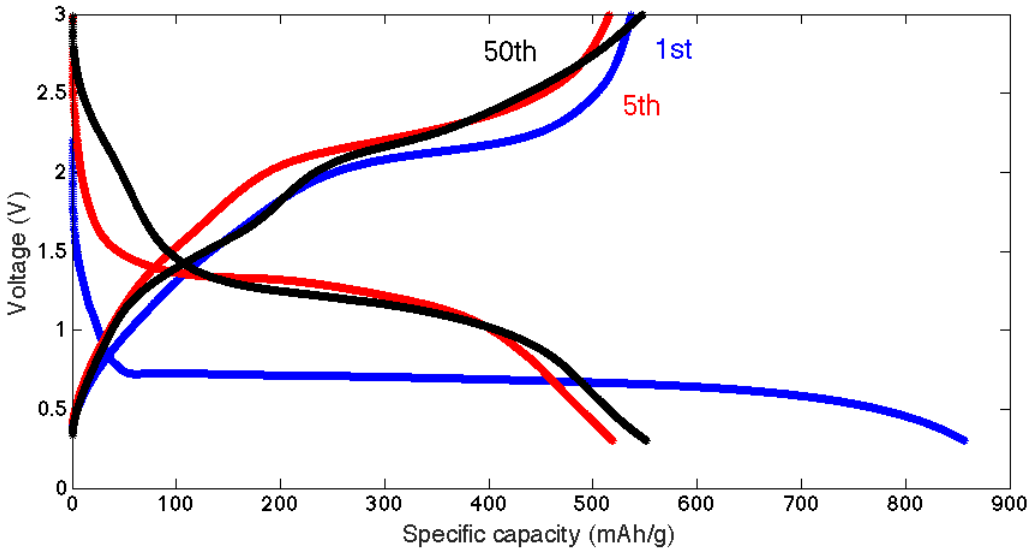

Figure 7.6: Charge-discharge voltage profile for 230nm nanowires battery at C/7

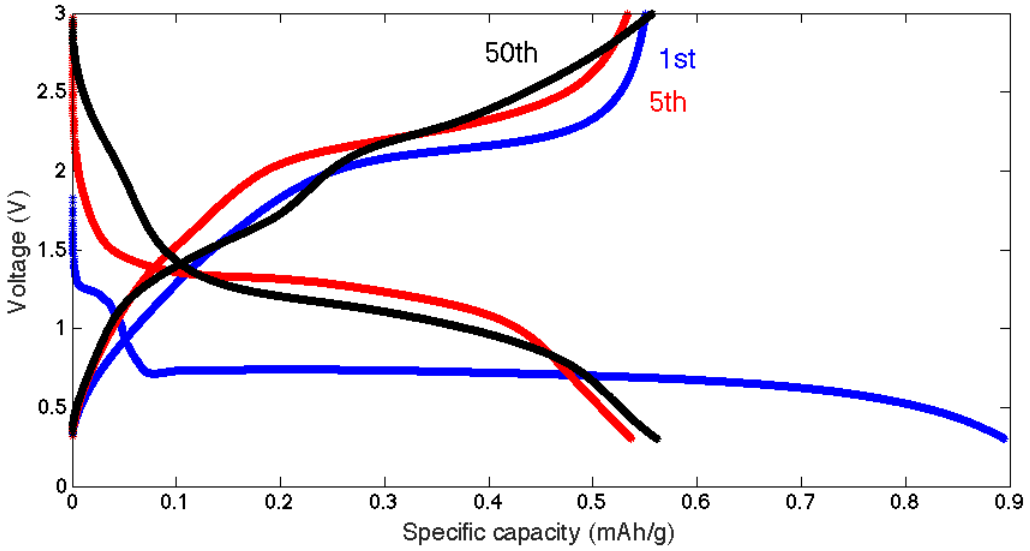

Figure 7.7: Charge-discharge voltage profile for another 230nm nanowires battery at C/7

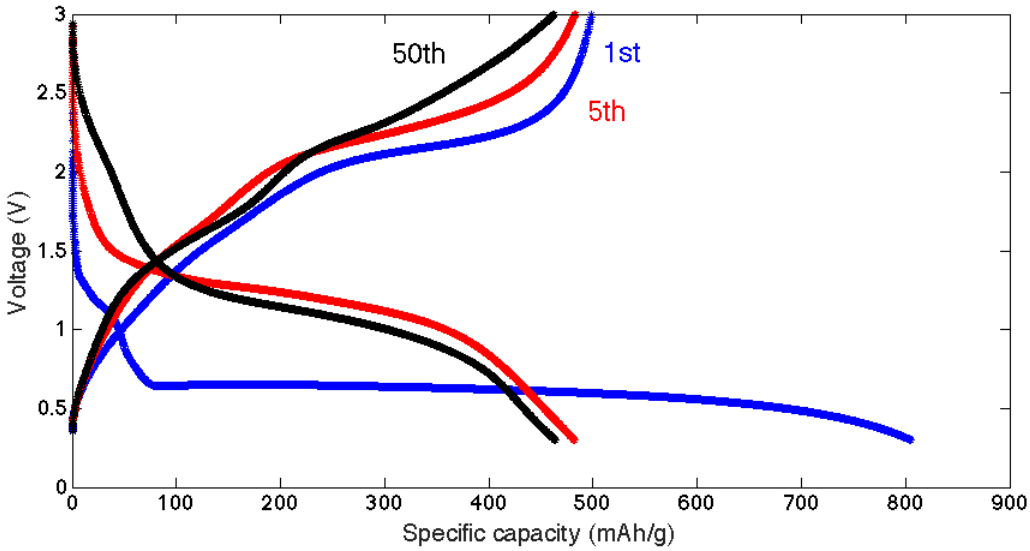

Figure 7.8: Charge-discharge voltage profile for 230nm nanowires battery at C/2

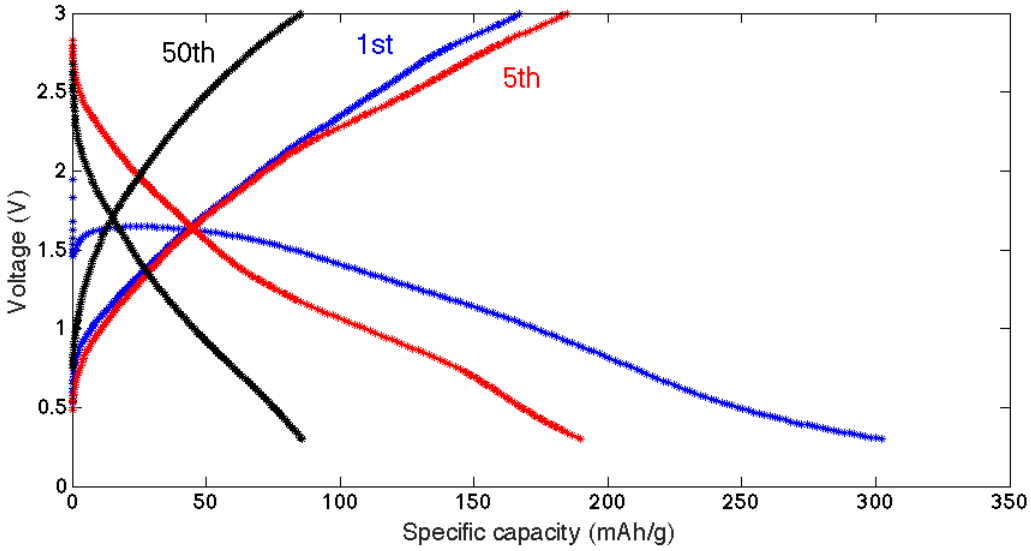

Figure 7.9: Charge-discharge voltage profile for 230nm nanowires battery at 2C

7.1.1.2.b 40 nm Batteries

During the first charge on 40 nm batteries, no very marked plateau is present. It is more like a slope during nearly the whole discharge process starting from 1.7 V to 0.6 V. The slope is higher when increasing the number of cycles. This slope is the results of pseudocapacitive effects which are more important because of the higher surface to volume of the 40 nm nanowires. This leads to hiding the lithiation plateau of the nickel oxide. A component of the big slope is also the SEI formation which is more visible because of the higher surface area.

The rest of the behaviours and the potentials associated to them are similar to the ones characterising the 230 nm nanowires.

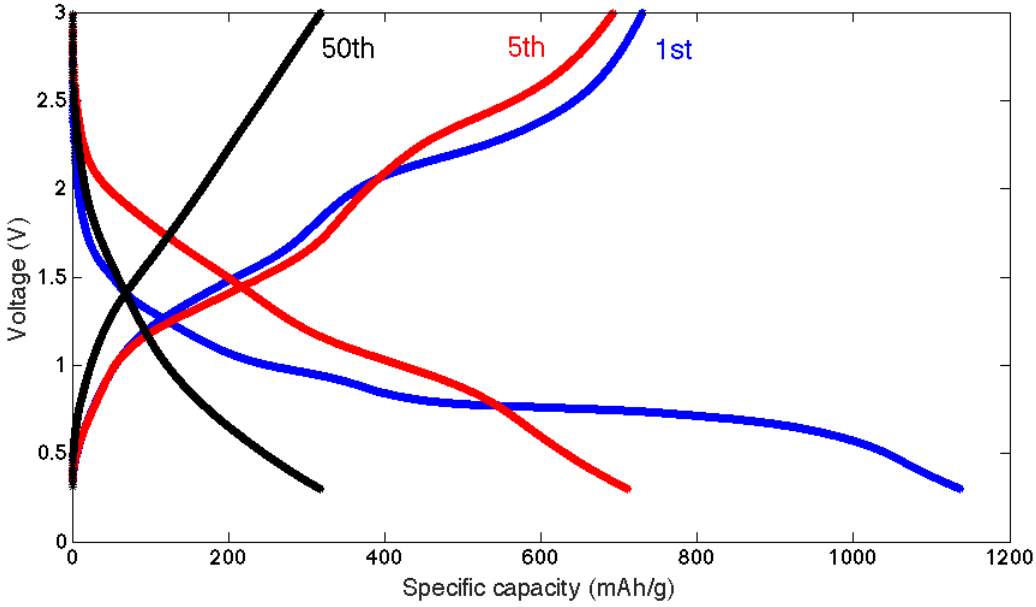

Figure 7.10: Charge-discharge voltage profile for 40nm nanowires battery at C/7

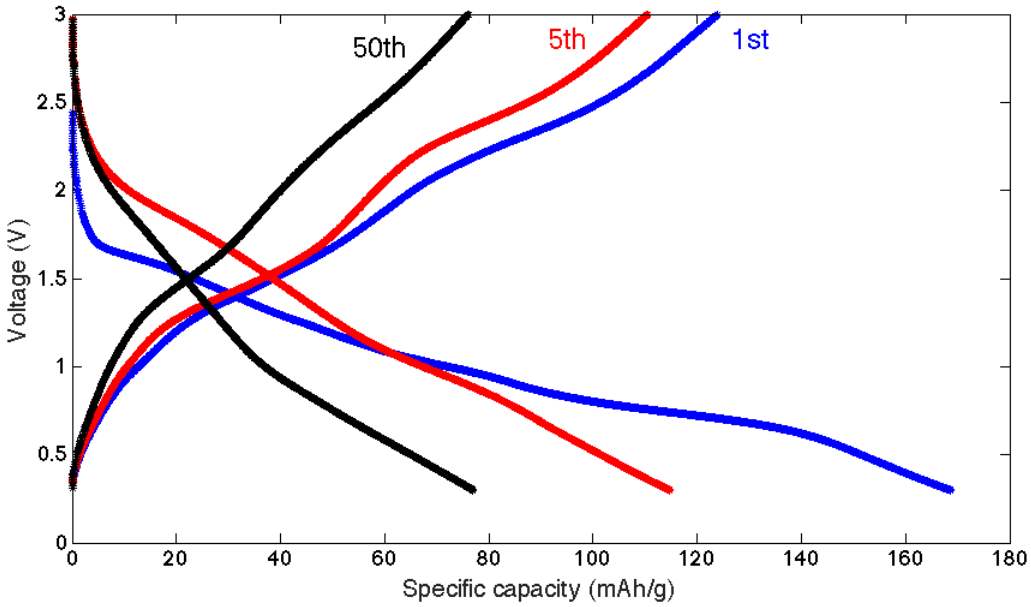

Figure 7.11: Charge-discharge voltage profile for 40nm nanowires battery at C/2

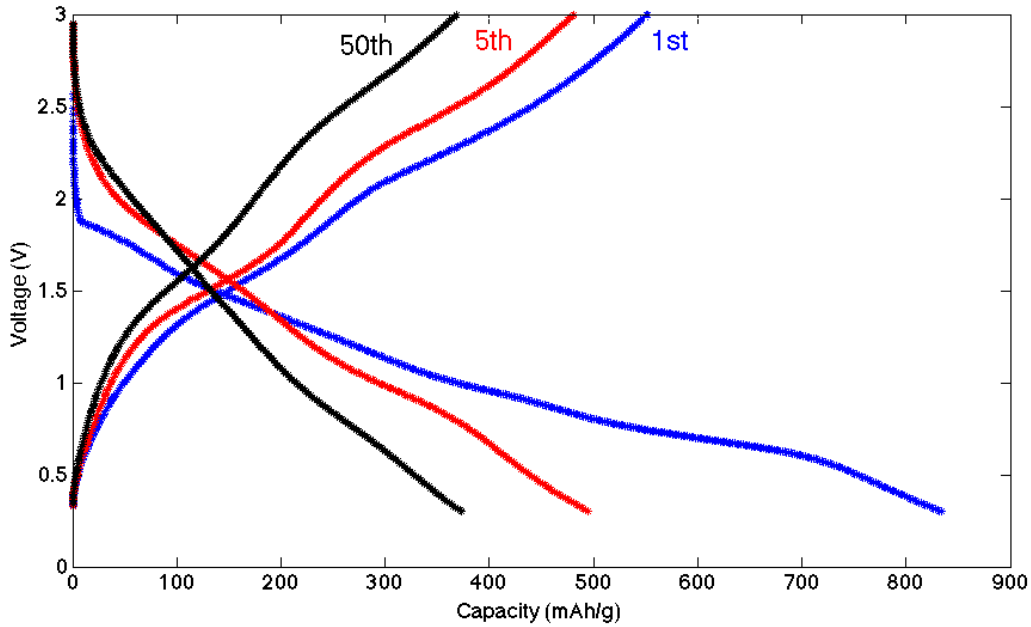

Figure 7.12: Charge-discharge voltage profile for 40nm nanowires battery at 2C

Comparison between 230 and 40 nm

The behaviour of the 230 nm nanowires is very similar to the submicrometer-sized particles studied in [13]. Conversely, the 40 nm nanowires are closer to the nanometer-sized particles. This behaviour is quite logical given the diameter of the nanowires.

230 nm nanowires have a higher specific capacity per mass at the beginning of the cycling test but tend to lose in capacity much faster than their 40 nm counterpart. This behaviour has again been verified in [13]. Also, all the plateaus are more marked for the 230 nm nanowires.

The potential at which the lithiation of the nickel oxide occurs indicates that such electrodes will be more efficient as cathode material in full-cell configuration in future batteries. Indeed, the more the discharge potential is low compared to Li/Li^+, the lower the difference in potential between the electrode being tested and the anode (the Li metal in this case).

7.1.1.2.c 230 nm Battery Cycled Between 0.01 V and 3 V

To observe the behaviour occurring during the lithiation of silicon, one battery has been cycled between 0.01 V and 3V as can be seen on figure 7.13. The specific capacity increase with cycle number but further cycles probably show the same behaviour as 230nm batteries cycled between 0.3 V and 3 V. A surprising fact is that the specific capacity is lower than the batteries tested without lithiation of silicon. This is a quite surprising result since, as said previously in the report, silicon possess a very high specific capacity. The lithiation of it would normally lead to a much greater specific capacity. However, on figure 7.14, it can be well seen that a new plateau at about 0.05 V appears during the first and fifth discharge steps. This is supposed to be due to a conversion reaction between lithium with one the component of the substrate. By comparing the literature, it appears that the silicon is the one being lithiated. Indeed, this phenomenon has been discovered to occur from 0.3 V but is really strong at 0.1 V. Taking into account that an overpotential often need to be applied since we are not in ideal conditions, this explains the plateau at 0.05 V on the graph. A new plateau at about 0.5 V during charge describes the delithiation of the silicon. It has been found that the delithiation of silicon occurs between 0.37 V and 0.62 V confirming our results[17].

Further discharges show the same increase in the potential of the major plateau concerning the reduction of the nickel oxide found previously.
The plateaus related to the lithiation and delithiation of silicon conserved, however, the same potential.

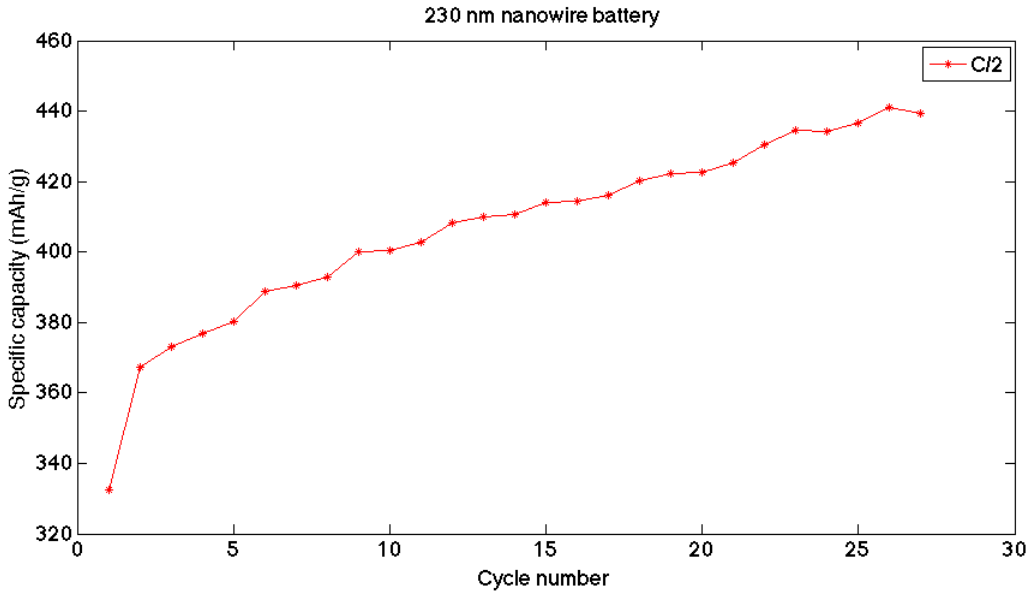

Figure 7.13: Galvanostatic charge-discharge cycles of 230 nm nanowires batteries to lithiate the silicium

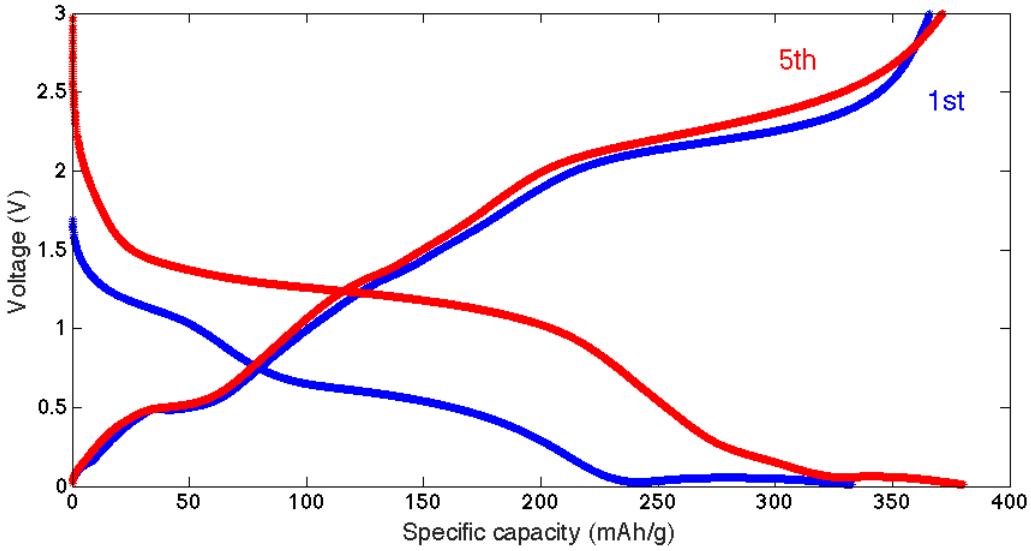

Figure 7.14: Galvanostatic charge-discharge cycles of 230 nm nanowires batteries to lithiate the silicium

Battery with 230 nm nanowires with different cycles rate

One battery has been made to observe the specific capacity of related to different cycle rates on the same battery. The cathode is made of 230 nm nanowires. A sequence of C/7, C/2, C, and C/2 has been done twice and finished by a speed of C/2. The different rates can be easily distinguished on the graph by the presence of several plateaus in the specific capacity in the first sequence on figure 7.15. When the C-rate becomes higher, the specific capacity decreases. This is consistent with the literature[12] and with the previous results obtained with the batteries tested each at one specific rate. When the rate come back at C/7, one can observe that the specific capacity returns nearly at its value from the previous cycles at the same speed. This shows that the kinetics effect occurring in the batteries are mostly reversible. However, for the rates at C/2, C and 2C, the specific capacity is lower during the second time, and the plateaus are no more present and become slopes indicating a faster decrease of the performance. This shows the effect of higher C-rate on the performance's fade, which is greater than at low C-rate speed making it impossible to recover the previous capacity of a lower C-rate cycle after some higher C-rate cycles.

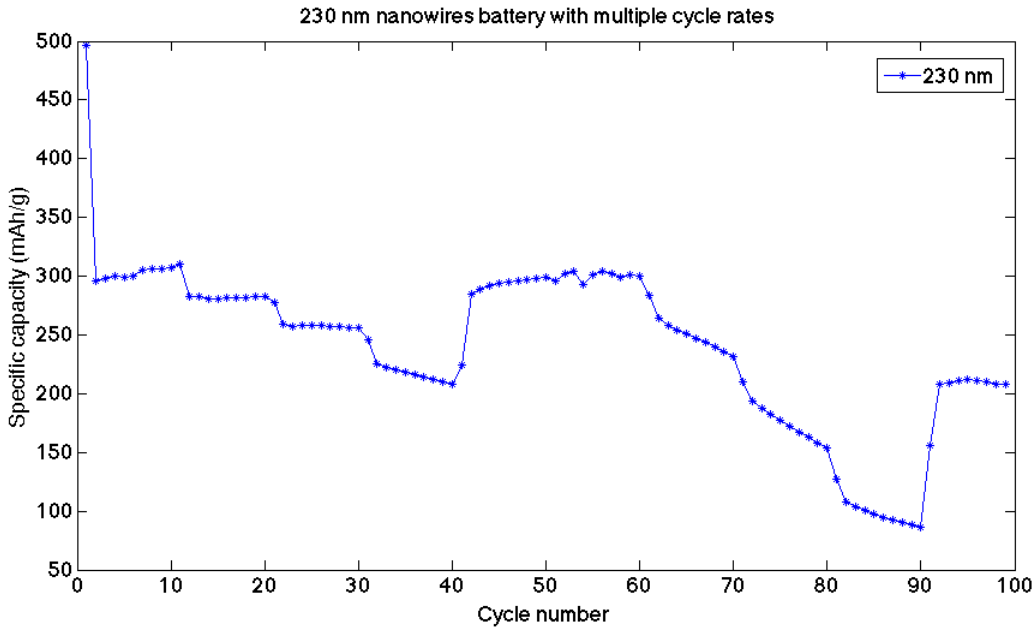

Figure 7.15: Galvanostatic charge-discharge cycles of 230nm nanowires batteries with multiple rates

7.1.2 Electrochemical Impedance Spectroscopy

7.1.2.1 Batteries Without Nanowires

The batteries based on the 2D NiO film shows a lower resistance than the batteries composed nanowires electrodes. This can be explained by the fact that carbon black is conductive. Nickel oxide on the other hand is semi conductor and therefore less conductive.

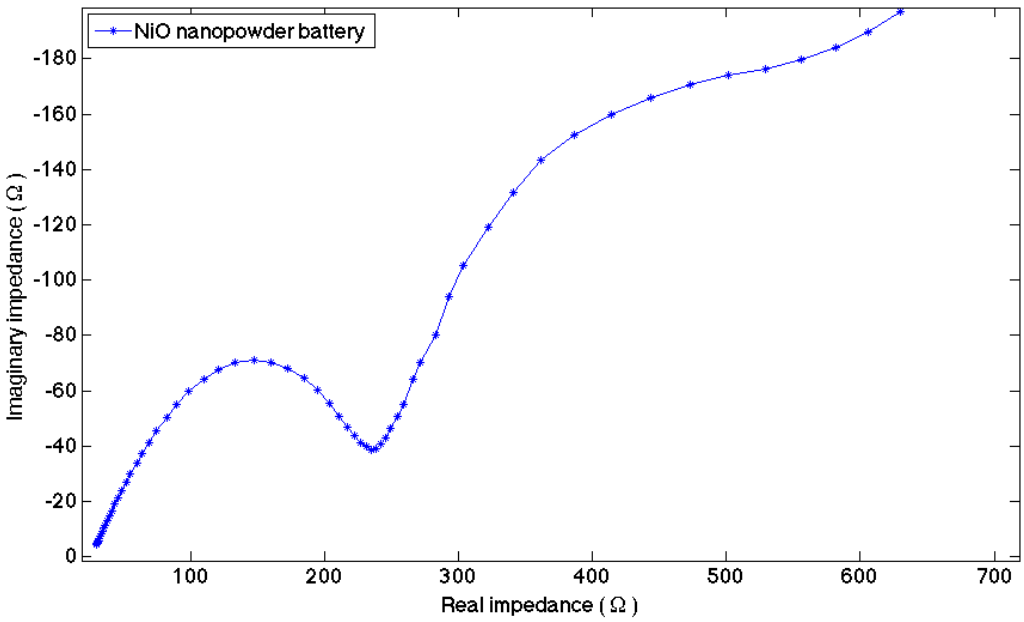

Figure 7.16: EIS test after cycling on the NiO film battery

7.1.2.2 Batteries With Nanowires

The batteries tested at a C-rate 4C show a higher film resistance of the SEI since the tail present in the low frequency, representing the diffusion mechanism within the electrolyte and active material regime, is shifted towards lower real impedance. This battery also shows a faster kinetic reaction behavior by having its real impedance shifted toward lower values. The battery tested at a C-rate of C/7 show a beginning of tail which has a lower slope than the two others. This is the consequence of larger active material particles. This could be explained that, at low C-rate, the oxidation of the metallic nickel is slower and has, therefore, the possibilities to grow bigger particles.

Also, this battery showed the lowest resistance which is consistent with galvanostatic charge and discharge cycle that revealed that this battery has the best specific capacity. If the resistance decrease, the specific capacity increase, this is thus verified for all 230 nm nanowires tested batteries.
This relation is however not checked for the 40 nm nanowires batteries.

The EIS test, conducted on the battery cycled between 0.01 V and 3 V, showed the same characteristic as previously explained. No new behaviour occured.

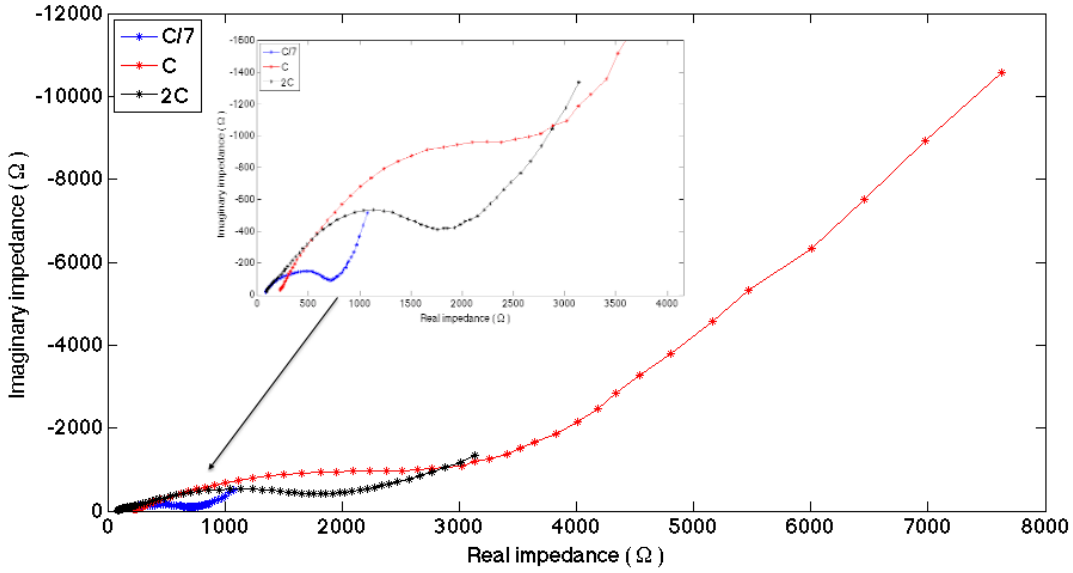

Figure 7.17: EIS test after cycling on 230 nm nanowires batteries at different speed

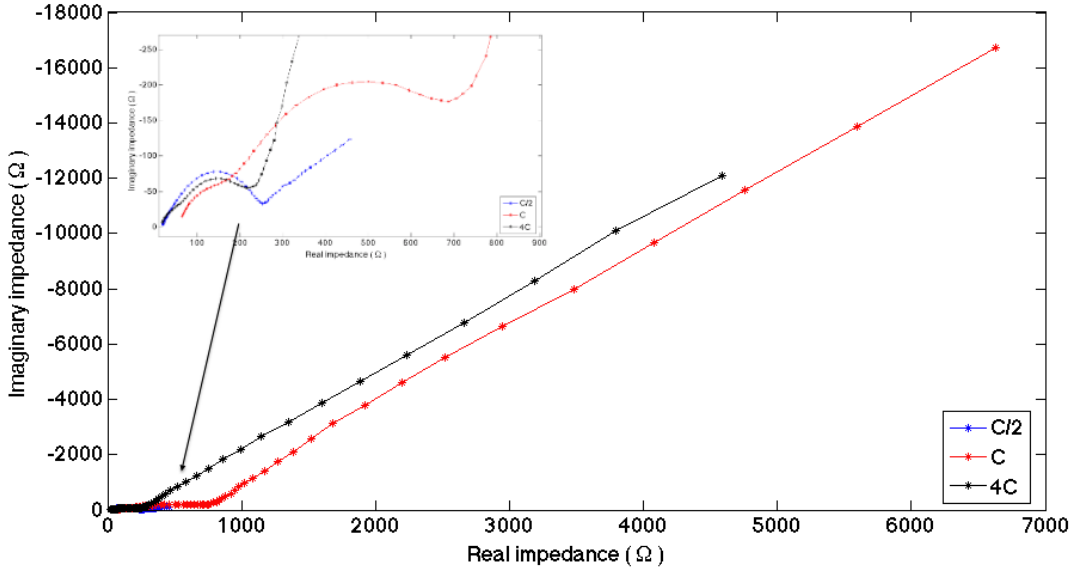

Figure 7.18: EIS test after cycling on 40 nm nanowires batteries at C/2, C and 4C

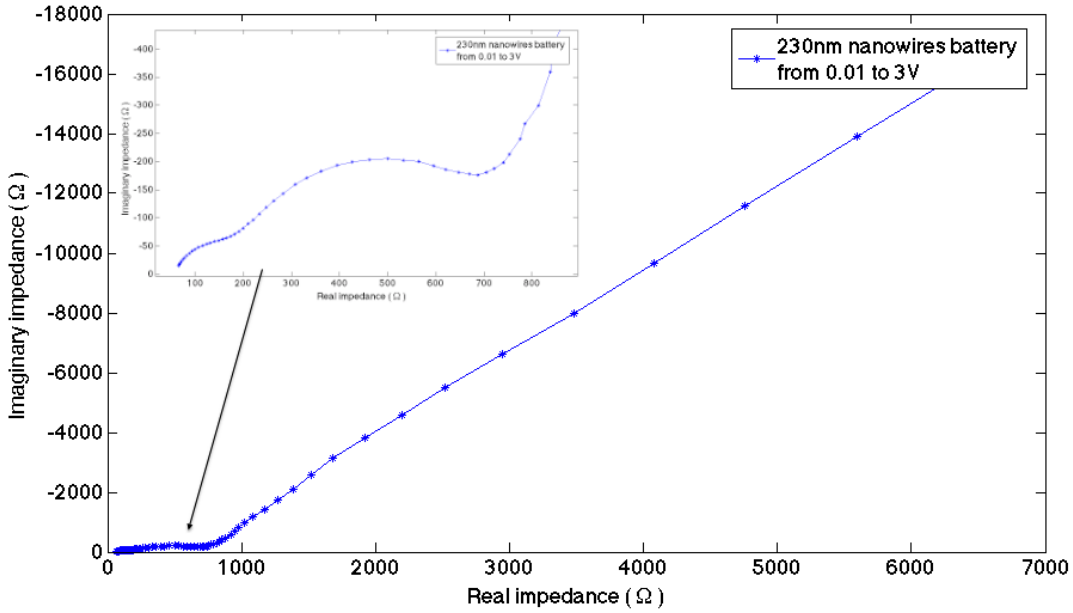

Figure 7.19: EIS test after cycling of the 230 nm nanowires battery cycled from 0.01 V to 3 V

Chapter 8

Supercapacitor Performance Testing

8.1 Electrochemical Characterisation

8.1.1 Without Nanowires

8.1.1.1 EIS

An EIS test has been conducted on the supercapacitors with the Cu substrate and with $Na2SO4$ and KOH as electrolyte before and after the charge-discharge cycles. Unfortunately, no usable information have been obtained from the EIS test before the charge-discharge cycles since no clear trend could be extracted from the data. The tests before annealing have been conducted twice on the same supercapacitor but removing it from the EIS and connecting it again result, in both cases, to the same unusable result. However, as it will be seen in section 8.1.1.2, these supercapacitors were functional. Therefore, the most plausible explanations on these incorrect measurements are a bad electrical contact between the supercapacitor and the EIS device or the EIS which was defective. As seen on Figure 8.1 to Figure 8.2, the results were random.

Another EIS test has been conducted on the same samples after cycling test leading to a more reliable result as seen on figures 8.3 and 8.4.
In the case of the supercapacitor with Na_2SO_4, a lower slope in the low-frequency region means a higher pseudocapacitive behavior than for the KOH(See figure 8.2). Also, this supercapacitor shows faster charge transport because of the shift of the high-frequency regime to the lower values of real impedance.

In the case of the supercapacitor with KOH, one can see a large two semi circle in the high frequency regime and a straight line in the low frequency regime. This means that the supercapacitor has a blocking behaviour at high frequency and a capacitive behaviour at low frequency[19].

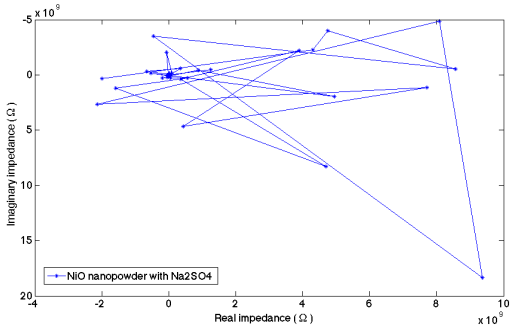

Figure 8.1: EIS test conducted on the supercapacitor made of NiO film with Na2S04 electrolyte before cycling test

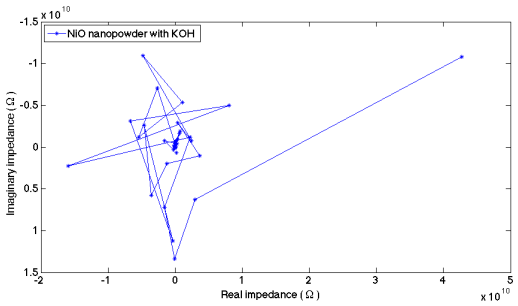

Figure 8.2: EIS test conducted on the supercapacitor made of NiO film with KOH electrolyte before cycling test

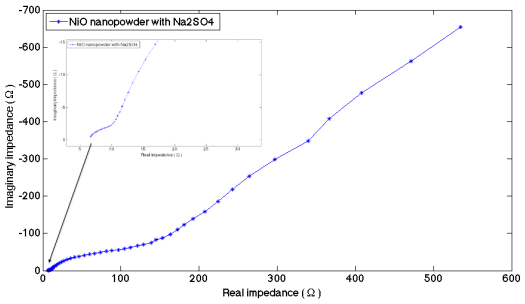

Figure 8.3: EIS test conducted on the supercapacitor made of NiO film with Na2S04 electrolyte after cycling test

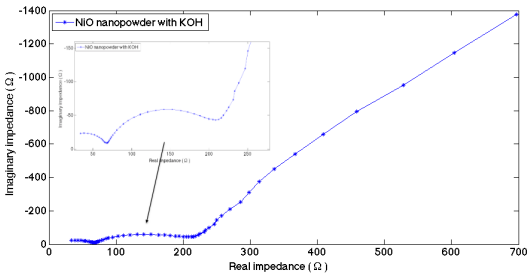

Figure 8.4: EIS test conducted on the supercapacitor made of NiO film with KOH electrolyte after cycling test

8.1.1.2 Galvanostatic Charge and Discharge Test

The reference supercapacitors made of Na_2SO_4, H_2SO_4 and KOH have been tested. These supercapacitors are references because the choice of the electrolyte for the supercapacitor made with nanowires depends on the results obtained during cycling of the references supercapacitors. All supercapacitors have been tested under a constant current of 0.1 mA/cm^2 between -0.2 V and 0.8 V for the ones with Na_2SO_4 and H_2SO_4 like in[18], and between -0.1 V and 0.2 V for the one with KOH as in [19]. The performance of supercapacitors is often expressed in term of specific capacitance per mass F/g. To convert the data obtained from the galvanostatic charge and discharge test that are expressed in mAh/g into F/g which is the unit used in the graphs of this section, the use of equation 8.1 is useful. During this work, all the data were expressed in mAh/g to be consistent with the units used for the batteries.

$$F = \frac{I \times T}{V \times m} \tag{8.1}$$

$$with \begin{cases} \text{F} & \text{The specific capacitance in F/g} \\ \text{I} & \text{The discharge current in amps} \\ \text{T} & \text{The discharge time in second} \\ \text{V} & \text{The discharge voltage in volts} \\ \text{m} & \text{The active material's mass} \end{cases}$$

8.1.1.2.a Na_2SO_4 Supercapacitors

On figure 8.5, one can see the variation of the specific capacity of two supercapacitors having Na_2SO_4 as the electrolyte. The blue curve is the one corresponding to the supercapacitor having its electrodes made of the film of NiO coated on copper. The red one corresponds to the same kind of supercapacitors but with aluminium instead of copper. The mass of active material on one electrode is 3.16 mg for the first and 4.63 mg for the second.

The specific capacity of the sample on Cu dropped rapidly during the first 30 cycles. This decrease is the signature of a chemical reaction that destroys the sample. This reaction is believed to be a reaction of Na_2SO_4 with copper that stopped after some cycles when a new layer has been formed on the copper metal protecting it from further degradation. After these 30 first cycles, a steady equilibrium seems to be reached leading to a nearly constant capacity of about two mAh/g with the number of cycles.

The behavior is completely different for the sample made with aluminium. Indeed, the capacity rises for the ten first cycles then decreased for about 70 cycles to the same specific capacity than the sample made with copper. After that, the specific capacity dropped severely to reach a value close to zero. A reaction of Na_2SO_4 and aluminium is suspected to be the cause of that. On figures 8.6 and 8.7, one can see the presence of an inflection in the charging curve at about 0.7V leading to the conclusion that a redox reaction occurs. This redox reduction correspond to the Ni(II)/Ni(III) redox process[18].

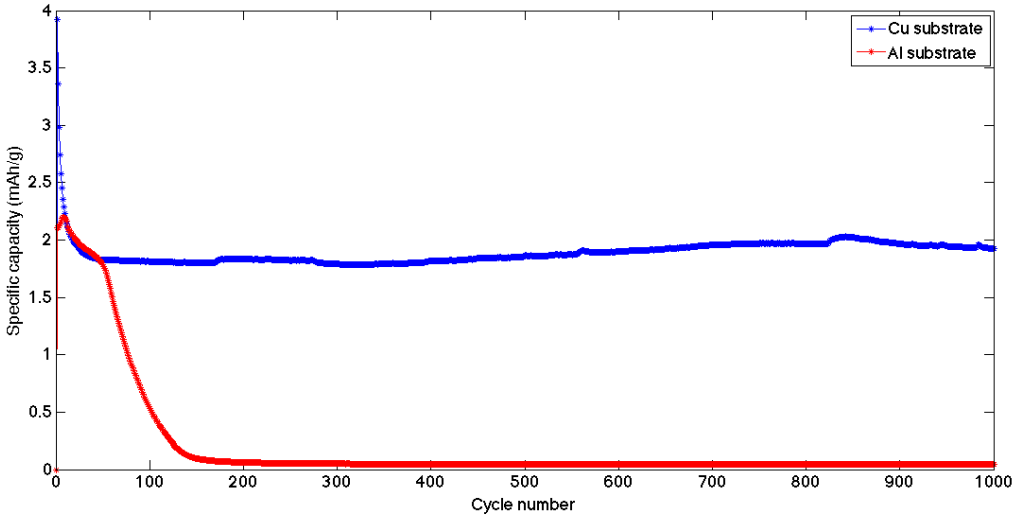

Figure 8.5: Galvanostatic charge-discharge cycles of NiO film symmetrical supercapacitors with Na2SO4 electrolyte

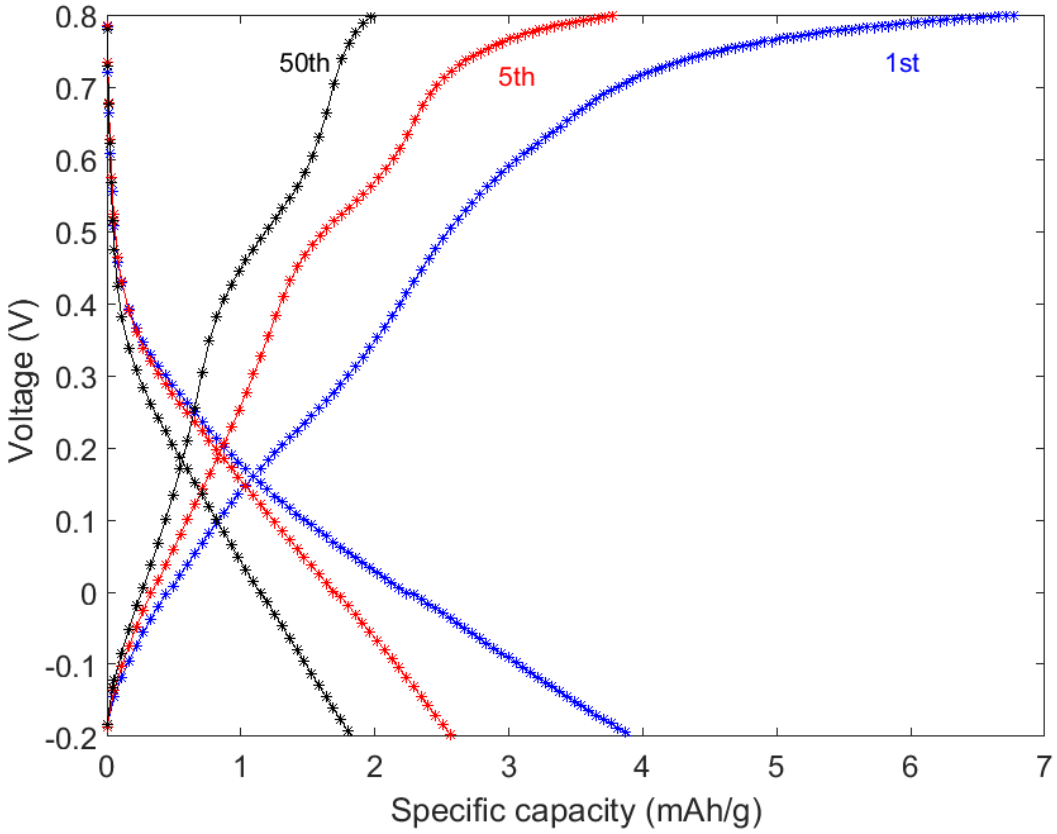

Figure 8.6: Voltage profile of the cycle test made on the supercapacitors with the NiO film on copper and Na2SO4 as electrolyte

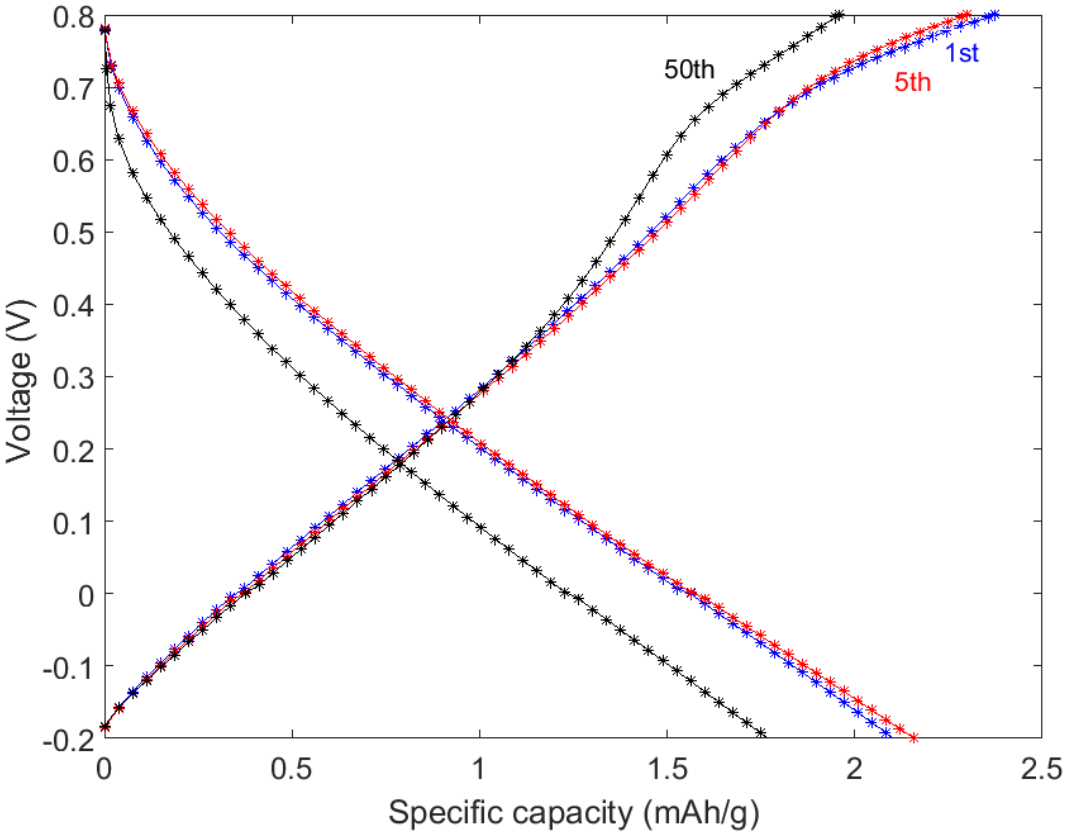

Figure 8.7: Voltage profile of the cycle test made on the supercapacitors with the NiO film on aluminium and Na2SO4 as electrolyte

8.1.1.2.b H_2SO_4 Supercapacitors

The second kind of reference supercapacitors that have been tested are the ones with H_2SO_4 as the electrolyte. As for the reference supercapacitors with Na_2SO_4, one has been done with copper and the other with aluminium as a substrate for the film. The mass of active material on the first electrode is 5.23 mg. For the second, the test did not work potentially due to the following equation:

$$Cu + 2H_2SO_4 \rightarrow CuSO_4 + SO_2 + 2H_2O \tag{8.2}$$

The other supercapacitor made with aluminium succeed better. It has a lower specific capacity than Na_2SO_4 based supercapacitors of 0.4 mAh/g to about 0.1 mAh/g from the first to the 1000th cycle More irregularities in the variation of the specific capacitance with the cycle number are also present.

The voltage profile of the supercapacitor made with aluminium and H_2SO_4 electrolyte show a strong redox reaction during charge a about 0.72V also attributable to the Ni(II)/Ni(III) redox process. Also, the rest of the graph is not linear indicating a pseudocapacitance effect.

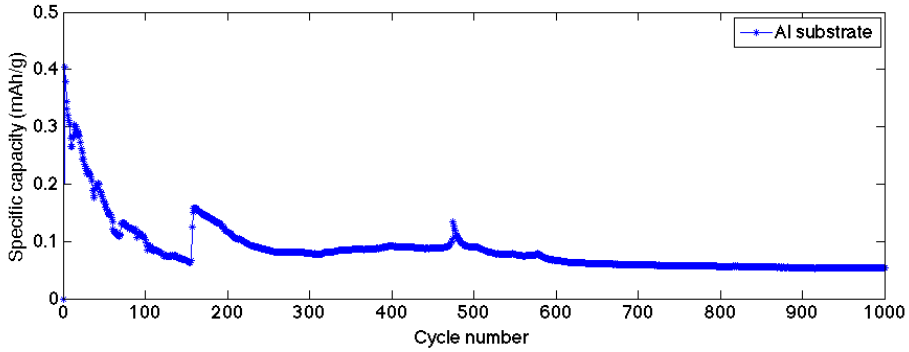

Figure 8.8: Galvanostatic charge-discharge cycles of NiO nanopowder symmetrical supercapacitors with H2SO4 electrolyte

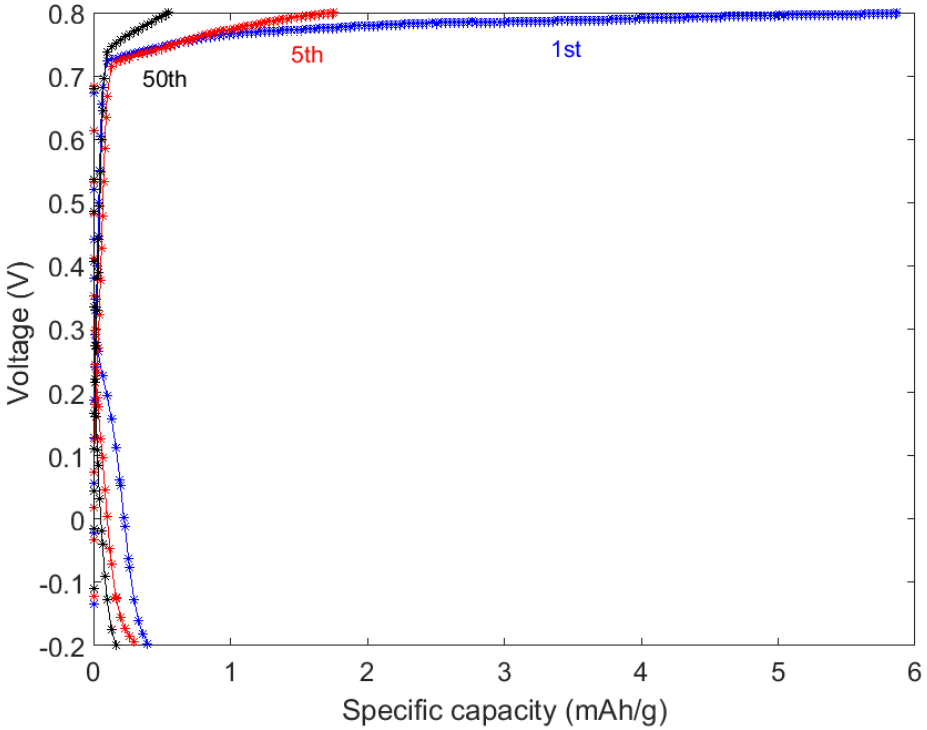

Figure 8.9: Voltage profile of the cycle test made on the supercapacitors with the NiO slurry on Aluminium and H2SO4 as electrolyte

8.1.1.2.c KOH Supercapacitor

The last reference supercapacitor to be tested was the one with KOH as electrolyte and Cu as a substrate for the electrode. The mass of active material was 2.2 mg. As seen on figure 8.10, the specific capacity dropped from about 30 mAh/g to 6 mAh/g. The fast decrease, in the beginning, is due to the corrosion of copper by KOH into copper hydroxide as seen on equation 8.3 and visible on figure 8.11. The formation of this layer of copper hydroxide is supposed to protect the copper film from further corrosion. The opening of the cell would have corroborated this supposition if the surface of the copper was blue because it is the color of copper hydroxide. This reaction only occurs during the first four cycles, as seen in the decrease of specific capacity on

figures 8.10 and 8.11. This reaction can be seen by the presence of plateaus in the charge and discharge curve of the first charge-discharge cycle at 0.3 V and 0.1 V respectively.

$$Cu + KOH = Cu(OH)_2 + K \tag{8.3}$$

Also, the rest of the graph is not linear indicating a pseudocapacitance effect.

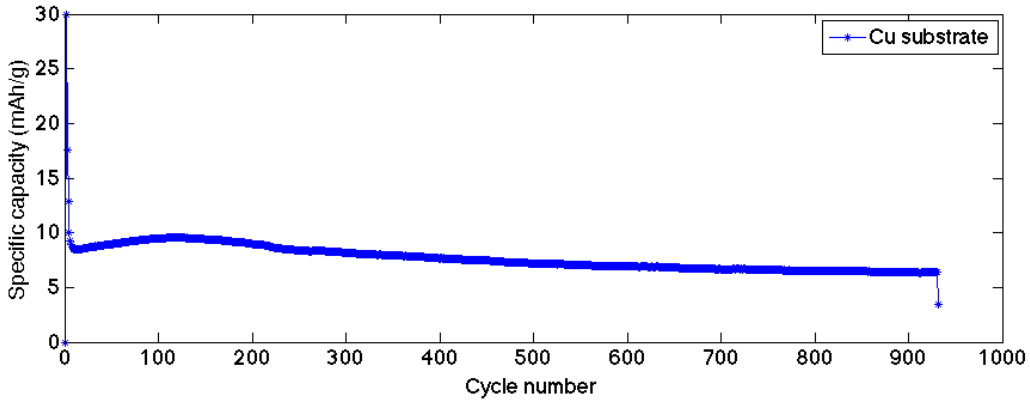

Figure 8.10: Galvanostatic charge-discharge cycles of NiO nanopowder symmetrical supercapacitors with KOH electrolyte

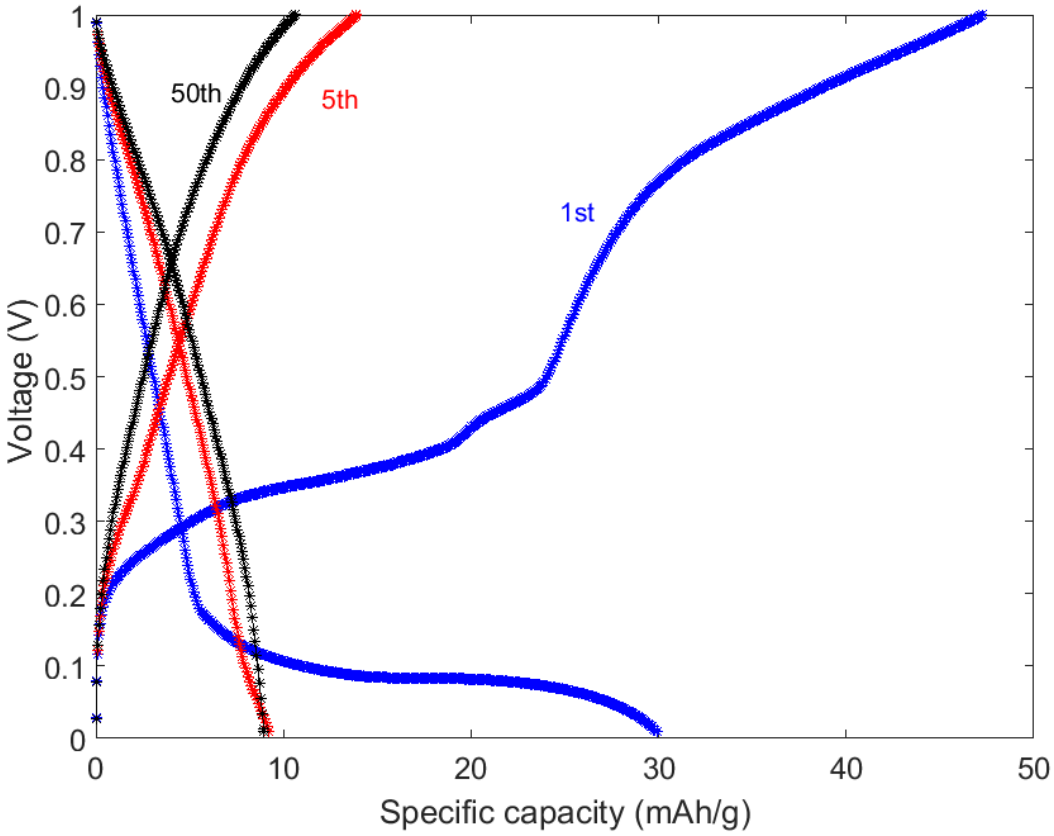

Figure 8.11: Voltage profile of the cycle test made on the supercapacitors with the NiO film on Aluminium and KOH as electrolyte

8.1.1.3 Cyclic Voltammetry

The cyclic voltammetry on the supercapacitor made with Na_2SO_4 shows an anodic current peak at 0.6 V to 0.7 V with increasing scan rate. There is also a cathodic current peak at about 0.2 V due to the Ni(II)/Ni(III) redox process. This anodic current had been detected by the galvanostatic charge and discharge test but not the cathodic current.

The cyclic voltammetry of the supercapacitor made of KOH shows a large current separation with a mirror image. This behaviour is characteristic of a capacitive behaviour.
The horizontal lines present in the graph are due to a limit current issue. Indeed, for lower scan rates, to obtain a better precision during the cycles, the limit current has been limited to a little more than 1 mA. However, it appears that the current exceeded this value leading to this horizontal behaviour. On figure 8.13,

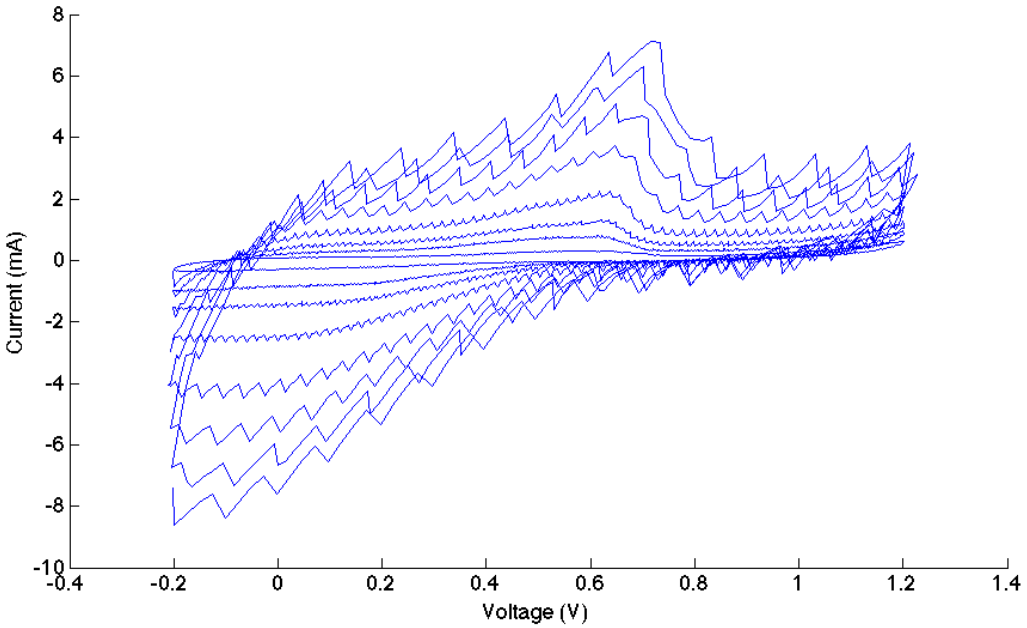

Figure 8.12: CV of the NiO film with Na2SO4 supercapacitor

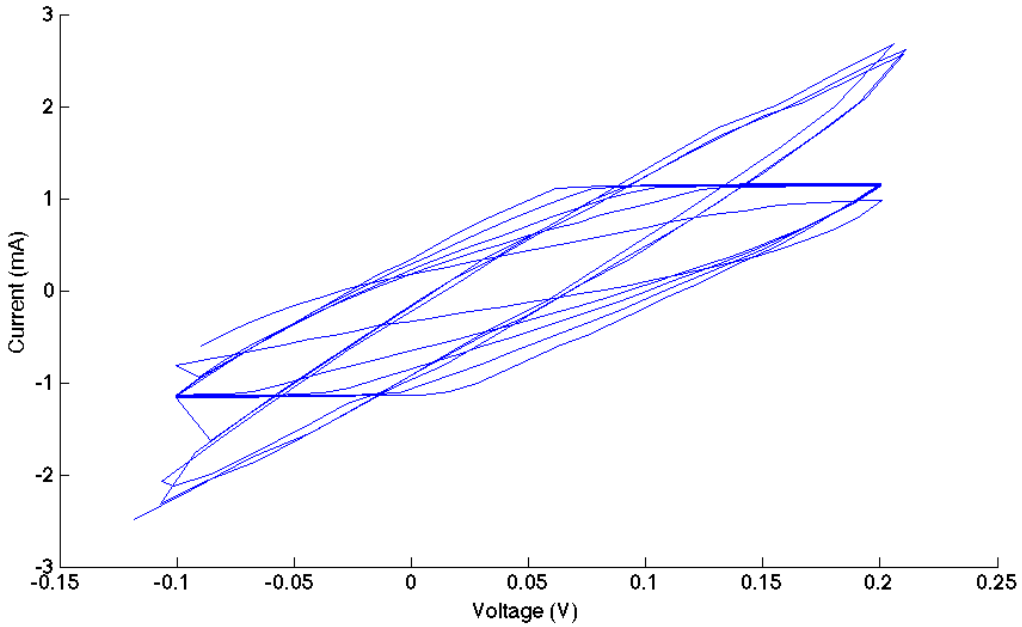

Figure 8.13: CV of the NiO film with KOH supercapacitor

8.1.2 With Nanowires:

Given the obtained results of the supercapacitors without nanowires, it has been decided to do supercapacitors with nanowires with Na_2SO_4 and KOH.

A problem occurred after the fabrication of the supercapacitors using KOH electrolytes. These expand and were destroyed after a few days after the fabrication and before the test. After looking which could be the cause of this, the answer has been found. KOH is corrosive for silicon and silicon dioxide[100]. Therefore, no useful data has been obtained since no test has been able to be performed.

8.1.2.1 EIS

The EIS test of the supercapacitor made of 40 nm nanowires and Na_2SO_4 unexpected results as can be seen in Figure 8.14.

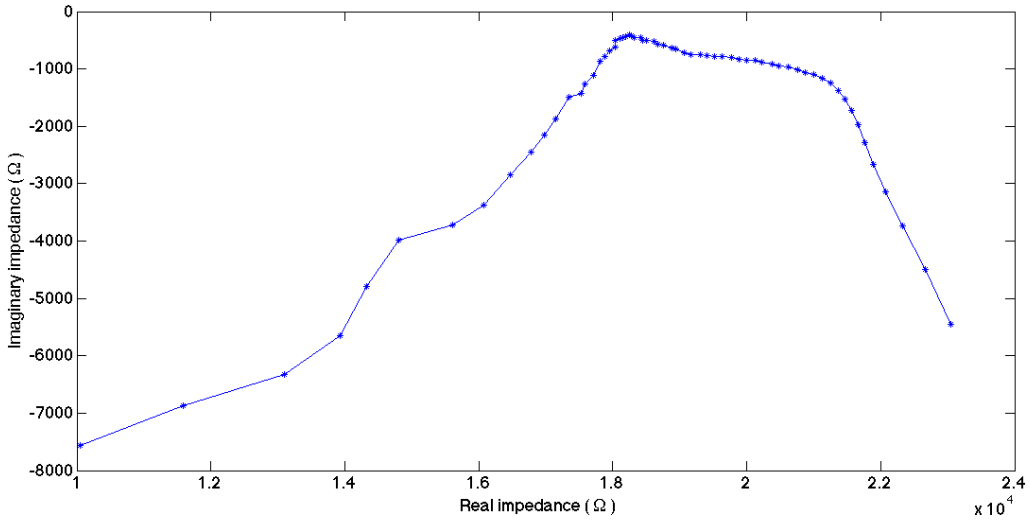

Figure 8.14: EIS graph of the supercapacitor made with 40 nm nanowires and with Na2SO4 as electrolyte

8.1.2.2 Galvanostatic Charge and Discharge

A galvanostatic charge and discharge test has been done on this supercapacitor. However, it appears that the test was far too fast, even if the same current density of 0.1 mA/cm^2 has been used. The result was only composed of straight lines that didn't give any detail about the chemical reactions occurring inside the supercapacitor. This test, in addition to not being conclusive, has been hard to start since the voltage rapidly exceeds the safety voltage limits that are however larger than the voltage range of cycling of the supercapacitor.

8.1.2.3 Cyclic Voltammetry

No useful information have been obtained from the from the CV test on the supercapacitor made of 40 nm nanowires with Na2SO4 electrolyte. As seen on figure 8.15, the plot is not smooth, and it seems that the precision of the graph is not sufficient, since all the points are aligned on different equidistant current values. More points have therefore been selected but the same result appears.

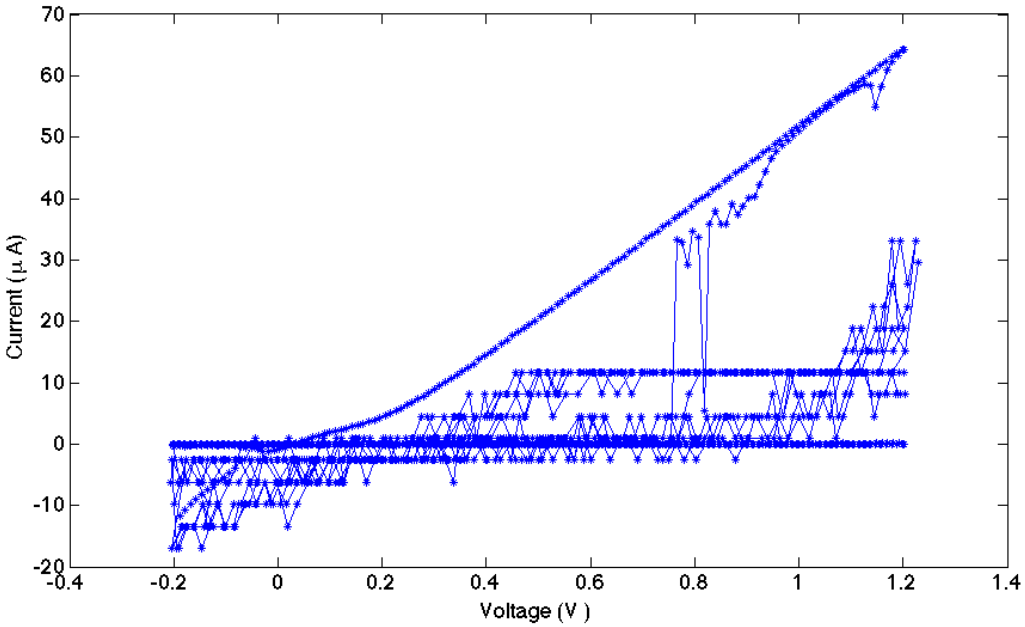

Figure 8.15: CV of the 40 nm nanowires with Na2SO4 supercapacitor

Chapter 9

Interdigit Electrode

9.1 Morphological Characterisation

9.1.1 Optical Microscopy

An observation with an optical microscope has been done in first place to look at the general aspects of the made interdigit electrodes.

The first one, represented on Figure 9.1, has been done using a power of 50 % (about 1.9 W), with one passage on each area, an internal frequency of 200 kHz, a speed of 20 mm/s and an overlap of 7.5 μm. The second, presented on figure 9.2, has been made using a power of 20 % (about 0.72 W) 20 passages on the same area, a frequency of 40 kHz, a speed of 200 mm/s and an overlap of 5 μm.

On the first one, one can see a horizontal line on the right. This line is an error during the laser use. A previous design composed of a straight line used to test the cut of nanowires and the surface of the substrate has not been changed, and instead of etching the surface with the right design shown on Figure 4.8, this straight line has been done. The process has been rapidly stopped, but since the process is extremely fast, the damaged was already done. However, this was the opportunity to test the power and number of passes needed to obtain a good result for the good design. It appears that the power used for this etching was too high. Indeed, one can see that some nanowires present on the side of the etched ares were destroyed. Also, in some unetched part of the electrode where nanowires are present, these do not stick on the platinium surface anymore. Also, a strange structure appeared on the two big vertical lines. These strange structures are supposed to be silicon that, under the powerful laser, sublimated and solidified itself into other shapes.

To avoid these imperfections, the power of the laser has been decreased to 20 % and 13 passes. These parameters come from a previous test done by Vivien Vandenkerckove at UCL. The result is shown on figure 9.2. On this one, one can see that the result is much better than the first one. Fewer nanowires were destroyed and the etching seems to be more homogeneous. The four places of different colors at the extremities of the large vertical etched zones were added to extend these zones because the silicon substrate was a bit longer than expected and the AutoCAD design was therefore too small.

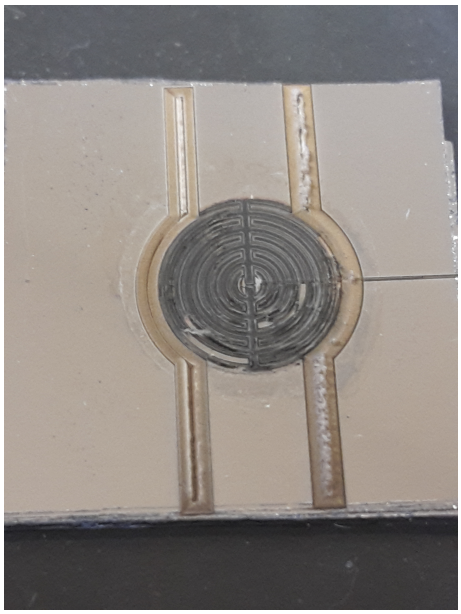

Figure 9.1: Picture of an interdigit electrode after its fabrication and before the annealing

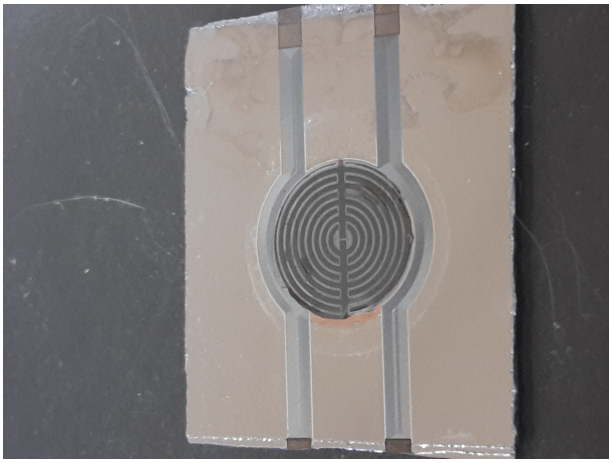

Figure 9.2: Picture of another interdigit electrode after its fabrication and before the annealing

9.1.2 SEM

SEM analysis have then been made on the previous interdigit electrodes to better charaterise their morphology. All the SEM analysis have been made on the interdigit electrode shown in figure 9.2

SEM images of the sample from figure 9.2 with nanowires of 230 nm in diameter has been done before its annealing. On figures 9.3 and 9.4, one can see two types of defect that occurred after the laser cutting. On Figure 9.3, one can observe that a part of the nanowires does not stick anymore on the substrate but that there are still present thanks to the facts that it is an interconnected structure that holds the nonfixed nanowires. On Figure 9.4, it can be seen that an entire strip has disappeared. It can be assumed that several factors taken simultaneously can be the reason:

- Too high number of detached nanowires
- Little width of one strip: By enhancing the width of one strip, it could be mechanically more stable because more nanowires are attached to the substrate. A side effect of this would be less interlacement between the two electrodes.
- Edge effect coming from the fact that during the deposition, a rubber band is disposed on the polycarbonate ring to prevent the leak of the electrolyte. This ring pushed on the polycarbonate making it stick a bit on the polycarbonate after each electrodeposition. The detachment of the rubber from the substrate-nanowires surface, and therefore, the slight pull exerted on the polycarbonate is more than likely the principal cause of this destruction.

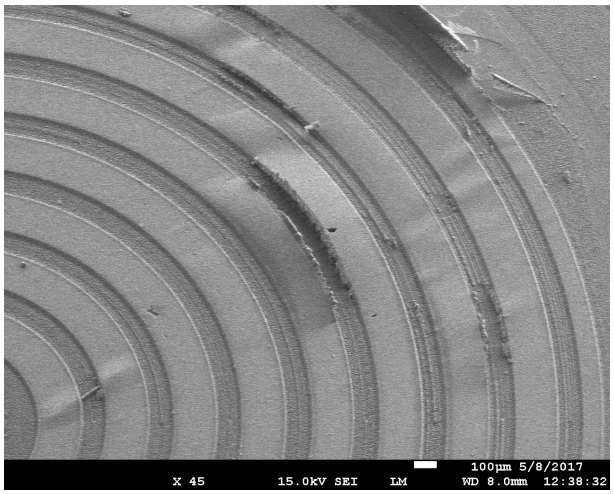

Figure 9.3: SEM picture of an interdigit electrode showing the partial detachment of some nanowires

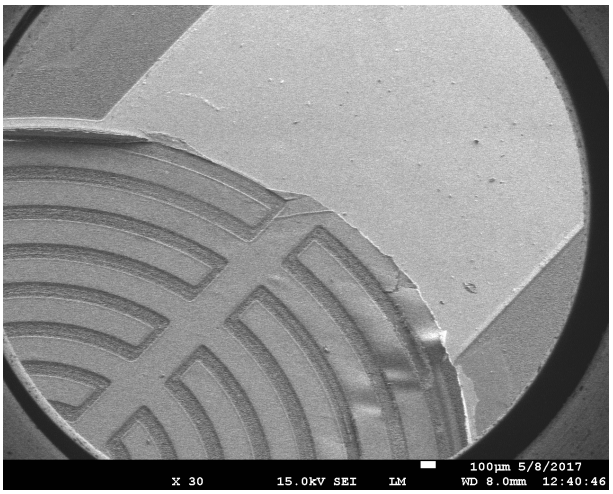

Figure 9.4: SEM picture of an interdigit electrode showing the destruction on an entire strip of nanowires

On figures 9.5 and 9.6, one can see two other kinds of problems that appeared. On Figure 9.5, it can be observed that a sort of little rod is present. This rod comes more than likely from a contamination of the surface before doing the electrodeposition since it can be seen that the nanowires in the extension of the axis of the rod are raised in comparison with the rest meaning that the bar is also present underneath them. Therefore, the nanowires came after and the contamination has preceded the electrodeposition. This contamination can be limited by cleaning the substrate before doing the electrodeposition. Also, this contamination is very unusual since it is the only sample in which this happened.
On figure 9.6, one can see the interface between the edge of the nanowires strip and the zone which has been etched by the laser. At this interface, nanowires seem to have melted. This melting is quite surprising since the picolaser second is designed to prevent such behaviour by vaporising the surface's material. The 3D nanostructure has thus been destroyed at these interfaces. This phenomenon could certainly be reduced using a lower power for the laser beam. The problem with this reduction will be a less efficient etching, and this will need more passes on the same zone from the laser that will maybe lead to the same or worst damages of the nanowires.

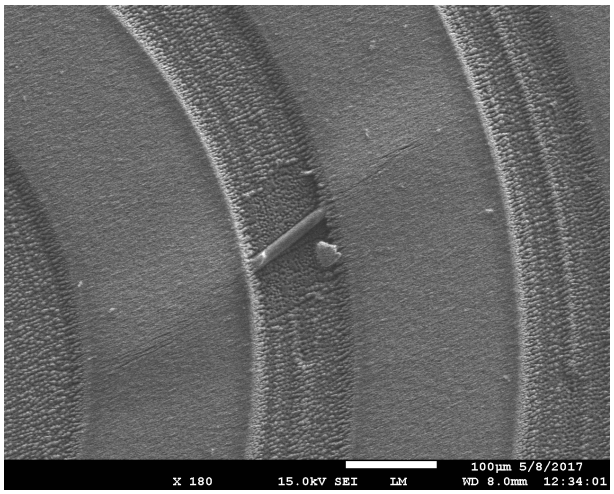

Figure 9.5: SEM picture of a contaminant that deposit before the electrodeposition

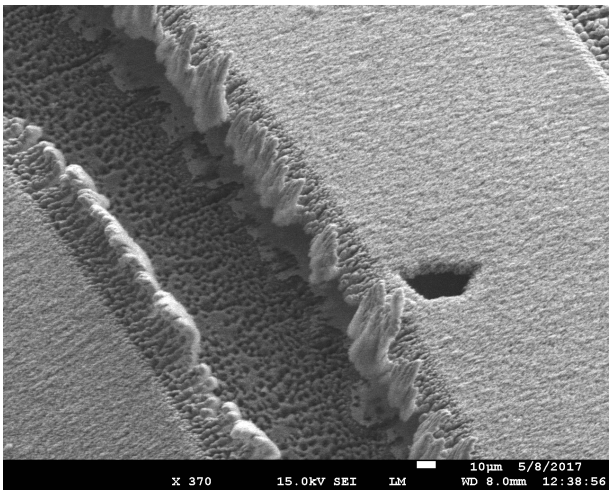

Figure 9.6: SEM picture showing the destruction of the nanowires on the edge of the laser etching zone

Figure 9.7 shows the width of the etched bands and the nanowires strips left intact. The width of the first one is of about 107 μm and the width of the nanowires strips of about 185 μm. These values are quite close to the theoretical values of the AutoCAD design, but it appears that the width of the bands etched by the laser is slightly larger than the 100 μm expected.

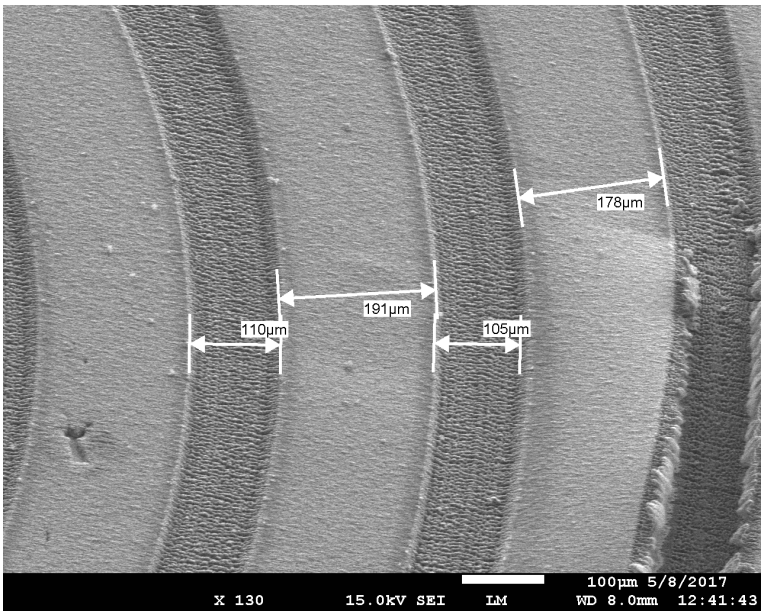

Figure 9.7: SEM picture of an interdigit electrode before annealing showing the width of the nanowires strips and etched bands

Figure 9.8 shows a SEM view of a place on the sample where nanowires detached from the substrate. The sample has been tilted in order to better see the place. One can well see the difference between the intact substrate and the etched substrate. The intact substrate is the one which is not etched by the laser according to the interdigit design.

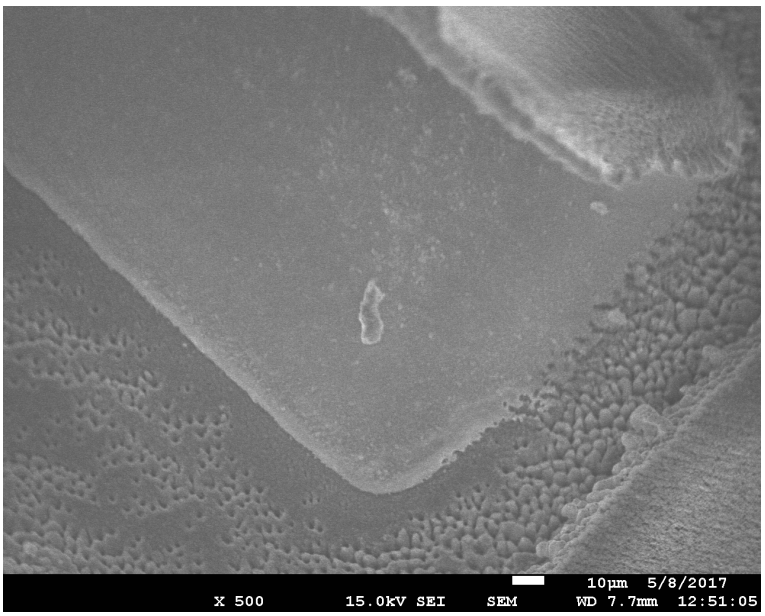

Figure 9.8: SEM view of detached nanowires, intact and etched substrate

Two SEM view have been done on the etched zone. The figure 9.9 shows the area inside the lateral zones. It can be seen that the surface is quite flat with the presence of holes, as well as the presence of more bright areas in some holes. These little holes are supposed to be the laser pulse impact on the surface. The figure 9.10 shows an area in the center of the interdigit design where the laser etched the surface and therefore the nanowires. One can see that the surface morphology is entirely different. This change can be explained by the presence of nanowires before the etching in the second case. Each round shape on this last is supposed to represent the base of one nanowire from the 3D interconnected structure. It appears that the nickel forming the nanowires was completely removed. This will be further developed in section 9.2.1 by an EDX analysis. The fact that the surface is not similar probably comes from the different topology of the surface of the substrate and the substrate + 3D nanowires. This means that the laser did not etch in the same way.

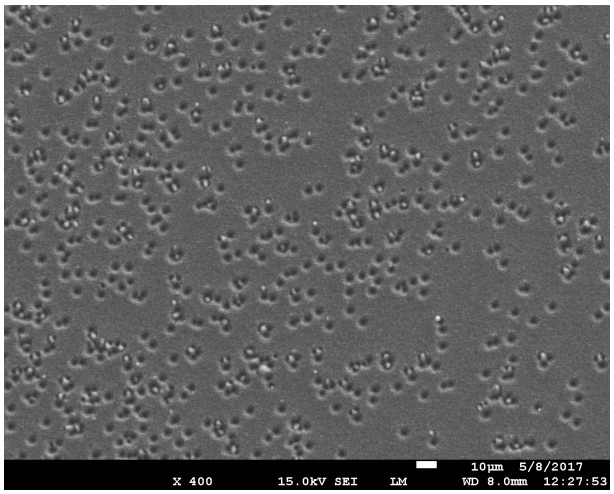

Figure 9.9: SEM view of the etched zone on the side (the two long etched zone).

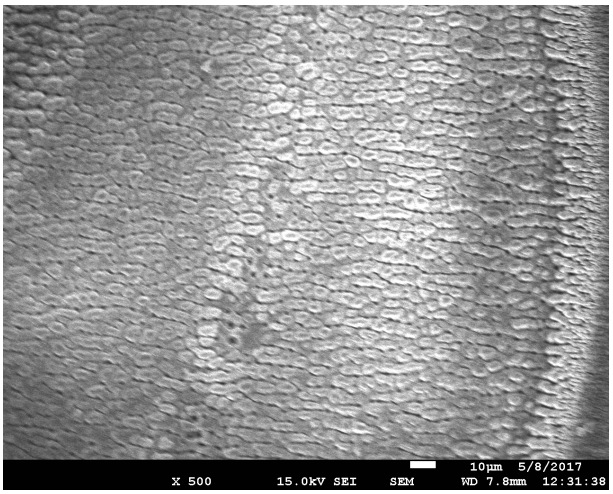

Figure 9.10: SEM view of the etched zone in the centre of the interdigit design

9.2 Chemical Characterisation

9.2.1 EDX

All the EDX analysis have been made on the interdigit electrode represented on figure 9.2.

EDX measurements have been done on two different places of the interdigit electrodes: In the large bands on the side of the electrodes (See table 9.1) and in the etched area in the middle of the interdigit design (See table 9.2). These measurements have been made to obtain the proportion of atoms present in these areas. These permits to see if the metal layers of the substrate and the nanowires have been etched by the laser. On both zones, there is the presence of carbon, oxygen, silicon, titanium, nickel, and platinium. The presence of the three last is the problem. Indeed, these atoms are electrically conductive and will prevent a good electrical isolation between the two electrodes. It appears that the presence of the nickel nanowires before etching lead to a different etching result. Indeed, nickel is still widely present in the second area as well as the platinium from the substrate surface. As can be seen, these two component composed a little more than 6% of the atoms composing the surface of this area and lead to a bad electrical isolation. The fact that nickel and platinum are still present lead to the conclusion that more passes will be needed or higher power to remove most of it. This will be discussed in section 9.4.

On the second zone, it appears that the etching was more complete since titanium, nickel,

and platinium only accounted for 0.32 % of the atoms present on the surface. The fact that the amount of nickel is not zero is because of the method of operation of the picosecond laser that consist, as explained in 4.5.1, to vaporise the surface's material. These vaporised particles can then fall back on others zones of the sample.

Concerning the other atoms, both zones contain about the same amount of carbon, silicon, and oxygen. The first probably comes from the rest of polycarbonate which has not been completely dissolved or from contamination by organic compounds from a contact with hands even indirect because carbon is very polluting. The last possibility is the carbon contamination from the carbon double tape used to fix the sample on the sample holder.
The two others come from the silicon oxide and silicon which make up the substrate. Less oxygen on the first zone lead to suppose that the laser etched more in the silicon oxide layer and therefore detects the silicon more extensively. This is in agreement with the topology of this zone before etching which was free of nanowires and therefore less material had to be etched.

Component	Mass %	Atom %
C	12.81	24.66
O	8.66	12.52
Si	75.90	62.49
Ti	0.03	0.01
Ni	0.03	0.01
Pt	2.56	0.3

Table 9.1: Summary of the atoms present on the etched zone on the sides of the electrodes

Component	Mass %	Atom %
C	7.47	17.94
O	8.65	15.61
Si	56.34	57.93
Ti	0.04	0.03
Ni	12.89	6.34
Pt	14.62	2.16

Table 9.2: Summary of the atoms present on the etched zone in the center of the the design

9.3 Electrical Measurement

The resistance between several zones of the interdigit electrode has been measured with a multimeter to verify if each zone was electrically isolated from the others. Unfortunately, it appears that the resistance between all the areas separated by an etched zone was of about 30 Ω and that the resistance between two points of the same area was of about 2 Ω or 3 Ω. There is therefore still too much electrical conductivity meaning that this interdigit electrode is not usable for supercapacitors.

9.4 Other Etching Structures

To better understand which problem could be to source of the electrical insulation problem, several tests varying each a parameter have been conducted on a substrate without any nanowires.

The first conducted test was the variation of the distance between the lasers passes. Indeed, when the laser etches a zone, it will discretise the area in several lines because the surface of the laser impact is much smaller than the area to cover. The increase of the distance from 1 μm to 20 μm decreased the electrical resistance from 400 $k\Omega$ to 200 $k\Omega$. The other parameters was a frequency of 40 kHz, a power of 20% or 0.67 W and a speed of 200 m/s.

The second test was the variation of the width of the etched zone. It would be expected that at most this width is large, the higher the electrical insulation is between the two adjacent part of the substrate separate by this etching. The width has been varied from 100 μm to 2 mm without obtaining a major change in the electrical insulation. The others parameters were a frequency of 200 kHz, a power of 100%, a speed of the 200 mm/s and a distance between the etched lines of 2 μm.

The third test varied the power from 20 % to 100 %. The consequence was surprisingly a decrease in the electrical insulation from 4.7 $k\Omega$ to 3.1 $k\Omega$. The other parameters were a frequency of 200 kHz, a speed of 200 mm/s, ten passes and a distance between the lines of 2 μm.

The fourth test varied the overlap. This overlap is defined by the distance between the center of two pulses beam impact on the target. By increasing the overlap and therefore diminishing the distance between the impact pulses, the electrical resistance increased by about 50 % but without exceeding 126 $k\Omega$ resulting in an insufficient electrical insulation.

Finally, another test has been made on a substrate were titanium and platinium have been deposited only on certain parts of the substrate. Therefore, between these zones, only silicon and silicon oxide are present. However, the electrical conduction is still too high.

The logical conclusion is that the problem comes from the silicon substrate itself.

Chapter 10

Conclusion

During this master thesis, electrodes composed of a 3D nanostructure of nickel-nickel oxide nanowires, on a silicon substrate, coated with titanium and platinum have been successfully made. Batteries and supercapacitors have been made with these electrodes, and tested.

Half of the electrodes were successfully incorporated into cells, and two-third of the batteries worked with more or less performance in function of the batteries. The supercapacitors made of these electrodes did not work.

For the working batteries, the results showed a poor coulombic efficiency during the first cycle, leading most of them to lose between 30% to 80% of their specific capacity. However, after some cycles, the coulombic efficiency become very close to one leading to a nearly stable performance in function of the number of cycles. This effect is more pronounced with the 40 nm nanowires electrodes, resulting in the conclusion that these are more electrochemically stable than the 230 nm nanowires electrodes. The first have however achieved higher specific capacity per mass than 40 nm nanowires electrodes, as well as the 2D NiO film electrodes, which are by far the worst of the three as expected. A quite large hysteresis curve is observed when looking at the voltage profiles, reducing the energy efficiency, which is consistent with the behaviour of transition metal oxides. The discharge potential of these electrodes is however not very high relative to Li/Li^+, and these should better be used as anodes instead of cathodes in future energy storage system. These 3D nanostructures are therefore very interesting in the battery field. The tests showed that it is possible to use silicon substrate inside batteries without damaging it, by choosing the potentials at which the cells are cycled. This has to be higher than 0.3 V.

The supercapacitors made with these electrodes did not work. EIS, galvanostatic charge and discharge cycles test did not show useful data. However, such nanostructures conserve their interest and research must continue in this field.

Concerning the supercapacitors, bad results were obtained. No electrochemically stable supercapacitor has been made with the 3D interconnected structure. The interest of enhancing the capacity and the power is still conserved.

The interdigit electrode is a fascinating design that will be able to improve the efficiency of electrodes further but unfortunately, no working electrode has been made, because of the insufficient electrical insulation of the silicon substrate.

Future prospects

Electrodes

Adhesion of the 3D interconnected nanowire network was one of the biggest challenges. Therefore, it would be interesting to test other covering layers, like nickel or silver[101], on the adhesion titanium layer, to enhance the adhesion between the nanowires, and the latest layer of the substrate. Copper has been tried as the last layer of the substrate, giving approximately the same success rate, regarding the adhesion obtained with the platinium. Unfortunately, most of them were destroyed during the malfunction of the drying oven, leading to the impossibility of having usable data from assembled cells with these electrodes.

It would be interesting to test some chemical attacks of the surface to create a more rough surface, or removing most of the thin oxide layer, which always forms in contact with air, to obtain a better adhesion.

The mechanical integrity of the 3D structure could be enhanced using less hard cooling conditions. Indeed, the passage from 350-450°C to ambient temperature, in a few seconds, was fatal to many samples. Doing a cooling in several tens of minutes could be beneficial.

The diameter of the nanowires could also be further decreased using polycarbonate templates with lower pore diameter, to reduce the effect of pulverisation of active material, which decreases at the nanometer scale.

Test optimum annealing

During the master thesis, just two annealing conditions were used with success. It would be interesting to test several other conditions, different temperatures and time, to obtain the optimum in term of cycle life, specific power and specific capacity of the cells.

Also, by annealing the 40 nm nanowires to obtain the same nickel-nickel oxide proportion as for the 230 nm nanowires, it would be possible to obtain higher specific capacity per surface, while maintaining the same electrochemical stability inherent to the behaviour of nanosized particles of nickel oxide.

Supercapacitors

The made supercapacitors did not work. This is probably due to the used electrolyte in combination with the used substrate. Other electrolytes should be used in order to reduce the side reaction that reduces the performance. Also, other substrates like stainless steel should be tried to avoid corrosion reactions, and enhance the performances.

Interdigit electrode

Several electrical insulation problems hindered the fabrication of a working interdigit electrode. No sufficient electrical insulation of the silicon substrate leads to nonfunctional interdigit electrodes. Therefore, it would be interesting to test different isolating covering layers on the silicon-silicon oxide substrate to obtain better electrical insulation when etched by the picosecond laser. Another silicon substrate, with a different doping and therefore a higher electrical resistance, could also be considered.

Bibliography

[1] IRENA(2015). Renewable power generation costs in 2014. Technical report, Internation Renewable Energy Agency, January 2015.

[2] Triple Pundit. Sustainable renewable energy storage: Are we there yet? `http://www.triplepundit.com/2014/09/storage-solutions-wind-solar-energy/`, note= 5-06-2017.

[3] Enerzine. Le japon s'essaye au stockage de l'électricité solaire. `http://www.enerzine.com/15/14273+le-japon-sessaye-au-stockage-de-lelectricite-solaire+.html`, note= 5-06-2017.

[4] Björn Nykvist and Måns Nilsson. Rapidly falling costs of battery packs for electric vehicles. *Nature Climate Change*, 5(4):329–332, 2015.

[5] Enerzine. Gigafactory tesla. `https://www.tesla.com/fr_BE/gigafactory?redirect=no`, note= 5-06-2017.

[6] Poulomi Roy and Suneel Kumar Srivastava. Nanostructured anode materials for lithium ion batteries. *Journal of Materials Chemistry A*, 3(6):2454–2484, 2015.

[7] Battery University. What's the best battery? `http://batteryuniversity.com/learn/archive/whats_the_best_battery`. 19-05-2017.

[8] D. Linden and T. Reddy. *Handbook of Batteries*. McGraw-Hill handbooks. McGraw-Hill Education, 2001.

[9] Naoki Nitta, Feixiang Wu, Jung Tae Lee, and Gleb Yushin. Li-ion battery materials: present and future. *Materials today*, 18(5):252–264, 2015.

[10] Subrahmanyam Goriparti, Ermanno Miele, Francesco De Angelis, Enzo Di Fabrizio, Remo Proietti Zaccaria, and Claudio Capiglia. Review on recent progress of nanostructured anode materials for li-ion batteries. *Journal of Power Sources*, 257:421 – 443, 2014.

[11] David J Lockwood. Nanostructure science and technology, 2005.

[12] Alexandru Vlad, Vlad-Andrei Antohe, Juan Manuel Martinez-Huerta, Etienne Ferain, Jean-Francois Gohy, and Luc Piraux. Three-dimensional interconnected nicore-nioshell nanowire networks for lithium microbattery architectures. *J. Mater. Chem. A*, 4:1603–1607, 2016.

[13] Ming-Yao Cheng, Yun-Sheng Ye, Tse-Ming Chiu, Chun-Jen Pan, and Bing-Joe Hwang. Size effect of nickel oxide for lithium ion battery anode. *Journal of Power Sources*, 253:27–34, 2014.

[14] Litty V Thekkekara, Baohua Jia, Yinan Zhang, Ling Qiu, Dan Li, and Min Gu. On-chip energy storage integrated with solar cells using a laser scribed graphene oxide film. *Applied Physics Letters*, 107(3):031105, 2015.

[15] Hui Wu, Gerentt Chan, Jang Wook Choi, Yan Yao, Matthew T McDowell, Seok Woo Lee, Ariel Jackson, Yuan Yang, Liangbing Hu, and Yi Cui. Stable cycling of double-walled silicon nanotube battery anodes through solid-electrolyte interphase control. *Nature nanotechnology*, 7(5):310–315, 2012.

[16] Yaser Abu-Lebdeh and Isobel Davidson. *Nanotechnology for lithium-ion batteries*. Springer Science & Business Media, 2012.

[17] Candace K Chan, Hailin Peng, Gao Liu, Kevin McIlwrath, Xiao Feng Zhang, Robert A Huggins, and Yi Cui. High-performance lithium battery anodes using silicon nanowires. *Nature nanotechnology*, 3(1):31–35, 2008.

[18] Abolanle S Adekunle, Kenneth I Ozoemena, Bhekie B Mamba, Bolade O Agboola, and Oluwafemi S Oluwatobi. Supercapacitive properties of symmetry and the asymmetry two electrode coin type supercapacitor cells made from mwcnts/nickel oxide nanocomposite. *Electrochemical Science Group*, 2011.

[19] V Ganesh, S Pitchumani, and V Lakshminarayanan. New symmetric and asymmetric supercapacitors based on high surface area porous nickel and activated carbon. *Journal of Power Sources*, 158(2):1523–1532, 2006.

[20] Battery university. Bu-104b: Battery building blocks. `http://batteryuniversity.com/learn/article/bu_104b_building_blocks_of_a_battery`. 09-04-2017.

[21] Battery university. Bu-307: How does electrolyte work? `http://batteryuniversity.com/learn/article/bu_307_electrolyte`. 15-05-2017.

[22] Battery university. Bu-105: Battery definitions and what they mean. `http://batteryuniversity.com/learn/article/battery_definitions`. 09-04-2017.

[23] Helena Berg. *Batteries for Electric Vehicles*, volume 1. Cambridge University Press, 11 2015.

[24] Matthew B Pinson and Martin Z Bazant. Theory of sei formation in rechargeable batteries: capacity fade, accelerated aging and lifetime prediction. *Journal of the Electrochemical Society*, 160(2):A243–A250, 2013.

[25] UsSolarInstitute. depth of discharge (dod). `https://ussolarinstitute.com/glossary/depth-of-discharge/`. 22-05-2017.

[26] Electropaedia. Battery life (and death). `http://www.mpoweruk.com/life.htm`. 20-05-2017.

[27] Battery University. Bu-808: How to prolong lithium-based batteries. `http://batteryuniversity.com/learn/article/how_to_prolong_lithium_based_batteries`. 20-05-2017.

[28] P Notten, H Bergveld, and W Kruijt. Battery management systems: Design by modeling. *Kluwer Academic Publisher*, 2002.

[29] Pallavi Verma, Pascal Maire, and Petr Novák. A review of the features and analyses of the solid electrolyte interphase in li-ion batteries. *Electrochimica Acta*, 55(22):6332–6341, 2010.

[30] Recharge. Batteries : Categories and types of batteries. http://www.rechargebatteries.org/knowledge-base/batteries/. 15-05-2017.

[31] Battery university. Bu-106: Advantages of primary batteries. http://batteryuniversity.com/learn/article/primary_batteries. 15-05-2017.

[32] Magnet academy. Daniell cell. https://nationalmaglab.org/education/magnet-academy/watch-play/interactive/daniell-cell. 19-05-2017.

[33] Chengjun Xu, Yanyi Chen, Shan Shi, Jia Li, Feiyu Kang, and Dangsheng Su. Secondary batteries with multivalent ions for energy storage. *Scientific reports*, 5:14120, 2015.

[34] Battery University. Bu-201: How does the lead acid battery work? http://batteryuniversity.com/learn/article/equalizing_charge. 19-05-2017.

[35] Battery University. Daniell cell. http://www.batteryuniversity.com/learn/article/lead_based_batteries. 19-05-2017.

[36] Battery University. Bu-203: Nickel-based batteries. http://www.batteryuniversity.com/learn/article/Nickel_based_batteries. 19-05-2017.

[37] Battery University. What the heck is a nicd battery? https://www.batterystuff.com/kb/articles/battery-articles/what-the-heck-is-a-nicd-battery.html. 19-05-2017.

[38] Wu Xu, Jiulin Wang, Fei Ding, Xilin Chen, Eduard Nasybulin, Yaohui Zhang, and Ji-Guang Zhang. Lithium metal anodes for rechargeable batteries. *Energy & Environmental Science*, 7(2):513–537, 2014.

[39] Héctor D Abrufia, Yasuyuki Kiya, and Jay C Henderson. Batteries and electrochemical capacitors. *Physics Today*, 2008.

[40] MassashusettsInstitute of Technology. Doubling battery power of consumer electronics. http://news.mit.edu/2016/lithium-metal-batteries-double-power-consumer-electronics-0817. 26-05-2017.

[41] M Rosa Palacin. Recent advances in rechargeable battery materials: a chemist's perspective. *Chemical Society Reviews*, 38(9):2565–2575, 2009.

[42] C. Julien and G.A. Nazri. Chapter 3 - intercalation compounds for advanced lithium batteries. In Hari Singh Nalwa, editor, *Handbook of Advanced Electronic and Photonic Materials and Devices*, pages 99 – 184. Academic Press, Burlington, 2001.

[43] Chaofeng Liu, Zachary G. Neale, and Guozhong Cao. Understanding electrochemical potentials of cathode materials in rechargeable batteries. *Materials Today*, 19(2):109 – 123, 2016.

[44] PLSG Poizot, S Laruelle, S Grugeon, L Dupont, and JM Tarascon. Nano-sized transition-metal oxides as negative-electrode materials for lithium-ion batteries. *Nature*, 407(6803):496–499, 2000.

[45] S. Zugmann, M. Fleischmann, M. Amereller, R.M. Gschwind, H.D. Wiemhöfer, and H.J. Gores. Measurement of transference numbers for lithium ion electrolytes via four different methods, a comparative study. *Electrochimica Acta*, 56(11):3926 – 3933, 2011.

[46] Maan Hayyan, Farouq S. Mjalli, Mohd Ali Hashim, Inas M. AlNashef, and Tan Xue Mei. Investigating the electrochemical windows of ionic liquids. *Journal of Industrial and Engineering Chemistry*, 19(1):106 – 112, 2013.

[47] Ruisi Zhang, Niloofar Hashemi, Maziar Ashuri, and Reza Montazami. Advanced gel polymer electrolyte for lithium-ion polymer batteries. In *ASME 2013 7th International Conference on Energy Sustainability collocated with the ASME 2013 Heat Transfer Summer Conference and the ASME 2013 11th International Conference on Fuel Cell Science, Engineering and Technology*, pages V001T05A005–V001T05A005. American Society of Mechanical Engineers, 2013.

[48] Ranganath Teki, Moni K Datta, Rahul Krishnan, Thomas C Parker, Toh-Ming Lu, Prashant N Kumta, and Nikhil Koratkar. Nanostructured silicon anodes for lithium ion rechargeable batteries. *Small*, 5(20):2236–2242, 2009.

[49] Zhuang Sun Peng Zhang Xuefeng Song, Xiaobing Wang and Lian Gao. Recent developments in silicon anode materials for high performance lithium-ion batteries. *Merck*, 2013.

[50] Sulin Zhang. Chemomechanical modeling of lithiation-induced failure in high-volume-change electrode materials for lithium ion batteries. *NPJ Computational Materials*, 3:1, 2017.

[51] Hui Wu, Gerentt Chan, Jang Wook Choi, Yan Yao, Matthew T McDowell, Seok Woo Lee, Ariel Jackson, Yuan Yang, Liangbing Hu, and Yi Cui. Stable cycling of double-walled silicon nanotube battery anodes through solid-electrolyte interphase control. *Nature nanotechnology*, 7(5):310–315, 2012.

[52] Jason Graetz, CC Ahn, Rachid Yazami, and Brent Fultz. Highly reversible lithium storage in nanostructured silicon. *Electrochemical and Solid-State Letters*, 6(9):A194–A197, 2003.

[53] LGH Staaf, Per Lundgren, and Peter Enoksson. Present and future supercapacitor carbon electrode materials for improved energy storage used in intelligent wireless sensor systems. *Nano Energy*, 9:128–141, 2014.

[54] Tao Chen and Liming Dai. Flexible supercapacitors based on carbon nanomaterials. *Journal of Materials Chemistry A*, 2(28):10756–10775, 2014.

[55] BE Conway. Similarities and differences between supercapacitors and batteries for storing electrical energy. In *Electrochemical Supercapacitors*, pages 11–31. Springer, 1999.

[56] Mouser electronics. High performance electrical double-layer capacitors. `http://www.mouser.com/pdfDocs/Murata-DMF-DMT_TechnicalGuide.pdf`. 24-05-2017.

[57] Marin S Halper and James C Ellenbogen. Supercapacitors: A brief overview. *MITRE Nanosystems Group*, 2006.

[58] Martin Chaplin. Electrolysis of water. `http://www1.lsbu.ac.uk/water/electrolysis.html`. 28-05-2017.

[59] Li Li Zhang and XS Zhao. Carbon-based materials as supercapacitor electrodes. *Chemical Society Reviews*, 38(9):2520–2531, 2009.

[60] Eunho Lim, Haegyeom Kim, Changshin Jo, Jinyoung Chun, Kyojin Ku, Seongseop Kim, Hyung Ik Lee, In-Sik Nam, Songhun Yoon, Kisuk Kang, et al. Advanced hybrid supercapacitor based on a mesoporous niobium pentoxide/carbon as high-performance anode. *ACS nano*, 8(9):8968–8978, 2014.

[61] Huiqiao Li, Liang Cheng, and Yongyao Xia. A hybrid electrochemical supercapacitor based on a 5 v li-ion battery cathode and active carbon. *Electrochemical and Solid-State Letters*, 8(9):A433–A436, 2005.

[62] Patrice Simon and Yury Gogotsi. Materials for electrochemical capacitors. *Nature materials*, 7(11):845–854, 2008.

[63] Rui Igreja and CJ Dias. Analytical evaluation of the interdigital electrodes capacitance for a multi-layered structure. *Sensors and Actuators A: Physical*, 112(2):291–301, 2004.

[64] Maher F El-Kady and Richard B Kaner. Scalable fabrication of high-power graphene micro-supercapacitors for flexible and on-chip energy storage. *Nature communications*, 4:1475, 2013.

[65] Litty V Thekkekara and Min Gu. Bioinspired fractal electrodes for solar energy storages. *Scientific Reports*, 7:45585, 2017.

[66] Radek Soukup, Jiri Navratil, Jan Reboun, and Tomas Rericha. A comparison of the interdigital electrodes prepared by aerosol jet printing and lift-off technique. In *Electronics Technology (ISSE), 2015 38th International Spring Seminar on*, pages 30–35. IEEE, 2015.

[67] Alexandru Vlad, Vlad-Andrei Antohe, Juan Manuel Martinez-Huerta, Etienne Ferain, Jean-Francois Gohy, and Luc Piraux. Supporting information for three-dimensional interconnected nicore-nioshell nanowire networks for lithium microbattery architectures. *J. Mater. Chem. A*, 4:1603–1607, 2016.

[68] HANOT H. and FERAIN E. Industrial applications of ion track technology. *Nuclear instruments and methods in physics research. Section B, Beam interactions with materials and atoms (Print)*, 267(6):1019–1022, 2009. eng.

[69] ESIEE : Paris. Depots de couches minces. `http://www.esiee.fr/fr/ecole/salles-blanches/equipements-et-procedes/depots-couches-minces`. 1-06-2017.

[70] A Ababneh, AN Al-Omari, AMK Dagamseh, M Tantawi, C Pauly, F Mücklich, D Feili, and H Seidel. Electrical and morphological characterization of platinum thin-films with various adhesion layers for high temperature applications. *Microsystem Technologies*, pages 1–7, 2015.

[71] H. Panda. *Handbook on Electroplating with Manufacture of Electrochemicals*. ASIA PACIFIC BUSINESS PRESS Inc, 2017.

[72] Yuliy D Gamburg and Giovanni Zangari. *Theory and practice of metal electrodeposition*. Springer Science & Business Media, 2011.

[73] Sung H Whang. *Nanostructured metals and alloys: processing, microstructure, mechanical properties and applications*. Elsevier, 2011.

[74] Industrial laser solution for manufacturing. Picosecond lasers come of age for micromachining. `http://www.industrial-lasers.com/articles/print/volume-28/issue-3/features/picosecond-lasers-come-of-age-for-micromachining.html`. 18-05-2017.

[75] Nanoscience Instruments. Sem components. `http://www.nanoscience.com/technology/sem-technology/sem-components/`.

[76] Susan Swapp. Geochemical Instrumentation and Analysis scanning electron microscopy (sem). `http://serc.carleton.edu/research_education/geochemsheets/techniques/SEM.html`. 13-03-2017.

[77] Material evaluation and inc engineering. Scanning electron microscopy (sem). `http://www.mee-inc.com/hamm/scanning-electron-microscopy-sem/`.

[78] University of Cap Town. Centre for imaging & analysis the sem vacuum system. http://emu.uct.ac.za/training/sem-school/the-sem-vacuum-system/.

[79] Azo optics. Astigmatism in optical systems. http://www.azooptics.com/Article.aspx?ArticleID=665.

[80] How Stuff Works Science. The key components of a scanning electron microscope. http://science.howstuffworks.com/scanning-electron-microscope2.htm. 31-05-2017.

[81] McSwiggen & Associates. Tech notes, wds vs eds. http://www.mcswiggen.com/TechNotes/WDSvsEDS.htm.

[82] Materials evaluation and inc engineering. Testing electrochemical capacitors part 1: Cv, eis, and leakage current. http://www.mee-inc.com/hamm/energy-dispersive-x-ray-spectroscopyeds/.

[83] P. J. Flanders. An alternating gradient magnetometer (invited). *Journal of Applied Physics*, 63(8):3940–3945, 1988.

[84] LakeShore Cryotechnics. Pmc micromag 2900 series agm. http://www.lakeshore.com/products/Vibrating-Sample-Magnetometer/PMC-MicroMag-2900-Series-AGM/Pages/Overview.aspx. 23-04-2017.

[85] ExplainThatStuff! Piezoelectricity. http://www.explainthatstuff.com/piezoelectricity.html. 23-04-2017.

[86] K. O'Grady, V. G. Lewis, and D. P. E. Dickson. Alternating gradient force magnetometry: Applications and extension to low temperatures (invited). *Journal of Applied Physics*, 73(10):5608–5613, 1993.

[87] NS Zhai, MW Li, WL Wang, DL Zhang, and DG Xu. The application of the eis in li-ion batteries measurement. *IOP Publishing*, 48(1):1157, 2006.

[88] Battery university. Bu-907: Testing lithium-based batteries. http://batteryuniversity.com/learn/article/testing_lithium_based_batteries. 16-05-2017.

[89] Corrosionpedia. Galvanostatic. https://www.corrosionpedia.com/definition/575/galvanostatic. 06-05-2017.

[90] Ecochemie. Galvanostatic charge-discharge of a li-ion battery with autolab. http://www.ecochemie.nl/download/Applicationnotes/Autolab_Application_Note_BAT02.pdf. 06-05-2017.

[91] Yanjing Chen, Mengyun Nie, Brett L. Lucht, Amitesh Saha, Pradeep R. Guduru, and Arijit Bose. High capacity, stable silicon/carbon anodes for lithium-ion batteries prepared using emulsion-templated directed assembly. *ACS Applied Materials & Interfaces*, 6(7):4678–4683, 2014. PMID: 24640970.

[92] Jung-Ki Park. *Principles and applications of lithium secondary batteries*. John Wiley & Sons, 2012.

[93] Gamry Instrument. Energy dispersive x-ray spectroscopy (eds). https://www.gamry.com/application-notes/battery-research/testing-electrochemical-capacitors-cyclic-voltammetry-leakage-current/.

[94] Peter T. Kissinger and William R. Heineman. Cyclic voltammetry. *Journal of Chemical Education*, 60(9):702, 1983.

[95] Sheng Han, Hong-Ying Chen, Chiu-Chieh Chen, Ta-Nien Yuan, and Han C Shih. Characterization of ni nanowires after annealing. *Materials Letters*, 61(4):1105–1108, 2007.

[96] Royal Society of Chemistry. Periodic table : Nickel. http://www.rsc.org/periodic-table/element/28/nickel. 11-05-2017.

[97] Azo nano. Nickel oxide (nio) nanoparticles - properties, applications. `http://www.azonano.com/article.aspx?ArticleID=3378`. 11-05-2017.

[98] Feng Leng, Cher Ming Tan, Michael Pecht, and JiYe Zhang. The effect of temperature on the electrochemistry in lithium-ion batteries. In *Next-Generation Electronics (ISNE), 2014 International Symposium on*, pages 1–4. IEEE, 2014.

[99] Binni Varghese, MV Reddy, Zhu Yanwu, Chang Sheh Lit, Teo Choon Hoong, GV Subba Rao, BVR Chowdari, Andrew Thye Shen Wee, Chwee Teck Lim, and Chorng-Haur Sow. Fabrication of nio nanowall electrodes for high performance lithium ion battery. *Chemistry of Materials*, 20(10):3360–3367, 2008.

[100] Inc MicroTechSystems. Alkaline etching of silicon. `http://www.microtechprocess.com/pdf/MTS_KOH.pdf`. 26-05-2017.

[101] Naoki Okamoto, Feng Wang, and Tohru Watanabe. Adhesion of electrodeposited copper, nickel and silver films on copper, nickel and silver substrates. *Materials transactions*, 45(12):3330–3333, 2004.

Chapter 11

Appendix

11.1 Calculation of Nickel Oxide Mass

The first step to obtaining the mass of nickel oxide present in the nanowires is to make an AGM measurement. During it, the variation of the magnetic moment of the sample in function of the applied magnetic field has been measured. Here, the most interesting results were the magnetic moment at saturation before and after annealing. These values have been showed in Table 6.1

11.1.1 Faraday's Law

Using the Faraday's law depicted in equation 4.3 and taking into account the cathodic efficiency ϕ for the deposition of nickel, the equation can be written as:

$$m = \frac{QM_w}{nF} \times \phi \tag{11.1}$$

with a charge of 2.2024 Coulombs and 1.207 Coulombs for 230 nm and 40 nm nanowires electrode respectively. ϕ equals 0.96 for the deposition of nickel, M equals 58.69 g/mol, F equals 96485 Coulombs and n equals to two exchanged electron.

The result is a mass of nickel metal before annealing of 0.591 mg and 0.353 mg for the 230 nm and 40 nm nanowires.

In order to obtain the value of nickel after the annealing, one has to do:

$$m_{Niaft} = m_{Nibef} \times \frac{\gamma_{aft}}{\gamma_{bef}} \tag{11.2}$$

with γ_{bef} and $m_{Ni_{bef}}$ the magnetic moment and nickel metal mass content before annealing, γ_{aft} and $m_{Ni_{aft}}$ the magnetic moment and nickel metal mass content after annealing.

The result is a nickel metal mass content of 52.44 % and 83.05 % for 230 nm and 40 nm nanowires respectively after annealing.

Knowing the density of nickel and nickel oxide, 58.69 g/mol and 74.69 g/mol, respectively, one can calculate the NiO mass:

$$m_{NiO} = \left(m_{Ni_{bef}} - m_{Ni_{aft}}\right) \times \frac{74.69}{58.69} \tag{11.3}$$

This gives 0.358 mg and 0.076 mg of nickel oxide for the 230 nm and 40 nm nanowires respectively.

11.2 Experimental Issues

During the master thesis, many things went wrong or didn't work as expected. It goes from machines that were broken for a longer or shorter time, bad stability of the nanowires, losses of pieces for the AGM or weird results

11.2.1 Electrodes Problems

11.2.1.1 Break of the Substrate

The break of the substrate did sometimes occur during the tightening of the bolts permitting to build the electrodeposition set-up. It appears that sometime, the stress created by this step broke some substrate.

Also, when manipulated with the tweezers, the substrate sometimes broke. This problem mostly occurred during the beginning of the master thesis when I wasn't comfortable to work with such little samples.

11.2.1.2 Detachments of Nanowires

This part was probably one of the most frustrating parts of this master thesis. Indeed, the detachment of the nanowires from the substrate could occur at all steps from the electrodeposition to the thermal drying. Indeed, 26 out of the 76 electrodes made during this master thesis were destroyed because of the detachment of nanowires.

11.2.2 Broken Machines

11.2.2.1 Electrodeposition Set-up

The first machine that showed problems was the electrodeposition set-up. At the beginning of the year, when the set-up was done, and the potentiostat turned on, it appears that the measured current was never stabilised. It oscillated between -5 V to 5 V. After some unsuccessful test testing that everything was well-connected, we finally found the source of the problem. One of the connecting wire was rusty. It seems a little stupid to not have to check this at the first place, but the problem did not occur all the time, so we did not think that the problem was linked to this since these were always used by other people.

11.2.2.2 The Tubular Oven

When all the steps to do the electrodeposition was mastered, it appears that the tubular oven used to anneal the samples was broken. The thermostat did not work anymore, and therefore the temperature could not be controlled anymore. From this arises the fact that some time has been lost waiting for the repair of the oven.

11.2.2.3 Malfunction of the Drying Oven

On April 10th 2017, after a planned power shortage of three days in the building were the drying oven is placed, this last went to high in temperature when it was turned on. It heated to 150°C instead of 70°C. Because of this, the plastic boxes containing nine electrodes melted on the electrodes and the nanowires. The oven has then been stopped, and everything which was inside was removed. During this operation, the plastic solidified and therefore clung to the electrode and nanowires surface making them unusable.
Also, even if some of them were still usable, it was no longer possible to identify individually

since the plastic deforms itself a lot and the place where the name of each electrode was written moved on each electrode. Indeed, four boxes were stacked on top of each other, and the electrodes from the top box fell to the bottom mixing them.

Another problem would be the annealing conditions that were therefore not the same as the conditions tested in AGM. Indeed, the ramp temperature and the time needed to achieve this 150°C was not accurately known and therefore, making a test sample to know the proportion of nickel oxide with the conditions that occurred in the oven would have been almost impossible. Without an AGM test, it would not have been possible to calculate the mass of active material, the NiO, and the galvanostatic charge and discharge test would have been incorrect.

Figure 11.1: Picture the melted boxes with the unusable electrodes inside.

Figure 11.2: Other picture the melted boxes with the unusable electrodes inside.

11.2.2.4 Malfunction of the Glovebox

In February, a problem with the glovebox occurred. A non-zero concentration of oxygen has been detected inside it. This was a huge problem since many components used inside it cannot be in contact with oxygen under penalty of being altered. Therefore, no cell assembly has been possible for some weeks. To not lose too much time, it was decided with my promoter Alexandru Vlad to start the production of supercapacitors. Indeed, these type of cells do not use lithium and therefore can be assembled in air.

11.2.2.5 Picolaser Failure

One of the longest machine failures that happened during this year is without a doubt the one from the picosecond laser. It occurs just after the meeting with my promoters where we decided to make interdigit supercapacitors. This failure lasted two months and a half until the end of April. The cause was one of the three motors that did not move anymore. Therefore, it was not possible to move the sample under the laser and to make any etching with it. The problem probably was an electrical connection problem. This cause has been discovered when the people from Winfab shutdown the machine, disconnected all the cables and plugged them all again. Everything seems to work again after that. As a result, only a few tests have been conducted since too little time was available.

11.3 Unusable Results

11.3.1 Electrodeposition

During some electrodepositions, it appears that on some areas, no nanowires were deposited. The most probable cause is the presence of air bubbles which were present on the surface before starting the deposition. This phenomenon has been reduced using a pipette to agitate the electrolyte at the bottom of the set-up at the interface between the polycarbonate membrane and the electrolyte.

Another strange phenomenon was a negative deposition current. This may have been due to a bad electrical contact of the electrodeposition circuit because when everything was dismantled and reassembled again, this problem disappeared.

11.3.2 Galvanostatic Charge and Discharge

Some batteries exhibited very low specific capacity when these were cycled. The values of specific capacities obtained varied between 10 mAh/g to 150 mAh/g compared to about 500 mAh/g for the good samples. These low values can be attributed to disconnection of a part of the nanowires from the electrode leading to a lower electron exchange from the anode to the external circuit. This disconnection may be attributed to the building process of the battery. During the fabrication process, the cellgard separator was deposited on the nanowires. Because these are very fragile, this step may have damaged the nanowires.

11.3.3 AGM

An AGM test on a sample composed of 40 nm in diameter nanowires annealed for 45 min at 350°C has been conducted. This test did not give valuable data. Indeed, to have reproducible data, the sample of origin was always cut in three pieces of 2 mm in diameter, and each of the three undergoes the same AGM test before and after annealing.

Rue Archimède, 1 bte L6.11.01, 1348 Louvain-la-Neuve **www.uclouvain.be/epl**